Detection, Prediction and Control of Epileptic Seizures

by

Md. Ashfaque Bin Shafique

A Dissertation Presented in Partial Fulfillment
of the Requirement for the Degree
Doctor of Philosophy

Approved October 2016 by the
Graduate Supervisory Committee:

Konstantinos Tsakalis, Chair
Armando Rodriguez
Jitendran Muthuswamy
Andreas Spanias

ARIZONA STATE UNIVERSITY

December 2016

ABSTRACT

From time immemorial, epilepsy has persisted to be one of the greatest impediments to human life for those stricken by it. As the fourth most common neurological disorder, epilepsy causes paroxysmal electrical discharges in the brain that manifest as seizures. Seizures have the effect of debilitating patients on a physical and psychological level. Although not lethal by themselves, they can bring about total disruption in consciousness which can, in hazardous conditions, lead to fatality. Roughly 1% of the world population suffer from epilepsy and another 30 to 50 new cases per 100,000 increase the number of affected annually. Controlling seizures in epileptic patients has therefore become a great medical and, in recent years, engineering challenge.

In this study, the conditions of human seizures are recreated in an animal model of temporal lobe epilepsy. The rodents used in this study are chemically induced to become chronically epileptic. Their Electroencephalogram (EEG) data is then recorded and analyzed to detect and predict seizures; with the ultimate goal being the control and complete suppression of seizures.

Two methods, the maximum Lyapunov exponent and the Generalized Partial Directed Coherence (GPDC), are applied on EEG data to extract meaningful information. Their effectiveness have been reported in the literature for the purpose of prediction of seizures and seizure focus localization. This study integrates these measures, through some modifications, to robustly detect seizures and separately find precursors to them and in consequence provide stimulation to the epileptic brain of rats in order to suppress seizures. Additionally open-loop stimulation with biphasic currents of various pairs of sites in differing lengths of time have helped us create control efficacy maps. While GPDC tells us about the possible location of the focus, control efficacy maps tells us how effective stimulating a certain pair of sites will be.

The results from computations performed on the data are presented and the feasibility of the control problem is discussed. The results show a new reliable means of seizure detection

even in the presence of artifacts in the data. The seizure precursors provide a means of prediction, in the order of tens of minutes, prior to seizures. Closed loop stimulation experiments based on these precursors and control efficacy maps on the epileptic animals show a maximum reduction of seizure frequency by 24.26% in one animal and reduction of length of seizures by 51.77% in another. Thus, through this study it was shown that the implementation of the methods can ameliorate seizures in an epileptic patient. It is expected that the new knowledge and experimental techniques will provide a guide for future research in an effort to ultimately eliminate seizures in epileptic patients.

To my parents, who constantly inspired me to pursue the sciences and be involved in research.

To my loving wife, for her untiring support.

ACKNOWLEDGMENTS

I owe my gratitude to several people who have advised, assisted, encouraged or inspired me during the course of this work. While dedicating a few words to them in this brief chapter would do little justice to their support and friendship towards me, I must mention that I will forever be indebted to them.

First of all, I would like to sincerely thank my advisor Dr. Konstantinos Tsakalis who so patiently guided me throughout my research that culminated into this dissertation. At times I have spent many hours a day, discussing problems that I faced and cannot remember any instance where he would not take ample time in explaining to me the intricacies of control theory and nonlinear dynamics. His teachings have deeply impacted my knowledge and skills and I feel honored to have been under his tutelage. I am greatly indebted to Dr. Armando Rodriguez for the effort he took to explain to me some of the complicated topics in control even after class time was over, just so I left with a better understanding of the topics he covered in class. I am thankful to Dr Leonidas Iasemidis for introducing me to the topic of epilepsy as an engineering challenge. I am thankful to Dr. Jennie Si for teaching me about neural networks, which I found profoundly invigorating. I thank Dr. Andreas Spanias and Dr. Jitendran Muthuswamy for serving on my thesis committee and providing me with guidance from time to time about my thesis. My sincerest appreciation goes to Dr David Treiman for his support and mentorship in the biological aspect of my study. His insight in epileptology helped me understand the dynamics better from a medical perspective as well as an engineering one.

My heartfelt thanks to Aaron Faith, Dr. Vinay Venkataraman, Dr. Balu Krishnan, Steven Marsh, Victoria Rodriguez, Garett Scott, Yiqiu Liu, Darpan Saha and Rakesh Joshi for being great friends who inspired intellectual discussions that led to deeper understanding of certain topics during the course of my study and also providing support in my work from time to time. In particular, I must mention that I could not have gained a profound understanding of nonlinear dynamics and chaos without the help of Dr Ioannis Vlachos; I

cannot thank him enough for the numerous hours of his time that I wasted by asking too many questions. He answered each very patiently.

My research work and the writing of this thesis would not have been complete without the enormous support of my mother and late father. From the bottom of my heart, I would like to extend my love and gratitude to them for nurturing me throughout the years through many sacrifices. I thank my family members for being a constant source of support and encouragement. My deepest gratitude to my friends and well-wishers for their encouragement and for believing in me; for picking me up when I was feeling low. That credit is largely also due to my loving wife, Samiha. I thank her for being the most patient person in the world and supporting me while I followed my calling.

Monetary support for this work has been provided by the National Science Foundation grant ECCS-1102390. This research was also partially supported through computational resources provided by ASU Research Computing and also the Extreme Science and Engineering Discovery Environment (XSEDE), which is supported by National Science Foundation grant number ACI-1053575.

TABLE OF CONTENTS

CHAPTER Page

CHAPTER Page

LIST OF TABLES

LIST OF FIGURES

Figure Page

Figure Page

Chapter 1

INTRODUCTION

1.1 Overview

Epilepsy is a chronic, noncommunicable medical condition that results in seizures, affecting a wide range of mental and physical functions in humans. The World Health Organization depicts that epilepsy affects 50 million people worldwide and annual new cases are between 30 and 50 per 100,000 people in the general population [158]; making it the fourth most common neurological disorder after Migraine, Stroke, and Alzheimer's [51]. Although Epilepsy occurs in all age groups, the highest incidence rates are among children and the elderly [32].

The known factors in causing epileptogenesis in humans are traumatic brain injuries, central nervous system infections, brain tumors and genetic abnormalities among many others [5]. Of the 2.2 million troops returning from Iraq and Afghanistan, 100,000 is estimated to develop post-traumatic epilepsy (PTE) [22], owing to the fact that traumatic brain injuries have a 50% incidence risk of epilepsy [92]. The CDC estimates 5.1 million adults and children combined, in the US, have been diagnosed with epilepsy as of 2016 (1.6% of total US population) [13]. The total indirect and direct cost of epilepsy in the United States is estimated to be $15.5 billion yearly. This estimate is based on a reported cost of $12.5 billion in 1995 converted to 2004 dollar value using Bureau of Labor Statistics data [13].

With a surface area of roughly 2,600 cm^2, and a thickness of 3–4 mm, the neo-cortex of a human brain is a thin, extended, convoluted sheet of tissue. It contains up to 28×10^9 neurons which are connected with each other and with cells elsewhere in the brain by a vast number of synapses, of the order of 10^{12} [99]. Epilepsy manifests itself in patients as epileptic seizures (ES) due to synchronous neural firing in the cerebral cortex. It has

been found that these paroxysmal electrical discharges may begin in a small neighborhood of the brain, in which case they are called partial seizures or focal seizures with single or multiple foci. Or, they may begin simultaneously in both cerebral hemispheres which are called primary generalized seizures [28]. Although, a more recent study has shown that even primary generalized seizures originate within local microcircuits and then propagate from that initial ictogenic zone [113]. After the onset of a seizure, partial seizures may remain localized and cause relatively mild cognitive, psychic, sensory, motor relapses or may spread to other regions of the brain and cause symptoms similar to generalized ones. Generalized seizures at their onset bring about altered states of consciousness and can also have a variety of motor symptoms, ranging from a minimal loss of motor action or brief localized body jerks to heavy convulsive actions known as tonic-clonic activity. Immediately after the seizure, the person may lose complete consciousness and wake up a few minutes later, never realizing what they went through.

The ancient Greeks thought of epilepsy as a disease that was "given by the Gods" to the patient (The Latin word Epilepsia is a translation of the Greek term *Epilambanein* which means "to take hold of" or "seize" [142]). This was primarily due to the fact that seizures would come and go, in a seemingly unpredictable fashion. For some patients it happens hundreds of times a day and for others, once every few years. The elusive property of seizures is what makes them difficult to treat. Approximately 60% of new onset epilepsy cases respond to existing antiepileptic drugs (AEDs) but 30% are pharmaco-resistant, having seizures that cannot be fully controlled with available medical therapy or without unacceptable side effects, [26]. However, in addition to the lack of efficacy for complete seizure control, there also is a substantial morbidity associated with the use of AEDs in patients, especially when polypharmacy is required.

The goal of epilepsy management is to make the patient completely seizure free, with minimal side effects or none at all from the anti-epileptic treatment. While surgical removal of the seizure focus is an important and effective therapeutic intervention; for

some of the people with uncontrollable epilepsy, because of multiple foci, seizure foci located within non-resectable areas of the brain and possible post-operative complications, resective surgery is unlikely to ever replace chronic treatment as the primary mode of epilepsy management in the large majority of patients with epilepsy. Patients with seizures who cannot be treated with AEDs and are not candidates for lobectomies are termed to have refractory epilepsy. This leaves us searching for alternative means of treatment for the nearly 15 million patients with refractory epilepsy worldwide in the form of Deep Brain Stimulation (DBS), Vagus Nerve Stimulation (VNS), Transcranial magnetic stimulation (TMS) etc. which have all shown promising results across a range of neurological and neuropsychiatric disorders [68].

An endeavor to control the occurrence of seizures must begin with identifying them accurately and in a timely fashion. Ever since its discovery in the 1920's by Hans Berger [103], the Electroencephalogram (EEG) has been utilized to diagnose conditions of the brain including seizures [144]. The EEG collection process and equipments have evolved considerably over the last decade and are sophisticated enough to incorporate as many as 256 recording channels with sampling rates up to 30 kHz. In the past, although fewer channels were being used to record data, [135] provides evidence that adequately sampling the human EEG across the full surface of the head requires a minimum of 128 sensors so as to not violate the spatial Nyquist sampling rate. Thus, using these data, a trained electroencephalographer would notice changes in the EEG and be able to diagnose that a seizure is occurring and also in cases of partial seizures, mark the focal electrodes. However, this method has a dire limitation in the fact that a timely intervention either by the use of drugs or electrical stimuli via DBS cannot be made effective since the seizure initiation can only be marked when a visible change occurs in the EEG, not to mention human error whereby the expert may fail to identify the seizure altogether. To this end, research has progressed greatly in the last three decades, aided by mathematical tools commonly used in the engineering principles of signal processing to help detect and even in some cases predict

seizures.

Until recently, the general belief in the medical community was that epileptic seizures could not be anticipated [94], although scientific intuition gave evidence for the contrary [114, 87]. Using tools from signal processing, in the late 1980s, Iasemidis and colleagues have reported on such mathematical methods that utilize nonlinear systems theory to assess the state of the brain [54, 62]. In their work they analyzed EEG data from epileptic patients to compute what is known as the Short Term Maximum Lyapunov Exponent (STL_{max}) [64, 62]. It was shown that as the brain transitions from interictal to preictal to ictal and then to postictal (see Appendix B) and back to interictal stages, the nonlinear dynamics of the brain evolves along the lines of chaos-to-order-to-chaos transitions [57, 125]; these changes were tracked through temporal evolutions of the STL_{max} metric and its statistical distance, the T-index. In [61, 60] the same researchers detail how the choice of different parameters in the STL_{max} algorithm can be fine tuned to reveal the change of the brain states between interictal to preictal in the order of minutes or even hours. These detection/prediction algorithms implied that finally it would be possible to think of a real time intervention strategy minutes before a seizure occurs.

Receiver Operating Curves (ROC) analysis showed the superiority of the STL_{max} algorithm over optimal random prediction schemes and over other linear and nonlinear "predictability" schemes. Other research groups followed and found transitions toward low-dimensional states and reduction of brain's complexity a few minutes before the occurrence of epileptic seizures [86, 83, 136, 81]. Through the use of support vector machines Williamson et al use space-delay correlation and covariance matrices to predict seizures [159] and have shown acceptable performance as well. Analysis of intracranial EEG (iEEG) from 18 patients show a characteristic decrease in phase synchronization among different brain sites minutes to several hours before a seizure [97]. With a different approach, [69] have reported that application of a periodic burst of stimulus can help predict seizures better and be used to control them; in a sense this can be thought of as an observability problem,

where the chance of predicting seizures is increased through minute stimulations. Most of these metrics use univariate measures, except for T-index of STL_{max}, thus [2] elicits many univariate and bivariate measures but ultimately concludes that bivariate measures are better in prediction. In a completely different approach, [75] describes a new portable method of seizure detection using motion sensors, that can prove very useful in clinical practice; 91% of seizures were detected within a median period of 17 seconds for tonic-clonic seizures. High-frequency electrical stimulation (HFES; 100–500Hz) triggered by automated seizure detections may have had promise [107]; however, attempting to abort a seizure by stimulating after detection is not a very effective method [89] even if done in close to real-time.

Equipped with the ability to "predict", the difficulties in designing and implementing effective seizure-suppressing controllers have motivated many to take a new look at the problem. The brain is not an unstructured, random collection of neurons guided by statistics. Thus, there is no need for brain models to be so. In their work with such theoretical models, Tsakalis et al have shown that a phenomenological seizure model can be justified by a failing feedback and seizure suppression can be well achieved by employing a *feedback decoupling* control strategy [146]. The implementation of such theoretical models required only weak knowledge of the detailed neuronal structure. It is noteworthy that the type of "epileptic" pathology that these networks can exhibit appears to be independent of the configuration of the network, that is, it is a generic property. It is also independent of the type of the oscillator used, e.g., see [147, 15] for similar results with physiologically motivated models of neuron-level populations and thalamocortical populations. Such methodologies, of looking for aggregate effects that quantify types of behavior should be contrasted with other types of detailed models (see e.g., [145, 25]), which are valuable but could obscure the important functional mechanisms of seizure generation for the design of a feedback controller. To achieve closed loop feedback control, sensory information about the system's states is necessary. One of the most prominent ways to achieve this is by the use of

observers, a.k.a filters. [6] uses a neural mass model based on that by Jansen and Rit [67] and implemented an Unscented Kalman Filter to estimate model parameters to be used eventually for control.

For the implementation of a feedback controller, the use of electrical stimulation presents itself as an attractive alternative for the treatment of epilepsy but the development of effective stimulation strategies and the mechanisms of operation are still not well understood. In addition to the extremely high complexity of brain operation and the variety of seizure types, there are only limited modes of data collection that can be used, both because of physical constraints and because of ethical regulations. The net result is that we are currently lacking a solid and widely acceptable model of seizure development, including seizure precursors or predicting mechanisms. As a few examples of the variety of models we cite [14, 55], whereby coupled oscillator networks were used to model the behavior of an epileptic brain during a seizure [38], which in a focal model of epilepsy shows that stimulation results in seizure elimination in 48% and improvement in seizures in 43% of patients [53], showing how using spectral power features from pre-ictal and inter-ictal data in a logistic regression classifier can improve chances of seizure prediction in dogs with focal epilepsy [6], which uses patient specific tuning of neural mass model parameters through the implementation of unscented Kalman filters to synthesize electrocorticogram (ECoG) data and [157], where micro and macro models were generated to see if epileptic spikes from human, rat and in-vitro gunea pig brain can be replicated in the models.

A natural succession to modeling the brain and its epileptic behavior would be to consider actual stimulation of it and observe efficacies of various implementations of stimuli. The more "traditional" line of work looks at the injection of a stimulus at the epileptic focus. Here, it is important to model the effect of the different type of stimuli on the observed brain behavior. For example, [11] shows that it is possible to either extend or truncate the tonic or clonic phases of the seizure by changing the frequency of stimuli. [95] shows that deep-brain stimulation (DBS) strongly reduced the sustained epileptic activity of focal

cortical dysplasia (FCD) for low-frequency (LFS, < 2Hz) and high-frequency stimulation (HFS, > 70Hz) while intermediate-frequency stimulation (IFS, around 50Hz) had no effect. Tassinari et al. [140] and Boroojerdi et al. [12] have reported in their study how TMS had affected seizure rates to decrease, also in [93] Lulic et al. reported promising results for VNS in patients with refractory epilepsy. Similarly, DBS, principally of thalamic structures, has been reported to reduce seizure frequency in humans [52, 73]. Using 3 and 0.3 Hz rTMS in complex partial epilepsy of mesiobasal limibic onset in rats has led to a decrease in epileptic spike frequency [143]. However useful these results are, there is still plenty of room for research in the control of this "divine" disease. One such area for study is the stimulation parameters for seizure control. As Kuncel et al. have shown that, in their algorithm, there are a total of 12964 possible combinations of stimulation parameters [77]. A search for the optimal parameter set is not in the scope of this study and so a known "safe" parameter set was chosen as described in Chapter 5.

Once the question of "when" a seizure is detected and/or predicted, in a manner of speaking, is answered, the next obvious question becomes "where" is it going to happen? Naturally, such a question can only be asked in cases of focal seizures. Focus localization has been approached as an information flow problem using transfer entropy metrics [124]. However, simpler linear metrics have been shown to produce similar or better results. Following Granger's famous 1969 paper on econometrics, which postulated the idea of causal relations between signals [40], Saito and Harashima utilized the notion of Granger causality in EEG to determine directional flow of information between different EEG channels [126]. Their methods were later modified into the concepts of partial directed coherence and generalized partial directed coherence (GPDC) by Baccala et al [8, 10, 9]. GPDC has been shown to effectively pinpoint focus in epileptic patients [138]. The localization of the seizure focus is not the end of the story. Our knowledge in systems theory elucidates that one needs to consider multiple stimulation points and durations to account for varying effectiveness of the stimulation. The development and maintenance of such "control efficacy" maps adds

new dimension to the seizure control problem. Simply put, it may not be necessary that stimulating the focus will abort a seizure; it is conceivable that sites surrounding the seizure may need to be stimulated as well. In our study we do take this effect into consideration.

While models, both computer and animal, allow us to study seizures and their control mechanisms, translating these work into human seizure control is still a challenge. There are an estimated 0.4 million Americans whose epilepsy cannot be treated with AEDs or surgery [22]. Currently, there are only two FDA-approved devices for treatment. One is a neurostimulator called RNS System developed by NeuroPace to reduce the frequency of seizures and is an implantable device [31]. The other is a vagus nerve stimulator developed by Cyberonics; this device is implanted in the chest to prevent seizures and has been FDA approved since the 90's. Both these devices claim to capture a patient's unique seizure patterns and apply appropriate electrical stimulation. The RNS worked only in a subset of patients and could provide only a 50% or more reduction in the rate of seizures two years post implant [49]. None of these treatments have provided a cure for the disease and even their effectiveness is limited [72]. Hence, there is a great need to develop a wearable device that can make this a treatable disease. Quite a number of research efforts, over the past two decades, have been carried out in combining control engineering and physiological functioning of the brain to develop theoretical and computational models combined with experiments on animals for epileptic seizure prediction and intervention [148].

One of the key impediments to the advances in this field comes from the fact that recording, analyzing and modeling brain activity is a data intensive task. Until recently our resources were largely limited by the computational tools available to us. Modeling and analyzing epilepsy can potentially involve a variety of metrics computed from real-time signals. The volume of the data can increase very rapidly when we consider the number of electrodes used (10 in a simple rodent study but beginning from 32 all the way up to 256 in most modern systems involving human subject studies) and the frequency of sampling (from 240Hz of the earlier EEG sampling rates to tens of kHz that may appear in some relatively

modern studies). And, while the intent and the paradigm followed by each investigator is to use one metric as a seizure predictor or detector, the possibility that the computational algorithm may require some form of tuning for different cases clearly demonstrates the need for extremely high computing capabilities aka, High Performance Computing (HPC). Finally, a great variety in the data can be found from simultaneous acquisition of EEG data with ambient data, muscle motion data and video data that, at the very least, can relate the observed electrical signals to the clinical behavior of the subject. The variety of metrics, the volume of data and its varying types is what has made the treatment of epilepsy a big data problem in recent years. Thus, latest advances in Big Data analytics are driving seemingly impossible tasks in analyzing epileptoform activity from the past, towards fruition today. In our work, however, we have focused on one type of data, i.e. EEG only but the analysis performed on these data are still quite computationally intensive.

Even with the advent of these new tools, control of epileptic seizures still remains an open ended question and the search for the "holy grail", the best prediction and control scheme, continues. This work is but a minute push in the positive direction towards the end goal.

1.2 Report Organization

This report is organized in 8 chapters. After the first chapter, i.e. this one -

- In Chapter 2, we introduce the concept of chaos and provide sufficient detail as a backdrop for it in the search for a solution to epilepsy as an engineering challenge.
- In Chapter 3, the development of the theory of largest Lyapunov from nonlinear dynamics is introduced and its relevance to chaotic systems and the epileptic brain.
- Chapter 4 describes the theory of generalized partial directed coherence; it's advantages over other mechanisms of measuring connectivity and therefore the reason for it being chosen in our study as a means to detect focal candidate sites.

- In Chapter 5, we provide detailed information about the experimental setup both hardware and software used to collect data and provide stimulation to the animals.
- Chapter 6 details the analysis and results from using a more robust method of computing the maximum Lyapunov exponent and provides evidence that it can be utilized to detect seizures.
- In Chapter 7, we use the same method shown in Chapter 6, albeit with a slightly different approach to preempt seizures by stimulating the brain.
- Chapter 8 provides the conclusions of the study so far and the scope of future work in this area of research.

Chapter 2

NONLINEAR DYNAMICAL SYSTEMS WITH CHAOS

2.1 Introduction

Mathematical models have enabled us to understand the universe we live in and to a great extent manipulate behaviors of physical, chemical and biological systems. While the accuracy of a model in an application is debatable, the fact that a fairly accurate model helps predict the system's behavior is not. This was clearly demonstrated by Pierre-Simon Laplace with his concept of universal determinism [132]. In his 1778 work, Laplace ingeniously explained the motions of the known celestial bodies in his time (sun, moon, and planets) with Newton's laws of motion and reduced the study of planets to a set of differential equations.

A century later, Henri Poincaré developed what is known as *state-space* - a set of system states defined over time. This helped study the evolution of a physical system over time by characterizing the system based on laws of physics with the application of differential equations, [115]. It is during this work that Poincaré observed the phenomenon of *sensitivity to initial conditions*. While studying the classical *three-body problem* involving the earth, the sun, and the moon, he found that they have orbits that are non-periodic, yet their periods are neither stable nor unstable. In other words, the periods are bounded within a region in their state-space, neither escaping to infinity nor settling to a fixed-point. However, as Poincaré pointed out, knowledge of the initial conditions of the states does not allow for their long-term predictability. Thus breaking away from Laplace's work of universal determinism. This point in time is regarded as the birth of "Chaos Theory", although it would take another century for this field of science to become mainstream.

A nonlinear dynamical system is said to be chaotic when it is sensitive to differences in initial conditions, is topologically mixing and has dense periodic orbits. The high sensitivity

to initial conditions is often referred to as *the butterfly effect* in pop culture. These minuscule differences in initial conditions may appear due to noise or machine accuracy in computation and can yield widely diverging outcomes for such nonlinear chaotic dynamical systems. Long-term prediction thus becomes impossible in general. Chaotic systems need not be complex in nature, they can be completely deterministic, implying that their future states are completely predictable with no stochasticity involved. Therefore, the study of mathematics that deals with deterministic systems with chaotic behavior is known as Chaos Theory and was first formalized by Edward Lorenz in 1963 [90].

> *Chaos: When the present determines the future, but the approximate present does not approximately determine the future.*
>
> - Edward Lorenz.

Ever since, Lorenz's discovery of chaotic phenomena in weather modeling, the field of chaos theory has exploded into many aspects of science and engineering. Chaos theory is used in cryptography by computer scientists, creating population models in biology, studying turbulence in fluid mechanics. In economics, it is utilized to predict stock market behavior but has had mixed results due to the tremendous complexity of such systems. Feedback, where humans anticipate and react to changes in the market by buying or selling stocks, exacerbates this complexity in stock market behavior. In astronomy, chaos has been used to describe the motion of many planetary bodies and in particular to better predict asteroid paths and whether or not they may come in contact with Earth. And, in more recent years it has been applied in the prediction and/or control of human brain dynamics. While this list of applications is by no means comprehensive, it does provide us with a notion of how ubiquitous chaos is in our modern lives. In the following we present a discussion of nonlinear systems leading to chaos. The conditions for chaos are provided with some examples for the reader to acquire some preliminary intuition about the matter.

2.2 Nonlinear Systems and Their Phase Space

A *dynamical system* is represented mathematically as a set of differential equations. The function that describes a dynamical system, establishes the time dependence of its states and is generally represented in the form

$$\dot{x} = f(x, u, t) \tag{2.1}$$

where, x, u and t represent the state, input and time variables respectively. If the system is *time-invariant* then t is no longer a variable and is dropped from the function. In this case the system is said to be *autonomous*. Sometimes an output equation will be added and the whole description is said to be a *state-space representation* of the dynamical system.

$$y = g(x, u, t) \tag{2.2}$$

Due to the nature of differential equations (difference equations in discrete time systems), dynamical systems exhibit *memory*; that is the value of the current states would depend on its past values. For instance, a swinging pendulum is a system where the current states, position and velocity of the pendulum, relies on knowledge of its past states. For most real-world systems, the differential equations that describe their behavior are nonlinear in nature. As an example, equation 2.3 describes the motion of a pendulum with force input at its pivot.

$$\ddot{\theta} + \frac{c}{mL^2}\dot{\theta} + \frac{g}{L}sin(\theta) = \frac{T_{max}}{mL^2}T \tag{2.3}$$

Here, θ (output) is the angle between the pendulum rod and the vertical and $\dot{\theta}$, $\ddot{\theta}$ are the corresponding higher order derivatives (angular velocity and acceleration). c is the coefficient of friction, m is the mass of the pendulum, assumed to be centered at the end of the rod of length L. T is the applied torque and is normalized to the maximum applicable value, T_{max} (dependent on the maximum torque of a motor). Typically, for the pendulum, the states are considered to be the angle θ and its angular velocity $\dot{\theta}$. As can be seen in this case, the non-linearity in the model appears from the presence of the sine term on

the system output θ; however non-linearity can appear in any other mathematical form for other systems. The validity of the model is also in question; we can have models that represent a system "closely" but never perfectly. This is one of the fundamental limitations of modeling real-world systems. The science of modeling is a juggling act between time and energy spent in creating an "accurate" model versus the benefits of the increased accuracy.

> *As far as the laws of mathematics refer to reality, they are not certain, and as far as they are certain, they do not refer to reality.*
>
> - Albert Einstein.

The *state space* (for discrete-time systems) or *phase space* (for continuous time systems) describes the set of values that the states in a system can take for the entire range of its operation. For instance, in the case of the pendulum, if the two states were represented on the two axes of a coordinate system, then a ring centered about $[0, 0]$ would describe the phase-space plot of the system. At no point in time can the pendulum have values for states outside the ring. Certain class of systems exhibit a behavior in which the phase-space is such that a large set of initial conditions will lead to the state-space trajectory converging to a point or an area; the region of initial conditions that do so is called a *basin of attraction*. Regions of phase-spaces with such behavior are called *attractors*. The four types of attractors are described in brief-

- Fixed-point: A fixed point attractor is one that comes out of a system whose eigenvalues are in the left-half-plane (stable systems). Typically systems that lose energy have fixed-point attractors; e.g. a pendulum with friction will always converge to the bottom position ($\theta = 0$, $\dot{\theta} = 0$), if there is no force input. The phase-space will show trajectories converging to the fixed-point from all local initial conditions (angular position and velocity). Intuitively, no matter where we start the pendulum off, after a certain amount of time, the bob will come to rest at the vertical downwards position.

- Limit Cycle: A limit cycle appears from systems whose states display periodic behavior. The trajectory takes the shape of a ring. A good example is the oscillator circuit used to generate tuning frequencies in a radio.

- Limit Torus: A limit torus, like a limit cycle has a periodic trajectory. However, in this case the system exhibits more than one natural frequency and any two of these frequencies being an irrational ratio makes for the trajectory to take the shape of a torus in the phase-space. An example would be an oscillator with two sinusoids where the frequencies form an irrational fraction.

- Strange attractor: Strange attractors are "strange" simply because the trajectories neither converge entirely into a fixed-point, nor do they escape like an unstable system, nor form a periodic orbit of a concentric nature and the trajectories are not quite on the same plane. The trajectories are locally bounded but never overlap. Nearby trajectories would seem to escape from each other, yet the distance cannot grow beyond a specific value. The dimension of these attractors are also *fractal* in nature due the trajectories not being on the same plane. A strange attractor is the cornerstone of a chaotic system's phase-space. The Lorenz attractor (Figure 2.3) is an example of such an attractor.

Having been introduced to the concept of nonlinear systems, their phase space and what strange attractors are, we are now ready to look deeper into chaotic systems and what separates them from random processes.

2.3 Chaotic Nonlinear Systems

David Ruelle and Takens are credited to have introduced the term *strange attractors* after Ruelle studied the Lorenz attractor in depth, [121]. It is worth mentioning that not all dynamical systems would have attractors in their phase space. Having briefly introduced the concept of phase-space and attractors in the previous section, we now move on to its relevance to chaotic systems. In the following, "state-space" and "phase-space" are used

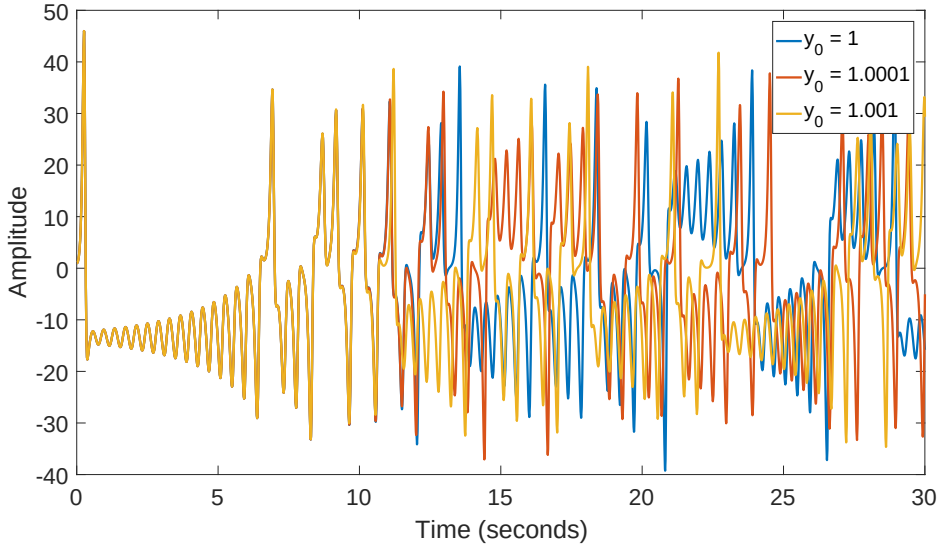

Figure 2.1: Plot of the y variable from the Lorenz equation. The initial conditions, y_0, were chosen as 1, 1.0001 and 1.001. As can be seen, even the slightest variation in initial conditions can make the output of y vary greatly over a 50 second evolution of time; even though they start off being similar near the beginning of the simulation. No noise was added to this data to emphasize that the sensitivity is indeed to initial conditions and not any external influence. The values for the parameters were $\sigma = 45.92$, $\rho = 16$ and $\beta = 4$, while the initial conditions for states other than y were fixed to $x_0 = 0$ and $z_0 = 1.05$.

interchangeably with the assumption that the reader understands that "state-space" is meant for systems described by discrete time systems and "phase-space" for continuous ones.

Edward Lorenz's discovery of chaotic behavior came as a culmination of two centuries of research in systems theory and mathematics. He found that using the same equations, the computer solution with rounding in three digits versus six, produced solutions that were entirely different from each other [105]. This is known as sensitive dependence to initial conditions and is one of the building blocks of chaos theory. In his 1972 paper titled "Predictability: Does the Flap of a Butterfly's Wings in Brazil Set Off a Tornado in Texas?" [27], Lorenz popularized the notion of the *Butterfly effect*. That the insignificant effect of the flapping of a butterfly's wings can lead to a tornado in another part of the world, all because a slight variation in the initial conditions was brought about, was the gist of the publication. However, a formal definition of chaos would not be put forward until much

later when Robert Devaney laid out the three essential properties for a system to be chaotic, [46]:

- Sensitivity to initial conditions.
- Topological mixing.
- Dense periodic orbits.

Figure 2.1 shows the effect of sensitivity to initial conditions. The output was generated from the differential equations of a Lorenz system, which is a nonlinear dynamical system comprised of three states. The initial conditions for states $[x, z]$ were kept the same while that for y was varied between $[1, 1.0001, 1.001]$. As can be seen from the Figure, in a short time, the state y evolved with a rather significant difference.

Topological mixing, implies that the system will evolve over time such that an *open set* in its state-space will eventually overlap with any other given region in the state-space. Mixing is a non-reversible process. Turbulence in fluids is an example of a chaotic system; the analogy allows us to imagine how two fluids can interact within a volume. As an example, Figure 2.2 shows how a set of points bounded in $[0, 1]$ evolves over six iterations of the *Logistic Map*, another example of a chaotic system. As is evident from the images, the process of mixing smears the blue circle from the first iteration into almost a blur in the closed region. after just six iterations. The sixth iteration shows that the points are almost completely scattered in the phase space. Had we progressed further in iterations, the mixing would have been homogeneous and irreversible. The logistic map has a state space function as given in Equation 2.4. In order to expand the state-space of the logistic map into two dimensions, a second state, y, was artificially created. The y variable being depicted modulo one at each step makes the points fold over within the unit square, otherwise the points may have escaped the region. This modulo operation implies that in Figure 2.2(d) - 2.2(f) the points near the top and bottom edge are in fact closer to each other than they appear; this is because the operation creates a cylinder parallel to the x axis.

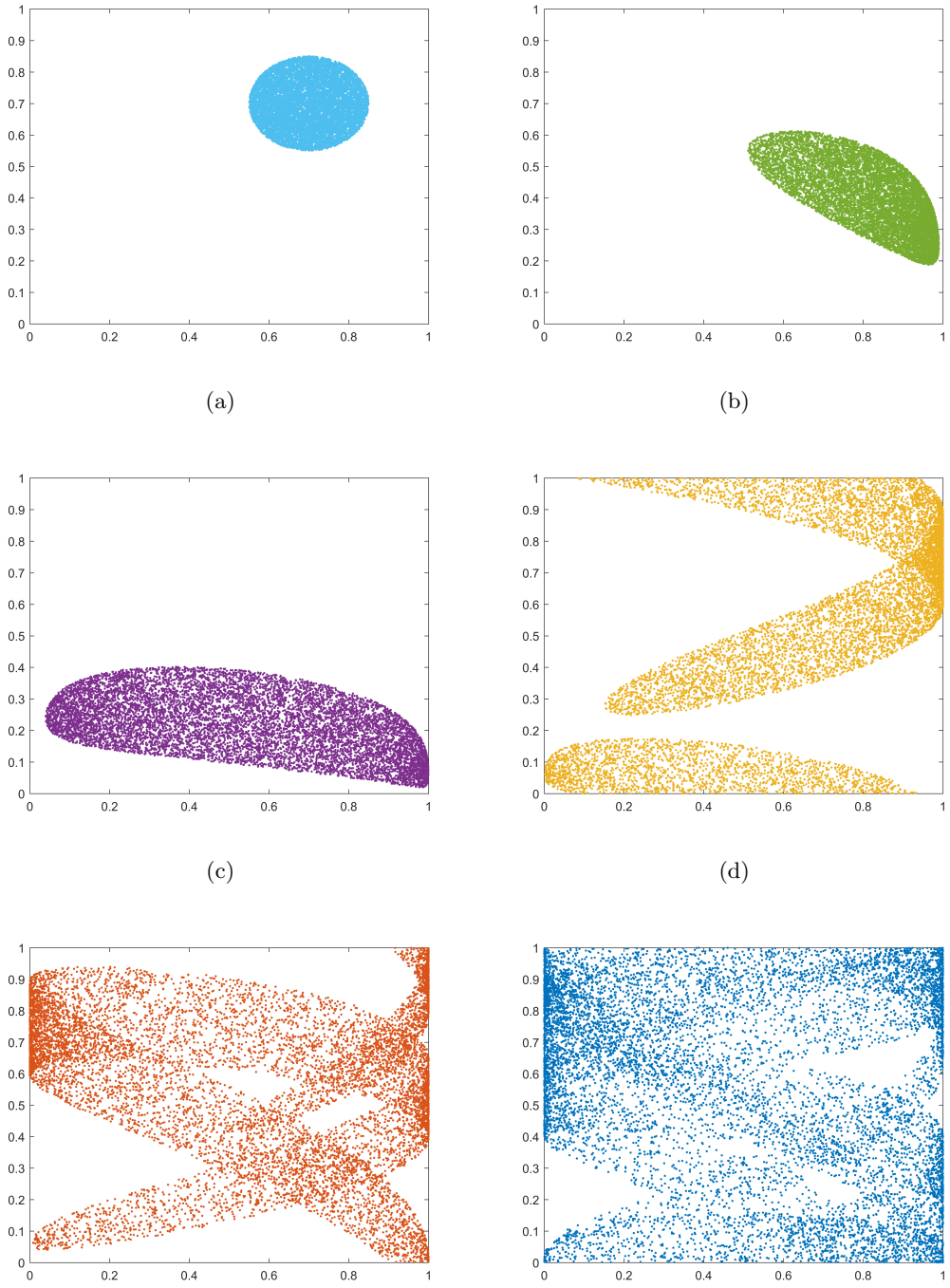

Figure 2.2: Six iterations of a set of states $[x, y]$ passed through the logistic map. (a) shows the first iterate (initial condition), which essentially forms a circle. Plots (b) through (e) show the second to the sixth iteration of the circular initial conditions. It can be seen that *mixing* occurs as we progress in iterations.

Finally, dense periodic orbits refer to the state-space trajectory of a system. The informal meaning or intuition of dense periodic orbits can be attained by thinking of trajectories in the state-space that can be arbitrarily close to each other. Figure 2.3 shows the trajectory of the Lorenz attractor in three-dimensional space. The solutions to the Equation were computed numerically using MATLAB and only 50 seconds worth of data are presented. This is why the "dense" nature of the orbits is not apparent, however longer simulations would have produced an output whereby the trajectories would seem to overlap each other; it must be emphasized trajectories never overlap in a chaotic attractor. More data would not necessarily imply that the attractor would grow (or shrink) in size, only that the trajectories would show more density. It is perchance that the shape of the Lorenz attractor looks similar to that of a "butterfly", finding another coincidence to the coining of the term "The Butterfly Effect".

So far, we have given conditions and their examples of how chaos comes about. We now look at two systems that show chaotic behavior. Equation 2.4 describes the logistic map in two dimensions. The logistic map, is an example of how chaos can arise from a simple system, i.e complex systems are not a necessity for chaotic phenomena. It must also be noted that the logistic map, a discrete-system that is represented by difference equations, can display chaoticity with a single state variable(x_k); y_k is artificially created in this example for the purpose of visualization in Figure 2.2 and is not considered a true second state of the system.

$$x_{k+1} = 4x_k(1 - x_k), \tag{2.4}$$

$$y_{k+1} = \begin{cases} x_k + y_k, & \text{if } x_k + y_k < 1 \\ x_k + y_k - 1, & otherwise \end{cases} \tag{2.5}$$

On the other hand we have Equation 2.6 which describes the Lorenz system. According to the Poincarè-Bendixson theorem, unlike discrete systems, continuous systems must have at least three dimensions in their phase-space to produce chaotic behavior. The lorenz system is a result of Edward Lorenz's work on weather prediction and forms the basis of

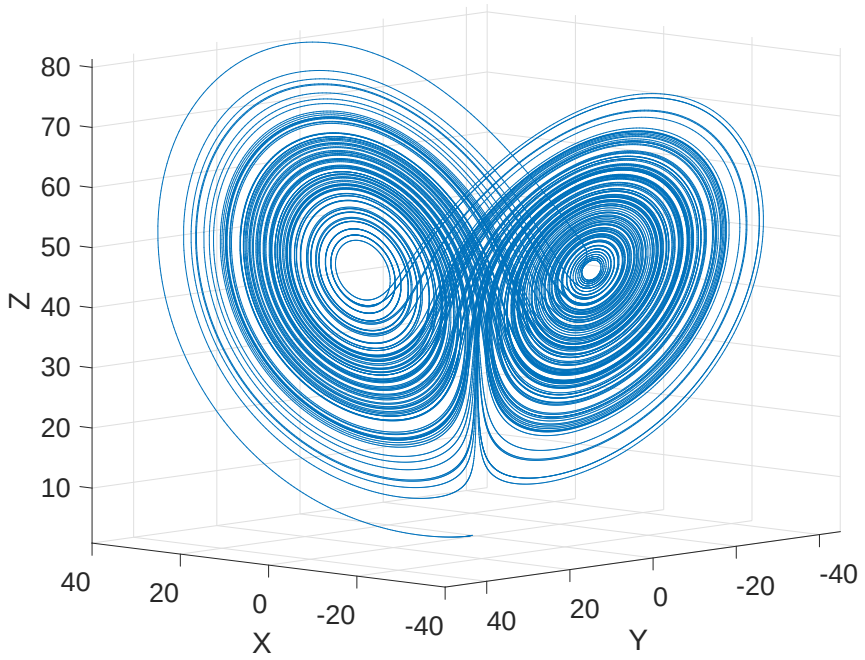

Figure 2.3: A diagram of the Lorenz attractor. This plot was generated via a 3-D plot in MATLAB. The Lorenz equations were solved using MATLAB *ode45* tool with a step-size of 0.001 seconds. The simulation was run for 50 seconds. It is worth noting that the picture could be made to look *dense* as a chaotic attractor by simply allowing for much more time evolution of the trajectory. For this simulation the values for the parameters were the same as used in Figure 2.1.

a mathematical model that describes atmospheric convection. By inspection it is apparent that this system is also deterministic; that is, knowing the exact initial conditions, we can tell the output after a certain time. This stands as an example that deterministic systems too can become chaotic under certain conditions. For the Lorenz system, those conditions are the values for the parameters σ, ρ and β (refer to Figure 2.1 for a set of values for these parameters).

$$\begin{aligned} \dot{x} &= \sigma(y - x) \\ \dot{y} &= x(\rho - z) - y \\ \dot{z} &= xy - \beta z \end{aligned} \tag{2.6}$$

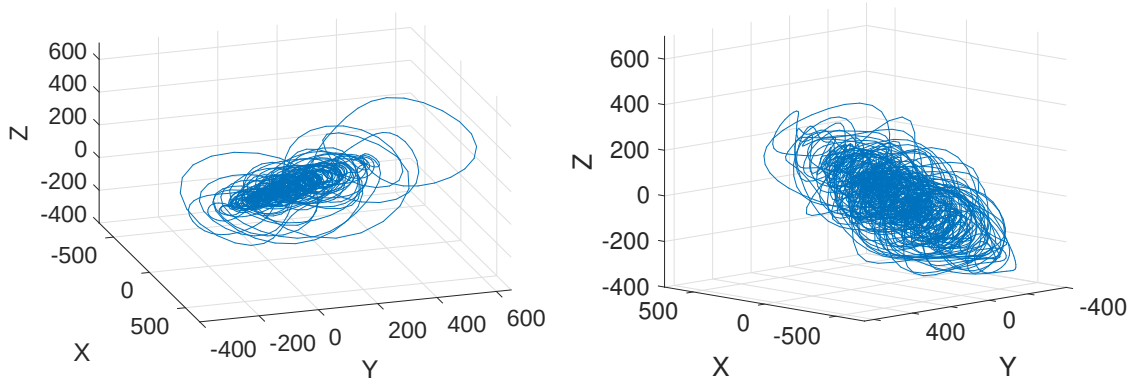

(a) (b)

Figure 2.4: Strange attractors from an epileptic animal EEG. (a) shows the attractor during an interictal epoch of 10 seconds whereas (b) shows the same for an ictal epoch. These attractors were created using 10 seconds of EEG data from the same first channel, expanding it into seven dimensions using Takens' embedding theorem methodology and then compressing into three dimensions, using orthogonal projection, for visual representation. The trajectories may seem like they cut each other in 3D but that will not be the case in higher dimensions of embedding. The attractor at seizure seems to occupy more volume indicating that the trajectories separate from each other more. This intuition will be corroborated with data presented later. The axis limits in both images are the same for X,Y and Z.

2.4 Conclusions

A description of chaotic system behavior is incomplete without comparing it to random or stochastic systems. It is imperative to understand the difference between chaotic systems and stochastic ones and be able to separate the two from given data. While a detailed discussion is irrelevant in our work, it suffices to say that in order to differentiate between a chaotic output and a stochastic output we need to start with a test state in the trajectory of the two systems and find the nearest neighbor to their respective test states in a nearby trajectory and measure the difference in the two states after a few discrete time evolutions. A chaotic system will have a difference which increases exponentially over time; the time evolution of the differences in a stochastic system, however, will be randomly distributed. For a more mathematical approach to distinguish between chaos and random noise, [42] shows how ν, the *correlation exponent* can be used to distinguish between chaos and random

noise and its relationship to the fractal (Hausdorff) dimension, D.

This has been but a concise introduction to the topic of systems theory and chaos. Dynamical systems, nonlinear dynamical systems and chaos are by themselves topics of their own, creating enormous interest in the scientific community. A more detailed description of these topics is out of the scope of this chapter and would lose focus from our subject matter - the treatment of epilepsy and the role of chaos as applied to its solution based on principles of mathematics and engineering. For a more detailed study of nonlinear systems and chaos, the avid reader is referred to an excellent book chapter in [134] or a tutorial in [112].

Understanding chaos is an important aspect to our method of studying epilepsy. The brain acts as a chaotic system and the basis for that will be presented in the later chapters. As an interesting addition to the discussion in this section we present Figure 2.4 which shows the orthogonal projection of attractors present in an epileptic brain. The attractors shown here originally are of much higher dimension but their projection was taken for suitable visualization on paper. Two epochs of data are used in the generation of these attractors. One that is interictal (in between seizures) and another that is ictal (during a seizure). Intuition from these images will be used later to better corroborate our findings.

Chapter 3

THE LYAPUNOV EXPONENT

3.1 Introduction

In the last few decades a great amount of mathematical and engineering principles have been brought into medical studies. This culminates from the idea that our body is primarily governed by chemical reactions and electrical signals. Thus, when it came to matters of the brain, it was apt to try and apply the already well developed theories of electrical engineering into interpreting its function on a neural level; since, neurons communicate with each other via electrical signals. Theories ranging from the use of Fourier analysis, to those of nonlinear dynamics and chaos were being reported in the literature. In recent days even the use of artificial neural networks have been brought in as well [160] to better model the behavior of the brain. It is essential at this point to note that modeling the output of the brain accurately, i.e the EEG from all channels, is overly ambitious due to mathematical and computational constraints and limited knowledge of the brain's underlying operations. However, modeling certain aspects or states of the brain may be viable.

More recently, improvements in nonlinear time series analysis techniques brought about better characterizations of the spatio-temporal dynamics of epileptic brain states, [82]. The Lyapunov exponent arises from nonlinear time series analysis as a metric for chaoticity of a nonlinear chaotic system. Thus, in their work, Iasemidis et al. have shown how the brain behaves as a strange chaotic attractor [64] and how during a seizure its chaoticity varies before, during and after a seizure. The Lyapunov exponent is a nonlinear dynamical measure; which means that since the brain is highly nonlinear and chaotic, the Lyapunov exponent, although a univariate measure, has been shown in a great number of studies to be a very effective tool to characterize human EEG data [64, 58, 152, 54, 60, 61, 100, 125]. Therefore, this method has been adopted in this study and implemented on EEG data

collected from rats albeit with some modifications.

3.2 Lyapunov Exponents

For dynamical systems, the Lyapunov exponent is a quantity that characterizes the separation rate of two nearest neighbor trajectories in the phase-space of the system. Nearest neighbor trajectories are found based on a distance metric, euclidean distance for example. Mathematically, the Lyapunov exponent can be described by the following linearized approximation

$$\delta L(t) \approx e^{\lambda t} \delta L_0 \tag{3.1}$$

where, δL_0 is the initial separation of the nearest neighbors and $\delta L(t)$ is their distance after time evolution t. In Equation 3.1, λ is the Lyapunov exponent along the direction being considered. In a dynamical system, there will be as many Lyapunov exponents as there are dimensions in its phase-space. The Lyapunov exponent in each case represents the separation rate in the directional orientation of the initial separation vector δL_0.

Of this spectrum of Lyapunov exponents, one in particular is of utmost interest in the study of chaotic systems - the maximum Lyapunov exponent (L_{max}). Its importance is due to the fact that L_{max} being positive is an indication of a system being chaotic. However, for a chaotic attractor to be present, the overall dynamics must be dissipative; i.e. the system must be globally stable and the sum of all the Lyapunov exponents must be negative [120]. The larger L_{max} is, the more chaotic the system. A system being more chaotic simply implies that the rate of separation is higher. This has been characterized as the Lyapunov time for chaotic systems and is strictly dependent on its dynamics. Electrical circuits that are chaotic have very short Lyapunov times (milliseconds) versus the solar system which has Lyapunov time in the order of millions of years.

Given a system model with n equations, computing the spectrum of Lyapunov exponents is achieved by solving all the equations for a set of nearby initial conditions and allowing them to expand through the equations. The growth of the vectors defined by the initial conditions is measured and at every time evolution a Gram-Schmidt Reorthonormalization

procedure is performed to ensure that the vectors maintain proper phase-space orientation and do not all lean towards the direction of the most rapid growth, [161]. The rate of the growth of these vectors can then be used to compute all the Lyapunov exponents. However, there are cases when a mathematical model of a system is not available, only experimental data. In those cases, particularly to estimate the chaoticity of a system, only L_{max} is required and can be estimated using the methods described in the following section.

3.3 Numerical Computation of Lyapunov Exponents

It has been shown in [58] that EEG in humans and animals are not random stochastic signals as they were thought of in the past. Rather, they can be described as electrical activity generated by a chaotic oscillator that is part of the brain's mechanism. Figure 2.4 is a graphical representation in three dimensions of an attractor generated from EEG data of an epileptic animal. This data is proof that the epileptic attractor is strange in nature. As such, the chaoticity of a strange attractor can be quantified by means of its Maximum Lyapunov Exponent (L_{max}). In the absence of a dynamical model (state equations), computing the Lyapunov exponent means relying on Taken's embedding theorem which allows a single observed variable to be expanded into a higher dimensional state-space. The Lyapunov exponent is then computed as a mean logarithmic deviation of the trajectories in the higher dimensional space over time. The following describes a few notable algorithm's that can achieve just that.

3.3.1 The Wolf Algorithm

The first step in computing the Lyapunov exponent is to create a delayed vector of observed values from a time series. [110] and [139] have shown that this delayed signal contains within them all the state variables of the system. This is due to the fact that delay coordinate embedding is a diffeomorphic transformation. That is to say the embedded trajectory has the same topology as the original trajectory in the phase-space of the system. In the case of EEG, this method can be used to reconstruct the multidimensional state space

of the brain's electrical activity from each EEG channel. For example, if $x(t)$ is a $n \times 1$ dimensional vector of duration T recorded from an EEG channel and sampled every T_s seconds, then $\bar{X}_i(t)$ is the $n \times p$ dimensional reconstructed signal such that

$$\bar{X}_i(t) = [x(t_i), x(t_i + \tau), \ldots, x(t_i + (p-1) * \tau)] \tag{3.2}$$

where, τ is the delay between successive components of $\bar{X}_i(t)$ and it rarely, if ever, is the same as T_s. If a phase space plot of the $n \times p$ dimensional vector $\bar{X}_i(t)$ were to be created, then it would look like that of a strange chaotic attractor, [58]. For reference, such an attractor is shown in Figure 2.4. The complexity of this attractor is measured by its dimension D and Iasemidis et al have shown that for a sinusoidal attractor, the value of $D = 1$ and for that of a chaotic attractor, such as those found in EEGs of epileptic patients, to be within $D = [2.5, 2.7]$.

A description of how D can be estimated from time series data via its state space correlation dimension ν is given by [3, 41]. The measure of chaoticity of these attractors can be defined via either their Kolmogorov Entropy [43] or their Lyapunov exponents [41]. As mentioned previously, an attractor is defined as chaotic if the largest of all its Lyapunov exponents (L_{max}) is positive.

The method for choosing p, the embedding dimension of the state space of the signal $x(t)$, was proposed in [139] to be $p \geq (2 * D + 1)$. Although the dimension of an attractor can be fractal, that of the embedded signal, p, cannot. It is worthwhile to mention that the brain is a nonstationary system and as such never reaches steady state; so its value for D is never constant. This is why the time window of $T = 10$ seconds is chosen so as to better satisfy the assumption of stationarity for the signal. While the embedding dimension , p, should be changed from epoch to epoch, the value of $p = 7$ is kept fixed for pre-ictal, post-ictal and interictal stages. The justification is that the existence of irrelevant information in dimensions higher than 7 might not influence the estimated dynamical measure by a great degree and also the reconstruction of the state space with high p suffers more from the short length of moving windows that are used to handle non-stationary data, [62].

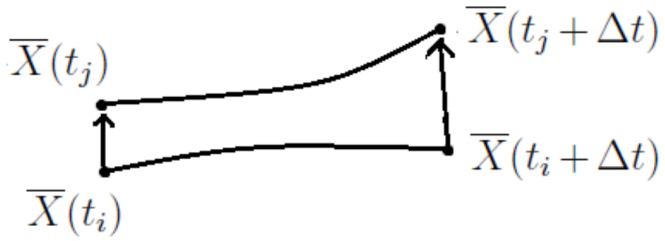

Figure 3.1: Diagram of a single evolution of the perturbed fiducial trajectory in Δt amount of time. The fiducial trajectory is the one associated with time t_i.

Originally, Wolf had proposed an algorithm to estimate L_{max} from stationary data [161], however, later, Iasemidis et al. modified this algorithm to compute what is known as the average short-term maximum Lyapuonv exponent (STL_{max}) for non-stationary EEG data on short time windows [61]. STL_{max} can be calculated as follows:

$$STL_{max} = \frac{1}{N_a \Delta t} \sum_{i=1}^{N_a} log_2 \frac{|\delta \bar{X}_{i,j}(\Delta t)|}{|\delta \bar{X}_{i,j}(0)|} \tag{3.3}$$

where, $\delta \bar{X}_{i,j}(0) = \bar{X}(t_i) - \bar{X}(t_j)$ is the displacement vector at time t_i, i.e. a perturbation of the fiducial orbit at t_i, and $\delta \bar{X}_{i,j}(\Delta t) = \bar{X}(t_i + \Delta t) - \bar{X}(t_j + \Delta t)$ is the evolution of this perturbation after time Δt. In other words, Δt is the the time over which $\delta \bar{X}_{i,j}(0)$ is allowed to evolve in the state space. When the evolution time, Δt, is given in seconds, STL_{max} has units in bits/sec. N_a is the number of local Lyapunov exponents that are estimated within a duration T of the data segment. This gives us the following relation between T, the length of a segment of data, and Δt, the evolve time:

$$T = (N-1)\Delta t \approx N_a \Delta t (p-1)\tau \tag{3.4}$$

Figure 3.1 is an attempt to diagrammatically show one evolution of the perturbation of the fiducial trajectory in a time Δt. Computations for STL_{max} are generally carried out by breaking up a data record into T second long windows for all channels.

3.3.2 The Rosenstein and Kantz Algorithms

The principal flaw in Wolf's algorithm was in the re-selection process wherein after every evolve time, Δt, a new candidate for the nearest neighbor to the fiducial trajectory is selected. This process lends itself to increased error in the presence of even the slightest amount of noise in the data and is also sensitive to attractor reconstruction parameters such as embedding delay and dimension [21]; rendering the Wolf method useless to any real data. In the '90s two other groups formulated new methods to estimate the Lyapunov exponent in order to circumvent this error [120] and [71].

In the Rosenstein method [120], Takens' embedding theorem is applied to reconstruct the state-space in higher dimensions. Then an initial fiducial trajectory is chosen along with its nearest neighbor trajectory. The average divergence between two points, one on the fiducial and another on its nearest neighbor trajectory, $L(t)$, at time t, is computed using the following equation,

$$L(t) = Ce^{L_{max}t} \tag{3.5}$$

where, C is a constant that normalizes the initial separation. In order to compute L_{max} numerically, the trajectories are allowed to evolve over the entire finite data set of time T. Then the log distance versus evolution time is plotted and the gradient of the initial part of the log distance curve is evaluated as the L_{max} for one trajectory pair. This is because we can take logarithms on both sides of Equation 3.5 to get

$$L_{max} = \frac{1}{t} ln \frac{L(t)}{C} \tag{3.6}$$

Similarly, for the rest of the data set, the process is repeated by moving forward, a number of samples at a time, in the phase-space and computing an estimate for L_{max} with the remaining data set. The average of all such L_{max} values is the final result from the Rosenstein algorithm. One has to be careful in how many times the operation is repeated since near the end not too many samples are left to see the divergence clearly.

The Kantz algorithm [71], also starts from computing the expanded phase-space

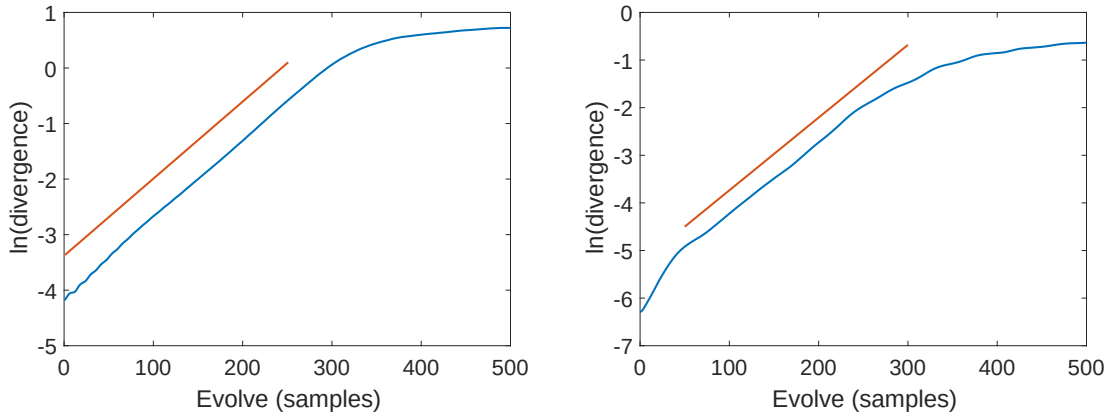

(a) (b)

Figure 3.2: Time vs log distance curves of the (a) Rosenstein and (b) Kantz algorithm applied to data from a Lorenz attractor sampled at 100Hz. The straight lines show the fit that is used and its gradient is the value for L_{max}. The value for L_{max} from (a) and (b) respectively are 1.3870 and 1.4877. 1.5 is the theoretical value; thus Kantz algorithm works better in this case.

trajectory. However, unlike the Rosenstein algorithm, instead of selecting a single nearest neighbor to track, the Kantz algorithm chooses a radius around the fiducial and computes the average of how all the trajectories within the radius separates from the fiducial. The log distance vs evolve time is plotted and like the Rosenstein algorithm, the gradient at the beginning of the plot is the value for L_{max}. This uses an exponentially greater number of trajectories and thus is more robust to perturbations in the signal. It must be noted that the first few points in the evolution is discarded since the maximal Lyapunov exponent at that time has not overtaken the other stable Lyapunov exponents. Also, the Kantz algorithm is not too sensitive to the embedding dimension and so a few of them can be used at the same time and the average of the L_{max} computed can be used as the final result. For a detailed explanation of the Kantz algorithm and its implementation in the TISEAN package, refer to [50]

Figure 3.2, shows how these two methods are employed in computing L_{max} for a Lorenz attractor. The data was sampled at 100 Hz. The log distance curve in both cases was allowed to evolve for 500 samples. The straight line has a gradient that is the estimate of

Table 3.1: Comparison of L_{max} values from the Kantz, Rosenstein and Wolf algorithms to the theoretical value.

Method	Value	Error %
Kantz	1.487	0.867
Rosenstein	1.387	7.53
Wolf	1.3318	11.21
Theoretical	1.50	N/A

L_{max}. The Kantz algorithm correctly estimates the value for L_{max} at 1.4877 followed by the Rosenstein L_{max} of 1.387. It must be noted that the Wolf algorithm can lead to greatly incorrect values as it did with an $L_{max} = 1.3318$ on the same data (see Table 3.1 for a comparison). Hence the Kantz algorithm, for its higher reliability in estimating L_{max}, is what we utilize in our work.

3.3.3 Parallel Computation of Lyapunov Exponents

Extensive offline investigations are required to optimize the input parameters for the Kantz algorithm and its output to suit our needs in seizure detection/prediction. Our choice of Kantz algorithm for computation of Lyapunov exponents of chaotic dynamical systems was presented earlier. The flowchart in Figure 3.3 shows the algorithm and it's parallel implementation using Matlab's *parfor*. These computations are naturally parallel and lend themselves easily to rapid prototyping for this application. In the implementation, Lyapunov exponents are calculated over windows of $T = 10$ seconds of data as mentioned in the previous subsection 3.3.1. Note, a single EEG recording can be as long as 178 hours (1 week) or more. These 10 second segments overlap with an offset of 2 seconds between two consecutive segments. The computations over 10 channels of EEG data (iteration counter i in Figure 3.3) are parallelized using *parfor*, a loop based parallelism mechanism provided in Matlab. But this limits the computation to just one node with multiple cores in a cluster. This, loop level coarse-grained parallelization over channels was used as the first step towards parallelization. It was found inadequate for the large number of offline computations needed for parameter optimizations. So, HPCmatlab (A cluster computing

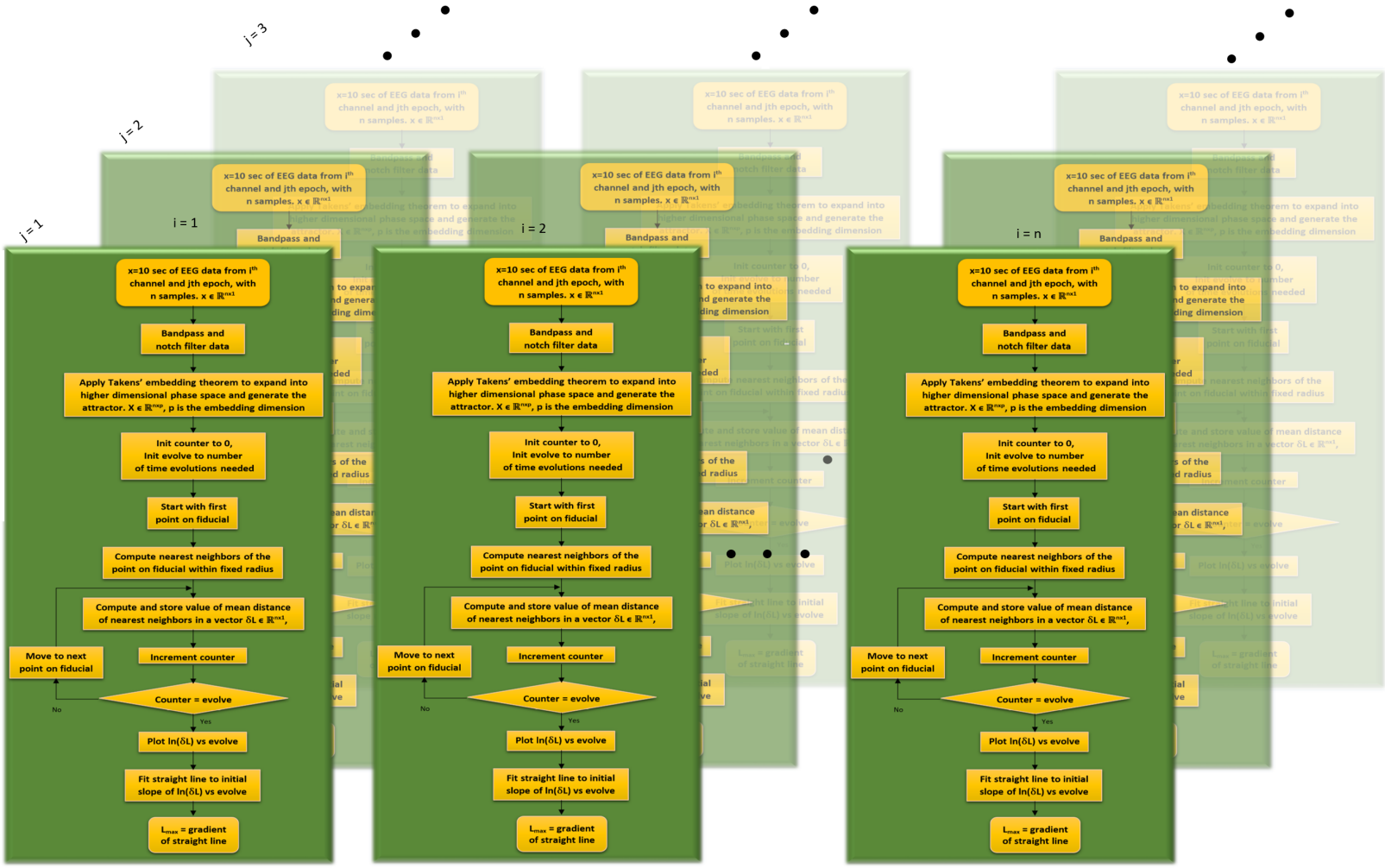

Figure 3.3: Flowchart showing the Kantz algorithm. The repetitions in i and j are to emphasize the process taking place in the parallel implementation, both in online and offline execution of the code. i is the iterate for the number of channels parallelized using *parfor* with n being the maximum number of channels. j is the iterate of epochs, parallelized using HPCmatlab with MPI. For offline computation, the value is limited by the amount of data stored on the disk. For the online case, however, it can go on as long as data is being collected.

tool developed at ASU, [44]) was used to divide the EEG data as work segments (j iterate) or epoch among Message Passing Interface (MPI) processes. Each MPI process calculates the Lyapunov exponent for its part of data segments (10 seconds) in the EEG data file and at the end, results from all processes are gathered in one single array on the root process. This has resulted in a hybrid programming model where data segments are distributed on different nodes via MPI and parfor is used within a node to parallelize the computation on 10 different channels.

In the case of real-time implementation, the i^{th} iterations are performed using MATLAB *parfor* the j^{th} iterates are basically advancements in time. So in essence L_{max} is computed for every 10 seconds of past data moving forward 2 seconds in realtime for all channels. The computer used to perform the real-time application is capable of acquiring data, filtering it and computing L_{max} for all channels within less than 0.6 seconds!

3.4 Entrainment and the T-index

The paired T-test is a well known statistical measure of relatedness. It is used to reject the null hypothesis that the means of two samples are the same.

$$H_0 : \bar{D} = \mu_1 - \mu_2 = 0 \tag{3.7}$$

$\bar{D}$ is the difference in the means of the samples. For a given pair of samples, the T-index can be computed as in Equation 3.8.

$$T_{ind} = \frac{\mu_1 - \mu_2}{\sqrt{\frac{\widehat{\sigma}_1^2}{n_1} + \frac{\widehat{\sigma}_2^2}{n_2}}} \tag{3.8}$$

where $\widehat{\sigma}_i$ and n_i are the standard deviations and number of samples of the respective data sets. For a specific case, as in this study, if the length and standard deviation of both pairs of samples are the same, the T-index can be computed as:

$$T_{ind_{ij}} = \frac{|\bar{D}_{ij}|}{\frac{\widehat{\sigma}_{ij}}{\sqrt{n}}} \tag{3.9}$$

The T-indices in this study were computed using Equation 3.9, at time t and a moving window of $T_{win} = [t, t - n * T]$ seconds across all possible pairs of Lyapunov exponents

that were computed on each electrode. It was seen previously that a window of 10 seconds help establish stationarity in the data and that is the length T used in computing Lyapunov exponents. If the true mean of the differences $\bar{D}_{ij}$ is equal to zero, and $\widehat{\sigma}_i$ are independent and normally distributed then T_{ij} is asymptotically distributed according to the t-distribution with (n-1) degrees of freedom. It was shown in [123] that these independence and normality conditions are satisfied. The null hypothesis in this case is that of desynchronization of sites i and j when $T_{ind_{ij}}$ is significantly different from zero at a predefined significance level α. The desyncrhonization condition between the electrode sites i and j, as detected by the paired t-test, is

$$T_{ij} > t_{\alpha/2,(n-1)} = T_{threshold} \tag{3.10}$$

where $T_{threshold}$, is the $100(1-\alpha/2)$ critical value of the t-distribution with (n-1) degrees of freedom. If $T_{ij} \leq T_{threshold}$ then the null hypothesis cannot be rejected, i.e. the sites may or may not be desynchronized. In this study $n = 60$ and $\alpha = 0.01$, which makes $T_{threshold} = 2.662$. So, whenever the value of the T-index is above 2.662, we can say with 99% confidence that the pair of electrodes are not entrained. This is a sufficient but not necessary condition. Iasemdidis et al. have shown that to make any claims about sites being entrained when the T-index falls below 2.662, there must be a progressive convergence over time of the T-index into a value less than the threshold [57]. In another study the same researchers use quadratic zero-one programming in order to select the best pair of sites (using T-index) and track their entrainment over time to correctly predict 90% of seizures [54]. Thus the time-profile of $T_{ind_{ij}}$, if chosen appropriately, may allow us to make a claim about synchronicity or entrainment of the two channels.

3.5 Conclusion

This chapter discussed the history and development of the Maximum Lyapunov Exponent and its formulation. The Lyapunov exponent, as was mentioned earlier, is a measure of chaoticity in a chaotic attractor. It was shown how among three methods of

computing L_{max} from sampled time series data, the Kantz algorithm stands out as the most robust. A measure of synchrony between two electrode sites was introduced through the use of the paired t-test. Results from the computation of L_{max} and their t-tests will be presented later. It will be seen that the time profile of L_{max} on all channels of EEG is quite distinct during a seizure and that certain other characteristics can help us generate a warning for an impending seizure. The progression to zero in the T-indices that Iasemidis et al. presented here will also be shown. The next chapter discusses a measure of connectivity known as the generalized partial directed coherence.

Chapter 4

GENERALIZED PARTIAL DIRECTED COHERENCE: A MEASURE OF CONNECTIVITY

4.1 Introduction

In 1969, when Clive Granger formulated his famous theory of causality [40], little did he know what a wide impact it will have on the understanding and usage of the idea of causal relationships in determining connectivity among systems. Its simple, really! Two signals can seem to be unrelated and independent by studying their present measurements; however, if knowledge of the past of one signal allows better prediction of the future behavior of the other, then it is said that the first signal Granger causes the second. Although Granger formulated this as an econometrics problem, it got wide acceptance in the engineering community in determining correlation and coherence between signals.

A formal definition of Granger causality as given in [164] starts with the assumption that a signal U Granger causes V. A model is constructed to express the relationship between the current output of V and its past information V^- and the past information of U^-. This function can be written as $V = f(V^-, U^-)$. From the values obtained in the sampled signal, the parameters in the model $f(V^-, U^-)$ have to be estimated and then the predictions of V based on V^- alone and on V^- and U^- are generated. In both cases, innovations in the predictions may be quantified by the variance of the prediction errors for two-dimensional modeling, $var(V|V^-)$ and $var(V|V^-, U^-)$. The Granger causality of U to V , $G_{U\to V}$, is then defined by

$$G_{U\to V} = ln\frac{var(V|V^-)}{var(V|V^-, U^-)} \tag{4.1}$$

A similar representation of Y Granger causing U can also be expressed by interchanging the variables in Equation 4.1. Knowledge of $G_{U\to V}$ and $G_{V\to U}$ means that a bi-directional causality between the signals can be measured separately. However, it relies on accurate

estimation of the model. Since many signals, especially electrophysiological ones, can be nonlinear and/or time-varying in nature, some researchers have attempted to create both linear and non-linear parametric models in their attempt to obtain a more reliable value for causality [164, 88, 48]. Another causality termed Gersch causality was proposed by Gersch in the '70s, however Albo et al. have shown that it fails to correctly identify the true source of a signal in a mix of three, if at least one of them has a high signal-to-noise ratio (SNR) irrespective of the actual connectivity pattern [4].

Since true connectivity in many electrophysiological signals, e.g. EEG, is unknown it is difficult to say with certainty whether one method of modeling is better than the other [17]. In most cases, simulated data are utilized in the beginning to fine tune the algorithm and then they are applied on actual sampled signals with a-priori knowledge of certain anatomy is employed to support neuronal connectivity paths. This is a fundamental problem when studying directional connectivity between brain areas. i.e, causality relationships between scalp EEG does not necessarily imply the same relationship is present between underlying neural sources. Thus [37] shows how the use of MVAR modeling and Independent Component Analysis (ICA) is able to determine the temporal activation of the neuronal sources as well as their approximate locations. In [18] Cheung et al. utilized a state-space based estimation of the multivariate autoregressive (MVAR) models for cortical connectivity assertions from EEG. Typically fitting an MVAR model to data also means that the noise or innovations from a parameter estimation problem be white, otherwise we may be left with biased models. The challenge is greater for nonlinear models, since in those cases the noise models must be nonlinear in nature too [47].

In the of case of EEG data, signals are acquired from a broad array of sensors distributed spatially over the human brain and a considerable amount of mixing of signals is involved. The human skull acts as a low-pass filter in both spatial and temporal domains, so in [135] Srinivasan et al. have shown that adequately sampling the human EEG would require a minimum of 128 sensors to respect a spatial Nyquist sampling theorem. Given such

large inter-connectivity patterns in the brain, it is necessary for us to develop fine tuned methods to estimate these connections as correctly as possible. Baccalá et al have done an extensive study using graph theoretical approach to describe the effective connectivity dynamics behind epileptic seizures in the brain. On the other hand, laying out a platform for identifying what is "coupling" versus what is "causal" (in a Granger sense) is also crucial; the effectiveness of coherence and partial coherence and also directed coherence and partial directed coherence computed from MVAR processes as metrics for coupling and causality respectively is evaluated in [29].

Although a rudimentary method of computing Granger causality was produced earlier, a more robust method would be welcome; one that deals not with stochasticity of signals, rather their inherent underlying dynamical properties. The potential benefit of having a model based measure fine tuned for a specific task such as quantifying coupling or coherence can be enormous in conclusively estimating the source of activity within the brain. One of the early lines of work to use the idea of Granger Causality in EEG was one by Saito et al. [126]. Their method known as the Directed Coherence (DC), was a unique decompositon of the ordinary coherence function into two directed coherences. The limitation being that the algorithm would break down as the number of channels increased beyond only 2. In their work, Kaminski and Blinowska [70], also attempted to formulate another measure for connectedness known as the Directed Transfer function (DTF). Although a good measure with the capacity to involve more channels, the DTF would rank interaction among brain sites, i.e. EEG channels, with respect to total inflow only of information from all channels into one.

In [8], Baccalá et al. tested the use of DC and Granger Causality on EEG data and consequently formulated the Partial Directed Coherence (PDC) [9]; this, unlike the DTF, would offer strength of connectivity as a matrix of information flow from every channel to the other. In [138] it was shown that a PDC of zero indicates an absence of a direct connection between time series. In [39] Gotman and Letvova proposes the use of coherence

and phase spectrum linearity to show that the amygdala is more likely to lead when seizures have regional onset while on the other hand the hippocampus is more likely to lead in focal-mesial seizures. Mean phase coherence as another measure for connectivity, as elicited in [97], shows that there is a preictal drop in synchronization; much like the results of Iasemidis et al using Lyapunov exponents [60].

Astolfi et al. used PDC and its squared value to show that using a SNR of at least 3 in the signals, both measures were able to correctly identify connectivity patterns, [7]. The use of Dual extended Kalman Filter (DEKF) to estimate time varying MVAR parameters was introduced in [106] to compute time varying PDC and show that seizures are detectable in neonatal epileptic patients. However, Schelter and colleagues have shown that PDC suffers from interpretability due to its normalization of all coherence measures to the $[0, 1]$ interval and thus proposed the use of a renormalized PDC measure [128]. Following their previous work, realizing that PDC suffered from correlated noise structures (mean and variance) in the innovations processes involved, Baccalá et al. formulated the concept of Generalized Partial Directed Coherence (GPDC) [10]. In their work, Yasumusa et al. [138] tested the performance of this GPDC algorithm on EEG data and helped to show how the focus could be located through its use. In more recent years GPDC has been used for the purpose of focus localization using EEG data correctly in 2 out of 3 patients [154]. The same researches later showed how magnetoencephalography (MEG) data can be analysed with GPDC to localize seizure focus with or without the presence of interictal spikes [76]. Other more direct forms of coupling have been investigated more recently. As an example among many, in [141] the authors used GPDC in order to assess information flow between medial prefrontal cortex (mPFC) and hippocampus of the rat brain, under isoflurane anesthesia and kainic acid-induced enhanced neuronal activity.

The use of GPDC in all these studies implies that it can be a very useful tool for estimating a measure for connectivity in determining the focus in epileptic patients. The GPDC algorithm is described in detail in the following section. Before proceeding to the

algorithm it must be mentioned that computing the GPDC takes a fair amount of processor time. A short section of data is first modeled using MVAR process, then the GPDC is evaluated at discretized frequencies of interest. Typically this frequency vector can have 100s of points. Although all computations are linear, evaluating GPDC for human data where the number of channels can be anywhere between 16 and 256 and the data are sampled upwards of 1KHz to 30KHz for days and even weeks in some cases, these computations can take in the order of days to complete. This calls for a parallelizable solution to the GPDC algorithm on EEG data. In our work we have utilized tools such as the supercomputing cluster available at ASU and the Gordon cluster at San Diego Supercomputer Center through the NSF XSEDE program. Another parallelizable approach through the use of GPUs for computing GPDC was presented in our work in [35, 36]; this solution implies that GPDC can be computed real-time without the need for complicated supercomputing structures. The next section describes the formulation of the GPDC algorithm.

4.2 Computing the GPDC

In computing the GPDC, the first step is to assume a set of simultaneously sampled time series with N channels and that they can be modeled using the following MVAR equation :

$$\begin{bmatrix} x_1(n) \\ \vdots \\ x_N(n) \end{bmatrix} = \sum_{k=1}^{p} A_k \begin{bmatrix} x_1(n-k) \\ \vdots \\ x_N(n-k) \end{bmatrix} + \begin{bmatrix} w_1(n) \\ \vdots \\ w_N(n) \end{bmatrix}$$

$$\Rightarrow \boldsymbol{X}(n) = \sum_{k=1}^{p} A_k \boldsymbol{X}(n-k) + \boldsymbol{W}(n) \tag{4.2}$$

where, p is the MVAR model order (lag), $\boldsymbol{X}(n)$ is the time series with N channels, $x_i(n)$ is the time series in the i^{th} channel, and $\boldsymbol{W}(n)$ is the vector innovations process having zero mean and covariance $\boldsymbol{\Sigma}_w$. Zero mean for the innovations process is necessary to have unbiased parameters from modeling. From Equation 4.2, it follows that the discrete time

transfer function of the MVAR process model can be written as

$$\boldsymbol{H} = \bar{A}^{-1}(f) = \left[I - \sum_{k=1}^{p} A_k z^{-k} \right]^{-1} \Bigg|_{z=e^{-2\pi j(f/f_s)}} \tag{4.3}$$

where,f is the range of frequencies of interest and f_s is the sampling rate. $\bar{A}(f)$ is a matrix of frequency dependent system coefficients with elements as shown below

$$\bar{A}_{ij}(f) = \begin{bmatrix} a_{11}(f) & a_{12}(f) & \cdots & a_{1N}(f) \\ a_{21}(f) & \ddots & \vdots & \vdots \\ \vdots & \cdots & a_{ij}(f) & \vdots \\ a_{N1}(f) & \cdots & \cdots & a_{NN}(f) \end{bmatrix} \tag{4.4}$$

Here, i and j are indices of the rows and columns respectively. The GPDC from channel j to i, computed at each frequency is then found by

$$\pi_{ij}(f) = \frac{\frac{1}{\sigma_i}\bar{A}_{ij}(f)}{\sqrt{\sum_{k=1}^{N} \frac{1}{\sigma_k^2}\bar{A}_{kj}(f)\bar{A}_{kj}^*(f)}} \tag{4.5}$$

Using Equation (4.3), we have

$$\bar{A}_{ij}(f) = \begin{cases} 1 - \sum_{k=1}^{p} a_{ij}(k)e^{-2\pi jFk} & \text{, if i = j} \\ -\sum_{k=1}^{p} a_{ij}(k)e^{-2\pi jFk} & \text{, otherwise} \end{cases} \tag{4.6}$$

where $F = \frac{f}{f_s}$ is the frequency at each point normalized to the sampling rate. In computing the GPDC as in Equation (4.5), the denominator normalizes the GPDC coefficients (Equations (4.7), (4.8)). The normalization is such that the following two conditions always hold

$$|\pi_{ij}(f)|^2 \leq 1 \tag{4.7}$$

and

$$\sum_{i=1}^{N} |\pi_{ij}(f)|^2 = 1 \tag{4.8}$$

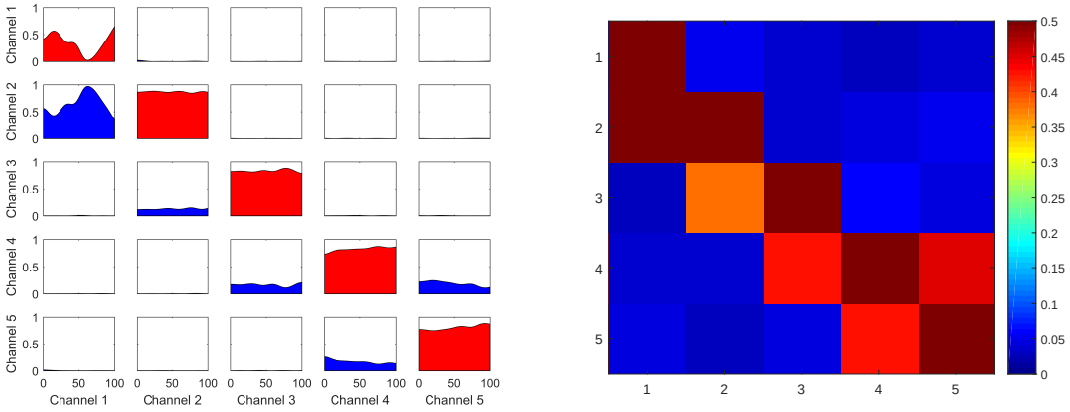

(a) (b)

Figure 4.1: (a) GPDC computed from simulated data generated using Equations 4.9 - 4.13. (b) Average GPDC computed by taking mean of all frequencies in each channel to channel interaction. This provides a simplistic view of the strength of interaction between channels.

This implies that the squares of each individual GPDC term evaluated at each frequency cannot be greater than 1 (Equation (4.7)) and also that the sum of the squares of the GPDC must equal 1 at all frequencies (Equation (4.8)) .

4.2.1 A Case Study Using Simulated Data

Here we present results from the implementation of the GPDC algorithm on simulated data. The data was generated using the following set of equations found in [9]

$$x_1(n) = 0.95\sqrt{2}x_1(n-1) - 0.9025x_1(n-2) + w_1(n) \tag{4.9}$$

$$x_2(n) = -0.5x_1(n-1) + w_2(n) \tag{4.10}$$

$$x_3(n) = 0.4x_2(n-2) + w_3(n) \tag{4.11}$$

$$x_4(n) = -0.5x_3(n-1) + 0.25\sqrt{2}x_4(n-1) + 0.25\sqrt{2}x_5(n-1) + w_4(n) \tag{4.12}$$

$$x_5(n) = -0.25\sqrt{2}x_4(n-1) + 0.25\sqrt{2}x_5(n-1) + w_5(n) \tag{4.13}$$

where, x_i corresponds to the signal in the i^{th} channel and w_i is the noise in the corresponding channel. Figure 4.1(a) shows the GPDC computed on data generated from this set of signals. The strength of interaction in the parameters of the delayed signals in the

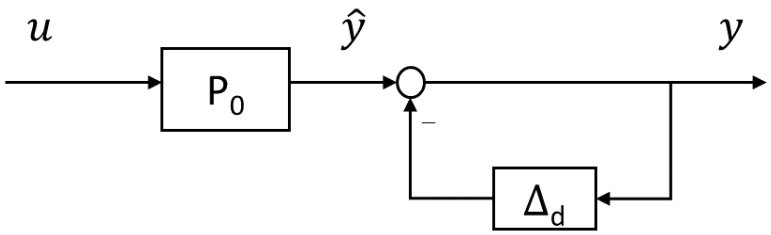

Figure 4.2: Uncertainty entry point in a model expressed in a divisive form.

equations are clearly reflected in the GPDC versus frequency plot. Figure 4.1(b) essentially produces a single value for each channel j to channel i interaction by taking an average over all frequencies. While the average was chosen as a metric to simply the results for this case, a better one would be to compute the L_2 norm for each channel to channel interaction since that would provide us a better estimate of the "energy" in the interaction.

4.3 Choice of GPDC Parameters

As was shown in section 4.2, the computation for GPDC begins with estimating a Multivariate Auto-Regressive (MVAR) Model of the data. MVAR modeling requires the choice of two crucial parameters. The first one is the model order, p, which is essentially the amount of delays considered in generating the MVAR model. Too low a value of p will underestimate the model, since not enough data points are being considered; too high a value has the problem of over fitting the data i.e. fitting noise. The second factor is the length of data (number of samples) that is used to create a model. If a system is stationary and linear, the length of the data is a non issue. As long as the signal is longer than the lowest frequency it contains, we can model the process appropriately. However, for non-stationary data the length must be small enough so that it seems stationary but not so large that the modeling error increases greatly. In this work, a method for determining a "good choice" of the length of the segment of data (in seconds), denoted hereon as T, and the MVAR model order, p, is shown.

Details of the different types of uncertainties that can appear in system models are

discussed in [166] . Following along those lines, we start by assuming a divisive uncertainty model as is shown in Figure 4.2. u is the input to the system , P_0, and $\hat{y}$ is its true (estimated) output. y is the output mixed with the uncertainty (noise). Thus the error of the system can be represented as $e = y - \hat{y}$. From Figure 4.2 we can write down a representation for P, the system with uncertainty as

$$P = P_0 \left(\frac{1}{1 - \Delta_d} \right) \tag{4.14}$$

and, using power spectrum notations

$$\Phi_y(j\omega) = P(j\omega)\Phi_u(j\omega) \tag{4.15}$$

$$\Phi_{\hat{y}}(j\omega) = P_0(j\omega)\Phi_u(j\omega) \tag{4.16}$$

where, $\Phi_y(j\omega)$, $\Phi_{\hat{y}}(j\omega)$, $\Phi_u(j\omega)$ are the power spectrum of the signals y, $\hat{y}$ and u respectively. From Equation (4.14) it follows that $\Delta_d(j\omega)$ can be written as

$$\Delta_d(j\omega) = \frac{P(j\omega) - P_0(j\omega)}{P(j\omega)} \tag{4.17}$$

$$\Delta_d(j\omega) = \frac{P(j\omega)\Phi_u(j\omega) - P_0(j\omega)\Phi_u(j\omega)}{P(j\omega)\Phi_u(j\omega)} \tag{4.18}$$

$$\Delta_d(j\omega) = \frac{\Phi_y(j\omega) - \Phi_{\hat{y}}(j\omega)}{\Phi_y(j\omega)} \tag{4.19}$$

$$\Delta_d(j\omega) = \frac{\Phi_e(j\omega)}{\Phi_y(j\omega)} \tag{4.20}$$

Thus, from a set of sampled signals the norm of the error system can be computed and a measure of modeling error may be estimated. It makes sense to consider the L_2 norm since it appears naturally in the signal spaces. In order to do this in practice, 5 hour windows of EEG data were collected from a rat. No stimulation was provided during this time. The 5 hour segments were then divided into T second long pieces. MVAR modeling is then performed on each T second long data by varying T between 5 and 50 seconds with increments of 5 seconds; in other words $T = [5 : 5 : 50]$ and simultaneously varying model order between 1 and 50 with unit increments for each value of p (i.e. $p = [1 : 1 : 50]$). The models obtained for each pair of values (T, p) were then tested on the data by computing

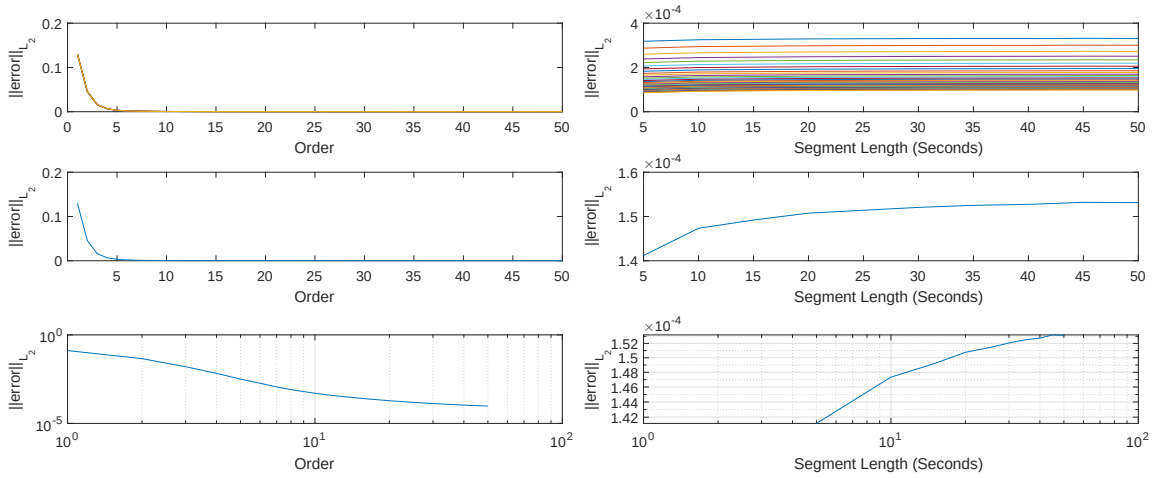

(a) (b)

Figure 4.3: MVAR modeling error from 5 hours of data collected from Rat 10 (non-epileptic) with respect to (a) changing order, p, and (b) segment length, T.

the residual error, e, between the actual data and the estimated data. The final step is to compute the L_2 norm of the error system. This was done by applying the following formula:

$$\|\Delta_d(j\omega)\|_{L_2} = \left\| \frac{FFT[e(t)]}{FFT[y(t)]} \right\|_{L_2} \tag{4.21}$$

where, $y(t)$ and $e(t)$ are the output and error signals respectively, FFT denotes the Fast Fourier transform operation. Using Equation 4.21 the L_2 norm of the error system for each pair of values of T and p are computed for each channel and all the $3600 \times 5/T$ segments of data. The average of the norms among each channel is computed and then averaged over all the segments of data giving us a single real value for each pair of (T, p). Finally we have a matrix of values for every combination of (T, p) which is used to produce plots as shown in Figures 4.3, 4.4, 4.5.

Figure 4.3 uses data from a healthy (non-epileptic) rat while Figures 4.4 and 4.5 is from epileptic animals. The reason for showing these three different cases is to emphasize on our properly chosen model order p, which we will justify shortly. The first subplot in Figures 4.3, 4.4, 4.5 (a) shows the L_2 norm of error vs. model order over all segment lengths. The

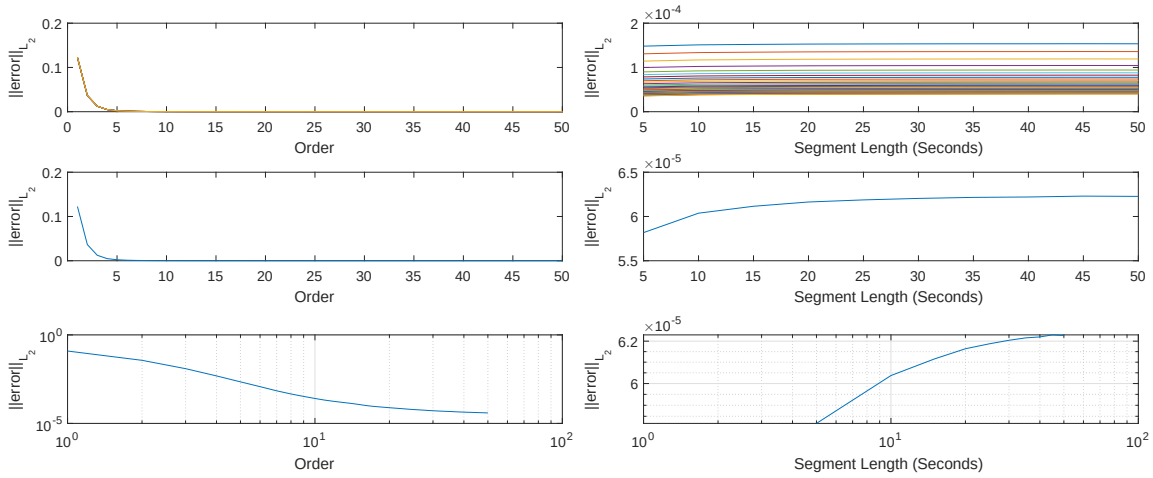

(a) (b)

Figure 4.4: MVAR modeling error from 5 hours of data collected from Rat 14 (epileptic) with respect to (a) changing order, p, and (b) segment length, T.

plots for the 10 cases of T in each case are indistinguishable in the plots owing to the fact that they are very close to each other. The second subplot is for error vs order by taking average of all segment lengths. Finally, the last subplot is the same as the second one but with logarithmic scale. The first subplot in Figures 4.3, 4.4, 4.5 (b) shows the L_2 norm of error vs. segment lengths over orders 12 through 50; it made little sense to consider orders smaller than that since under-fitting would cause too much error and bias in our interpretation of the results. The second subplot is for error vs segment lengths by taking average of the chosen model orders between 12 and 50. Once again, the last subplot is the same as the second one but with logarithmic scale.

Careful consideration of the second and third subplot in Figures 4.3, 4.4, 4.5 (a) shows that the error does not significantly decrease after model order is increased beyond 20. Therefore in this study $p = 20$ was chosen for all GPDC computations. Likewise, a scrutiny of Figures 4.3, 4.4, 4.5 (b) shows that the error norm increases with increasing length of the segments. This is justifiable because, even for the maximum MVAR order of 50, a segment length of 50 seconds when the data is sampled at 512 Hz may have too many samples and cause under-fitting. So choosing a very high value for T is unadvisable. On the other hand,

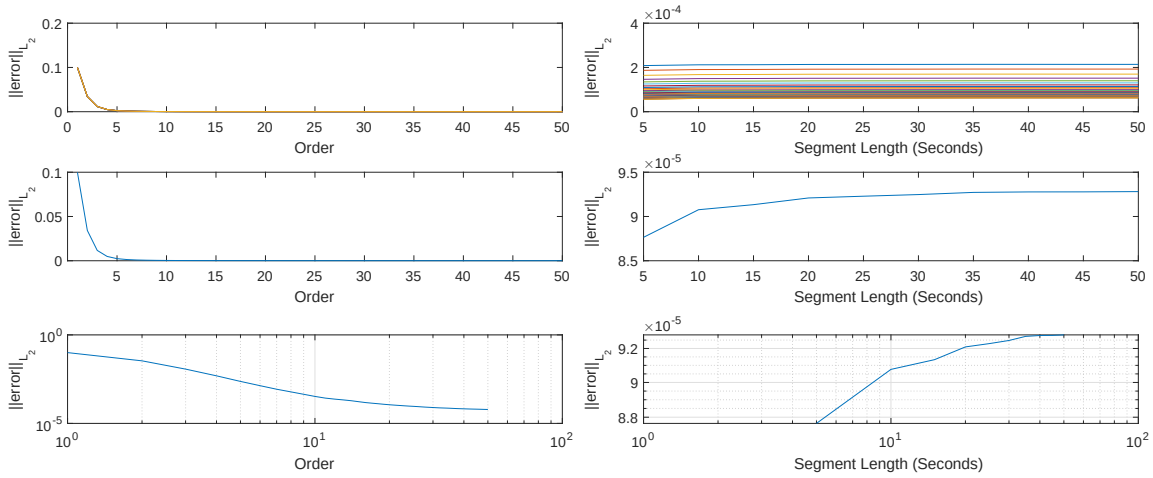

(a) (b)

Figure 4.5: MVAR modeling error from 5 hours of data collected from Rat 13 (epileptic) with respect to (a) changing order, p, and (b) segment length, T.

choosing too small a value for T will cause over-fitting and that should be avoided too. Thus, as a compromise the segment length is chosen as $T = 10$ seconds which still provides a relatively low error; this is also in lieu of the value used in computing the Lyapunov exponent where $T = 10$ seconds helped uphold stationarity properties. Therefore from here on, all computations of MVAR models are done with this value of segment length.

4.4 Conclusion

The algorithm for computing the Generalized Partial Directed Coherence was described in this chapter. One remark that must be mentioned about the scaling term in the denominator of Equation 4.5 is that it provides a ranking of outflow of information/energy with respect to total outflow of information from x_j to all other channels x_i. This is in stark contrast to the DTF method in [70], where interaction of the channels is ranked with respect to total inflow of information to each individual channel. For detection of the focus sites in an epileptic brain, where the focus is assumed to drive other parts of the brain into a seizure, it is worthwhile to be able to look at both outflow of information as well as inflow. The GPDC as a metric for causality allows us to achieve just that. For any

interested reader, an excellent review paper has been presented by Baccalá et al on the topic of directed coherence and Granger causality in [8].

Chapter 5

EXPERIMENTAL SETUP

5.1 Introduction

In this chapter we look at the experimental techniques and setup used during the course of this study. A number of different components came together in the proper setup of a test-bed for studying epilepsy. The animals, and how they were made epileptic is discussed first. Next, we describe in detail the electronics involved in collecting data and performing stimulations in multiple sites of the brain followed by a description of the actual stimulation waveforms utilized in the study. The software environment (GUI) that helps control all these functions are briefly touched upon as well. All in all, by the end of the chapter the reader would be left with a thorough understanding of the entire procedure of carrying out such experiments.

5.2 Preparation of Animals

The animals used in this study were male Spraque Dawley rats [45], weighing between 200 - 225 grams, from Harlan Laboratories. All animal experimentation used in the study were performed in the Laboratory For Translational Epilepsy Research at Barrow Neurological Institute (BNI) upon approval by the Institutional Animal Care and Use Committee (IACUC). The protocol for inducing chronic epilepsy was described previously in [156]. This procedure generates generalized convulsive status epilepticus (SE) [24] . Although electrical stimulation can be used to produce SE in animals [91, 104], it has been shown that it is not the most effective method. Thus, status epilepticus was induced by intraperitoneal (IP) injection of lithium chloride (3 mmol/kg) followed by subcutaneous (SC) injection of pilocarpine (30 mg/kg) 20-24 hours later. Following the injection of Pilocarpine, the EEG of each rat were monitored visually for clinical signs of SE noted

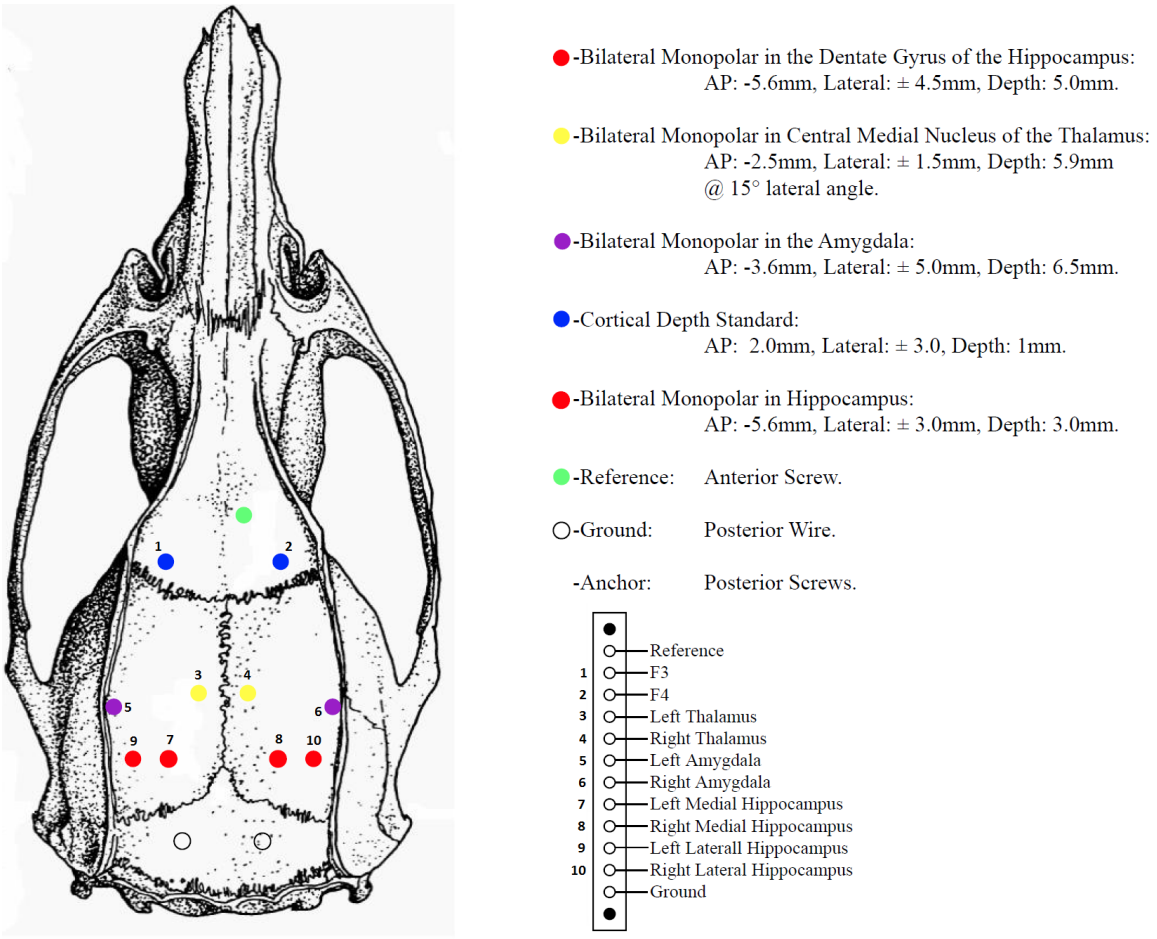

Figure 5.1: Diagram of surgical placement of electrodes in the rat's brain (top view).

behaviorally by the presence of a Racine level 5 seizure (rearing with loss of balance [119]). At EEG Stage V (approximately 4 hours after pilocarpine injection) SE was stopped using a standard cocktail of Diazepam 10 mg/kg, and Phenobarbital 25 mg/kg, both IP. The rats were then kept under visual observation for 72 hrs within which all measures were taken to stop them from deceasing. In the event that none of the methods to keep them alive worked, the animals were euthanized.

After SE was successfully induced in the animals, they were allowed five weeks for the seizure frequency to stabilize. Following this five week period, the animals were taken into surgery and an electrode array, as shown in Figure 5.1, were implanted into their brain. Not including the reference and ground connections, each rat had 10 electrodes implanted. From

this point onward, the electrode names are abbreviated from what is shown in the Figure to F3, F4, LT, RT, LA, RA, LM, RM, LL, RL, corresponding to channels 1 through 10 as recorded in the EEG. After surgery, each animal was allowed a week before being connected to an EEG machine. The referential voltages from each of the 10 electrodes mentioned was then recorded using an EEG machine, an Intan RHD2000 development board or Xltek Neurolink IP 128 depending on the circumstance.

5.3 Electronic Components and Hardware

Here we describe the different components that form the recording and stimulation setup used in the experiment. A wholistic view is developed near the end.

5.3.1 EEG Recording Unit

For the purpose of recording EEG, although in the latter stages of the study we used an Intan RHD2000 Development board (Figure 5.2 [65]), initially an Xltek Neurolink IP 128 machine from Natus Medical Inc. was being used [102]. The disadvantage to using the Xltek system was that we could not collect data in real-time in order to perform closed-loop control experiments. Apart from providing real-time access to data, the Intan device is also capable of sampling at very high speeds, approximately 32KS/s per channel. It also has a number of hardware and software filters that can be programmed to modify the cutoff frequencies. Along with all these capabilities, the Intan system is equipped with an impedance measurement unit that we utilized in order to estimate impedances of the electrode sites. These measurements were later used to calculate "safe" stimulation parameters for the study.

The Intan EEG system is controlled from a desktop computer using MATLAB and an API provided by Intan Technologies. All the hardware and DSP filter configurations on the board can be setup using this API, including sampling rates. The board has a large enough buffer ($\approx$130 MB) for the ADC to sample the data and store in real-time. The buffer serves up the data to the MATLAB program when it is polled. The software setup is described in

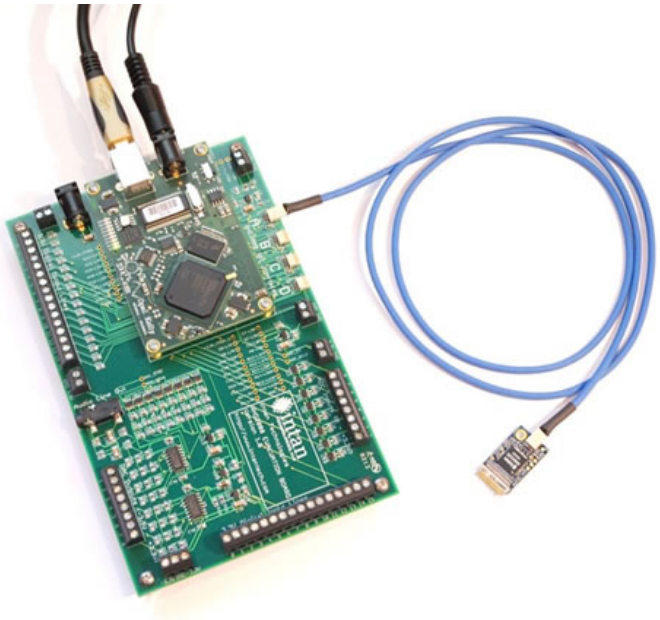

Figure 5.2: Intan RHD2000 Development board connected to an RHD2216 16 channel amplifier and digitizer. Image reproduced from [65] with permission.

a later section (subsection 5.3.4).

5.3.2 Electrical Stimulation

Deep Brain Stimulation (DBS) protocols in several animal models of epilepsy have shown some effectiveness in controlling epileptic seizures with high frequency stimulation targeting the subthalamic nucleus, anterior thalamic nucleus, caudal superior colliculus, substantia nigra, and hippocampus [153, 79, 165, 107]. Some researchers have shown the effectiveness of DBS using neural oscillator models as well [122, 95]. All these investigators used stimulation parameters in - frequency ranging from 50-230 Hz and bipolar constant current pulses between 30-1000 μsec at current intensities from 0.1 to 2 mA. In contrast, low frequency (between 1 Hz and 30 Hz) stimulation resulted in an increase of seizure susceptibility or synchronization of EEG.

In this study, the stimulation is applied between pairs of electrodes (amygdalar, hippocampal, thalamic, frontal) according to the results from certain analysis; i.e. whenever a seizure warning is issued by our seizure warning algorithm or in the case of the offline

Figure 5.3: Front view of the digital stimulus isolator from A-M Systems. The current and voltage levels must be manually selected using the corresponding knobs.

stimulation - in an open-loop manner for a fixed duration on various pairs of electrodes. A stimulation switching circuitry was developed in-house for the purpose of stimulating any pair of sites at will (described in subsection 5.3.3). Deep Brain Stimulation (DBS) of the animal was achieved by means of a Digitial Stimulus Isolator from A-M systems [1]. This stimulator (Figure 5.3) has a control port which requires a 3 digit binary code. This code can generate an output of:

- A DC offset,
- A positive DC level from offset, and
- A negative DC level from offset.

In our case, the DC offset was chosen to be 0 V, the high and low levels were 0.1 V respectively so as to create a bi-phasic rectangular pulse wave. The frequency of this wave can be chosen by carefully timing the three binary codes that are sent to the stimulator. For this purpose an Arduino Mega 2560 microcomputer was used. The microcomputer receives stimulation parameters from a code implemented in MATLAB 2014b running on a Windows-10 desktop computer. The Arduino then implements the timing for the switching between the three levels to create the shape of the stimulation used in this study as shown in Figure 5.4.

5.3.2.1 The Stimulation Parameters

A description of the stimulus parameters needed to obtain the waveform in Figure 5.4 and what types of stimulation was used during this study follows. It must be noted that this stimulation method was used in open-loop stimulations only.

- +ve Pulse Duration: this is how long the pulse stays high. In this study we used 150 μSec.
- -ve Pulse Duration: this is how long the pulse stays low. In this study we used 150 μSec.
- Time Period: a gap of zero DC voltage is applied after each positive and negative pulse to keep the total charge applied to the brain tissue within tolerable limits. The time period in this study was 4 msec leading to a frequency of 250 Hz.
- Packet On Time is the duration these short pulses were applied in one burst. 30 seconds was used in this study.
- Packet Off Time was applied to provide a break in stimulation and was chosen as 90 seconds in this case.
- Stimulation Duration was the time for which the entire packet train was applied. This was 20 minutes. There was a gap of 40 minutes between each Stimulation Duration.

For the epileptic rats involved in this study, EEG recording was started as soon as it recovered from surgery. Typically a few weeks of data were collected prior to the start of stimulation. This was to establish baseline data for the rat. For animals that went through open-loop stimulation only, the regime involved applying 5 hours of stimulation to each electrode pair, amounting to a total of 45 electrode pairs for all the 10 electrodes. A 3 hour break of stimulation was provided before switching between the pairs. It must be pointed out that within the 5 hours of stimulation time the parameters provided in Figure 5.4 was applied. The stimulation pairs were chosen randomly so as to be consistent with

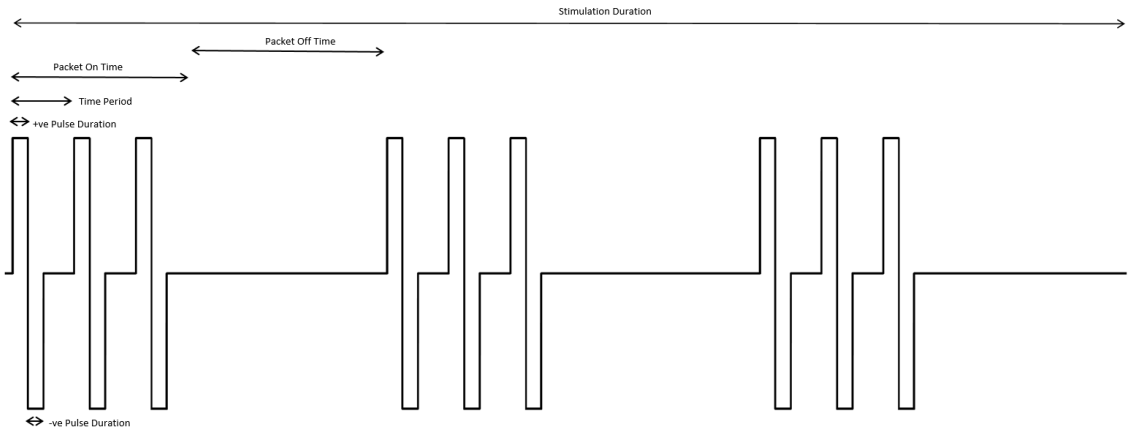

Figure 5.4: Shape of one type of open-loop stimulation applied to a pair of electrodes implanted in the rat's brain.

the principles of appropriately designed engineering experiments; namely - Randomization, Replication and Blocking [96]. The switching of electrode pairs between collecting EEG and allowing stimulation to pass through without damaging the EEG machine was achieved by implementing a switching circuit comprised of multiple gates and is described in more detail later (subsection 5.3.3).

In the more recent experiments, a different type of stimulation was provided. We found that the long durations of "packet Off time" was not providing enough control input to affect the brain state the way we wanted it to. In order to remedy this, we switched to a stimulation method whereby the stimulation frequency was set to 500 Hz and the positive and negative pulse durations were set to 300 μsec. There was no Packet Off Time altogether. This pulse width modulation like technique allowed for more stimulation energy to be applied. The only other parameter that was changed in that case was the "stimulation duration". The electrical stimulation we used in our closed-loop experiments had a current rating ranging from 100-750 μA and "stimulation duration" of 10 - 20 minutes. Considering possible induced tissue damage by electrical stimulus, the maximum current intensity of 750 μA falls under the safe allowable charge density limit of 30 μC/cm^2 as reported by [77] for deep brain stimulation; given the size of the stimulating electrode and pulse parameters chosen. While these specific values of the stimulation parameters are being utilized in our

work, their optimization can become a project on its own right and is not considered at this point.

The function for calculating the parameters for stimulation is as follows

$$\text{Charge density} = \frac{\text{Voltage applied} \times \text{Pulse Width}}{\text{Impedance} \times \text{Electrode Surface Area}} \tag{5.1}$$

In our experiments, the voltage applied on the electrodes was always fixed to 0.1 V. Pulse width varied between 150 - 300 μSec. The surface area of the electrode was calculated using $Area = \pi r^2 + 2\pi rh$, where the radius, r, of the electrodes is 87.5 μm and have a cylindrical non insulated surface of height, h, 500 μm. Thus, giving us a total of 0.003 cm^2 of exposed surface area for the electrodes. From impedance measurements collected through the Intan system, the average impedance for each electrode was approximately 500 KΩ in magnitude (ignoring phase). The result of the charge density suggests that our choice of stimulus parameters kept the charge density orders of magnitude below the recommended value of 30 μC/cm^2.

5.3.3 Switching Circuit

Since one of the primary goals of this study was not only to apply stimulation but also to determine what modality of stimulation locations would be most beneficial in seizure suppression, we needed to implement a method of being able to stimulate in different areas

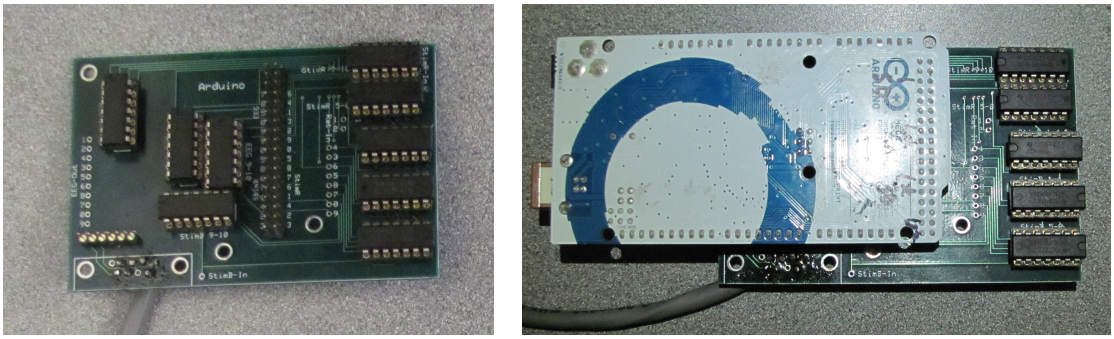

(a) Switching circuit (b) Switching circuit with the Arduino attached on top

Figure 5.5: Actual switching circuit being used in the study. The ICs contain 4 high speed solid state relays.

of the brain at will. The stimulator provided by A-M systems could only stimulate in a pair of sites, however, given the 10 electrodes we were using in our study, we needed to stimulate a possible 45 pairs! Thus we designed and implemented a switching circuit to be able to propagate the stimulation signal to any chosen pair of brain sites at a given instance. The actual switching circuit that was built on a PCB board is shown in Figure 5.5. This controller can choose which pair of sites to stimulate when commanded from an Arduino Mega and appropriately disengage the EEG channels during stimulation so they are not damaged by the much larger stimulation voltages and currents.

5.3.4 Software Environment

The main data acquisition and analysis is performed on a desktop computer equipped with an Intel® Core I-7® 4790 processor running at 3.60 GHz clock speed with 4 cores

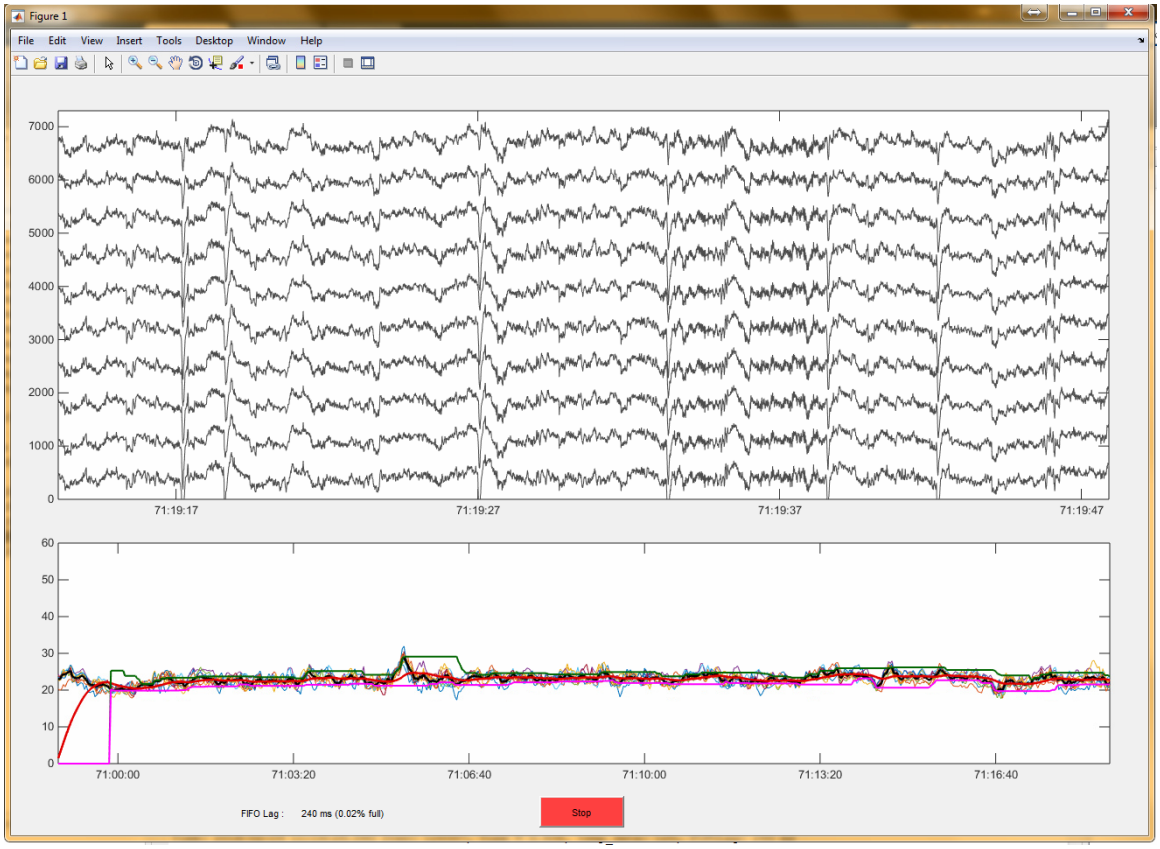

Figure 5.6: Software GUI used for recording EEG data and displaying the computed L_{max} values as well as performing closed-loop control experiments.

and 16GB of DDR3 SDRAM. This system utilizes a MATLAB 2014b installation that in conjunction with the Intan API and MATLAB built-in Serial communication protocol controls the Arduino Mega and performs data acquisition from the Intan EEG system. Once the data are in, the MATLAB program performs analysis on the data and based on the algorithm implemented (open-loop or closed-loop) sends out stimulation "start" and "stop" commands to the Arduino Mega. Figure 5.6 shows a screenshot of the GUI developed. This GUI allows the user to visualize the EEG in the top panel and the computed Lyapunov time profiles in the bottom panel.

For any offline computation performed on our data, we utilized a Dell Precision T3500 computer equipped with a Six Core Intel® Xeon® Processor W3690 series, 3.46GHz clock speed, 12M L3 cache, 6.4GT/s and 24GB, 1333MHz FSB, DDR3 SDRAM. Alongside that, at times when the volume of data exceeded the capacity of a single computer, ASU super-computing resources as well as those in the NSF funded XSEDE systems were utilized. The super-computing resources were availed mostly during parameter tuning of certain algorithms when multiple parameters sets were varied and the analysis performed on the same data sets. These calculations tend to take tens of hours, even with the help of massively parallelized code running on computing clusters.

5.4 The Big Picture

As mentioned previously, the Intan RHD2000 development board and its 16 channel amplifier was setup as the EEG acquisition machine. The rats used in our study have 10 EEG channels, a ground and a reference channel. We collect EEG data from 10 electrodes located in different parts of the rat brain (see Figure 5.1). The EEG channels go through a switch board into the Intan EEG data acquisition system. The Intan board has an amplifier that conditions the signals so that its 16bit ADC has sufficient resolution in the EEG waveforms which are typically in the 100s of μV range. Once digitized, the data is collected in a FPGA buffer until a MATLAB program polls it from the buffer over USB. The MATLAB code operates every two seconds and it brings in two seconds worth of data

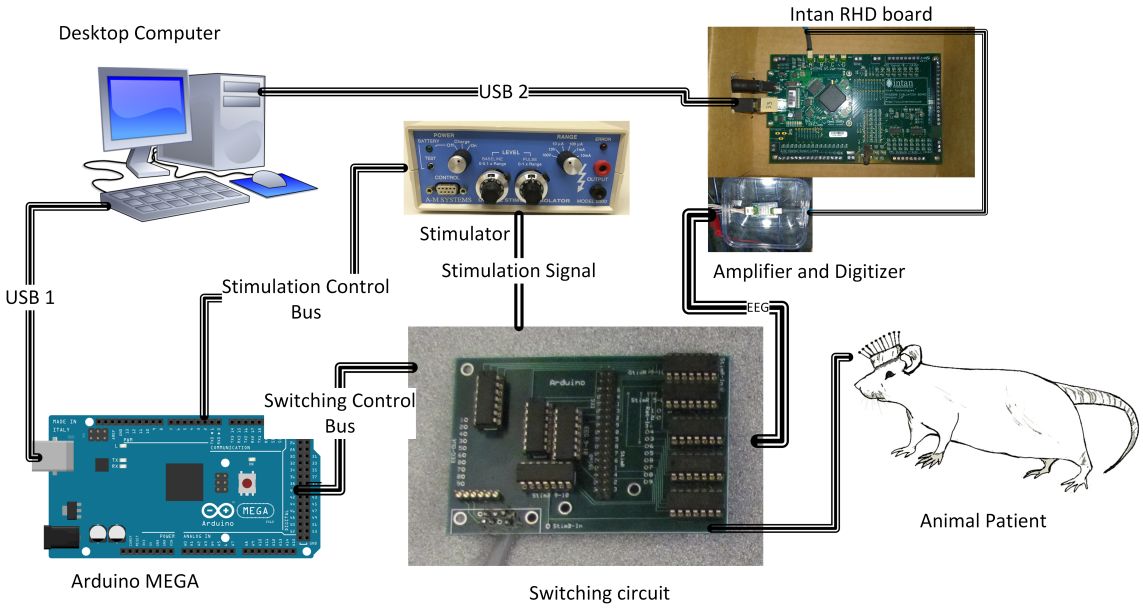

Figure 5.7: Block diagram showing the experimental setup used. The Switching circuit is controlled by the Arduino Due which in turn receives commands from the MATLAB program running on the computer. The switching circuit enables us to stimulate any pair of electrodes at will. The stimulation signal is generated from the A-M systems stimulator.

that are sampled from the ADC at 512Hz from all channels. On MATLAB, either the offline fixed stimulation code or the seizure warning algorithm decides on when and how to stimulate and those parameters are sent over emulated Serial Port(USB Virtual COM port) to the Arduino MEGA. The MEGA then commands the stimulator ([1]) to provide stimulation on its output port. At the same time, the Arduino also commands the switching circuit so that it disconnects a chosen pair of electrodes from the rat to the EEG board and connects them to the stimulator so that the stimulation signal can pass through to the rat brain. When stimulation needs to be switched off, the Arduino commands the stimulator to switch off and reconnects the EEG channels to the rat electrodes. Figure 5.7, shows the entire setup just described and a more detailed diagram of the switching circuit and its operation can be found in Appendix A.

Chapter 6

SEIZURE DETECTION

6.1 Introduction

As elucidated in Chapter 1, epilepsy is a neurological disorder characterized by seizures which are recurrent perturbations of normal brain function. One of the challenges in the field of epilepsy management is the process of detecting seizures. Currently, the established practice is to admit patients into long-term epilepsy monitoring units where epileptologists and trained technicians review continuous EEG (cEEG) recordings over days/weeks. While there have been many methods introduced in the literature on seizure detection [150, 34, 117, 33, 111, 97, 152], several of which involve the use of Neural Networks, none can yet show detection of seizures with 100% Sensitivity and 100% Specificity (see Appendix B). The poor result is mostly due to the fact that an intermediate metric is computed from EEG data based on linear measures, e.g. statistical measures [133, 127], frequency and power spectral analysis [137], before the actual seizure detection metric is implemented. The brain is not an unstructured, random collection of neurons guided by statistics, neither is its behavior linear in nature. Thus, it does not lend itself well to being modeled by such measures. So, while yielding decent results for academic purposes, these methods were not accurate enough for deployment in clinical settings [125].

Using a different seizure detection paradigm (i.e. without using EEG data) implemented in [75], Kramer et al show the use of patient movement data collected by accelerometers during a seizure event to detect it. However, this method is ineffective since not all seizures manifest themselves clinically. Lehnertz et al elicits the use of nonlinear time series analysis as a great tool for efficient use in detection and prediction of epileptic seizures [83]. Notably, among these methods, is the use of Lyapunov exponents in computing chaoticity of an epileptic brain. Following the work of Takens [139] and Wolf [161], Iasemidis et al [59, 61, 62]

have shown how to estimate the Lyapunov exponent, a nonlinear measure, from delay coordinate embedding of sampled EEG data. In this work, using Lyapunov exponents computed from the Kantz algorithm, we have brought to light a fundamental flaw and thereby difference in outcomes in estimating the Lyapunov exponent versus one computed from the modified Wolf algorithm as suggested by Iasemidis et al. Chapter 3 describes the maximum Lyapunov exponent (L_{max}) and the its computation, which when done correctly as we have shown, can be used to produce a reliable estimate of L_{max} from data.

The method implemented in this study utilizes knowledge of chaotic systems and Lyapunov exponents as nonlinear measures that more accurately describes brain activity, allowing for a seizure detection scheme with extremely high Sensitivity and high Specificity (see Appendix B). The accuracy is due to the implementation of the Kantz algorithm as shown in subection 3.3.2, which provides more reliable estimates of L_{max} compared to the other two algorithms. Due to the nonlinear nature of the analysis and the exponentially greater number of trajectories tracked, as compared to the Wolf and Rosenstein algorithms, this method is computationally expensive. However, the expense of compute time does provide us with the benefit of producing a reliable seizure detection mechanism which will aid medical practitioners and patients in epilepsy.

Typically the number of patients admitted at a time between Epilepsy Monitoring Units (EMU) and Intensive Care Units (ICU) in a hospital can become overwhelming, owing to the fact that epilepsy is such a common neurological disorder. Technicians and doctors simply cannot keep up with sifting through volumes of EEG generated in such short period of time. Owing to this, studies have shown that nearly 30% of ICU patients are left with undiagnosed seizures due to this manual and labor-intensive process that is prone to human error [23, 78]. Untimely detection of seizures increase the morbidity of patients and can lead to mortality in certain cases. It also means that the patients have to stay in the hospital longer, thus adding to cost. It is our hope that the newly invented implementation of the automated seizure detection mechanism in this dissertation will help alleviate much

of that burden, equipped with its high true positive and low false positive detection rate (see Appendix B).

6.2 Siezure Detection Results

From our work, we have seen that the use of Kantz algorithm enhances the results for L_{max} computation not only in simulated data from chaotic systems but also in real EEG data collected from animals. Careful and long hours of tuning the kantz parameters allowed us to arrive at these results. In certain cases, choosing certain "wrong" parameter values have produced negative L_{max} values which absolutely do not make sense for a chaotic system; therefore one must be extremely careful in the implementation of L_{max} estimation algorithms. Figure 6.1 shows a comparison of the three different methods applied to the same set of EEG data from animal labeled Rat 7 during the study. A seizure as marked

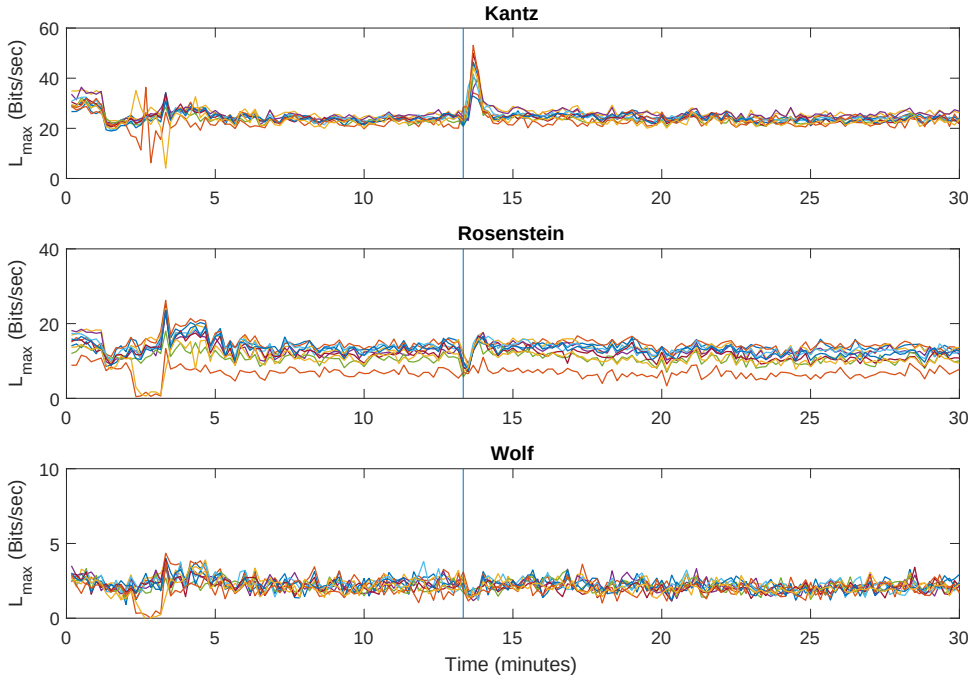

Figure 6.1: Comparison of L_{max} vs time on the same set of EEG data, where L_{max} is estimated from (a) Kantz, (b) Rosenstein, (c) Wolf algorithms respectively. Clearly the one computed from Kantz shows a distinct shape during the seizure at time 13 minutes. The blue vertical line marks the beginning of the seizure.

visually by inspecting EEG is seen to occur at about 13 minutes. The plot shows L_{max} over time, where L_{max}, for each channel, was computed for 10 seconds of data moving forward in time with a 2 second overlap. It is interesting to observe that during the seizure, while the Kantz algorithm shows a distinct peak in the L_{max} time profile, that from the Wolf shows none and the one from the Rosenstein algorithm shows a drop but it is not consistent over many other seizures. Also, the Rosenstein algorithm seems to be more susceptible to noise as is evidenced by the differing value of one channel compared to the rest; this channel had more noise in its EEG data. At this point it would be prudent to mention that the intuition gained about the shape of the epileptic attractor during interictal and ictal epochs (refer to Figure 2.4) does support the idea that during a seizure L_{max} would have a higher value since the trajectories seem to separate from each other more in Figure 2.4(b) than in Figure 2.4(a).

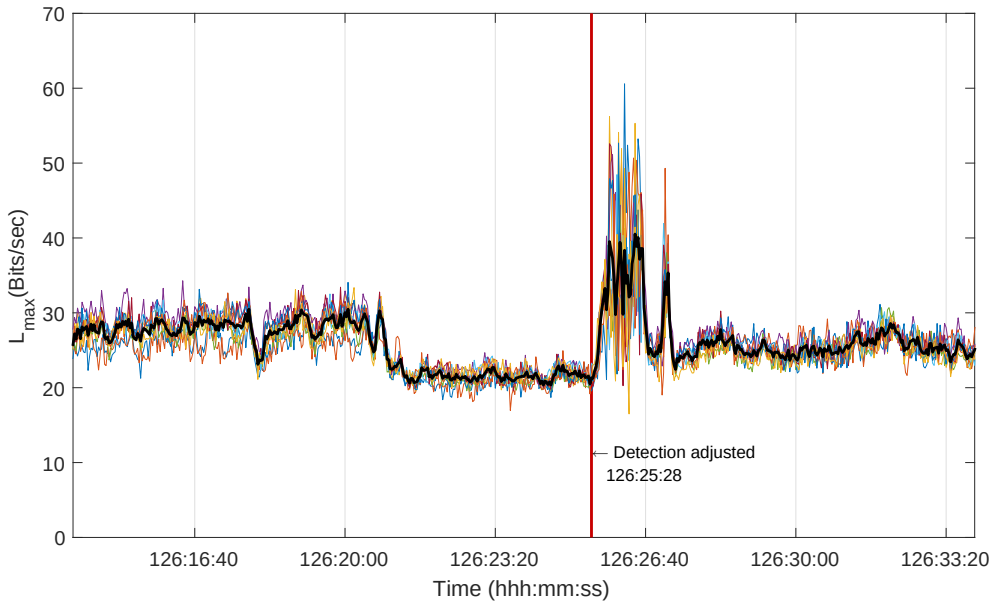

Figure 6.2: Plots of Maximum Lyapunov Exponents computed using Kantz algorithm on all 10 channels of a rodent; the thick black line is the mean of the L_{max} from the channels at each time point. The L_{max} was computed using 10 seconds of data, sampled at 512 Hz, moving forward every 2 seconds in time. The red vertical line marks the beginning of the seizure event at time 126 hours 25 minutes and 28 seconds from the beginning of recording. As can be seen the Lyapunov drops a little a few minutes before the seizure, then at the seizure, rises to a higher value than its mean.

Following this, we now draw attention to Figure 6.2, where the L_{max} temporal profile computed using the Kantz algorithm is shown in higher resolution. The data used was acquired from Rat 13. Here, it can be seen clearly that the L_{max} profile drops from its mean level of roughly 30 bits/sec to a lower value almost 5 minutes prior to the seizure start; this in turn can become useful as a seizure precursor measure and be used to stimulate in order to attempt a seizure abortion. We have seen this drop in all seizures analyzed over 3 animals so far.

At this point it would be interesting to point out that Iasemidis et al made a conjecture that during a seizure the brain changes state from chaotic to ordered to chaotic. We can ascertain this logic by scrutinizing the temporal evolution of the L_{max} plot obtained using their modified Wolf algorithm in Figure 6.1. We contend that the use of Wolf algorithm and its weakness to noisy data obscured some of the dynamics before, during and after the seizure. Using the optimized Kantz algorithm we show that a seizure in fact consists

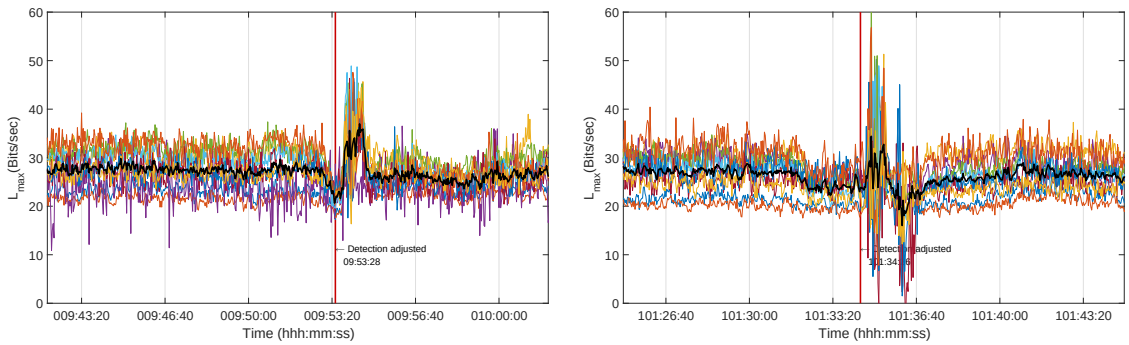

(a) (b)

Figure 6.3: Plots of Maximum Lyapunov Exponents computed using Kantz algorithm on all 10 channels of Rat 12. The thick black line is the mean of the L_{max} from all the channels at each time point. The L_{max} was computed using 10 seconds of data, sampled at 512 Hz, moving forward every 2 seconds in time. (a) Shows a seizure detection event at time 9 hours 53 minutes and 28 seconds from the beginning of recording; the seizure start time as seen from the EEG was 9 hours 53 minutes and 52 seconds. The red vertical line marks the beginning of the seizure. As can be seen the Lyapunov drops a little a few minutes before the seizure, then at the seizure, rises to a higher value than its mean before resetting to its interictal value after the seizure is complete. (b) Shows the same temporal profile for a separate recording file approximately 2 weeks later. Here the seizure detection algorithm shows the start time as 101 hours 34 minutes and 26 seconds compared to the start marked visually from EEG at 101 hours 34 minutes and 36 seconds.

of a transition from an interictal (chaotic state) to a preictal brain state where the brain transitions from chaotic to ordered (less chaotic) and then ictally to unstable, exponentially growing, which in L_{max} terms is manifested as extremely chaotic, and finally to the original chaotic levels postictally. In Figure 6.2, this is characterized by the drop of the L_{max} profile from its mean value of 30 bits/sec to about 20 bits/sec at 126 hours and 21 minutes approximately, then the abrupt transition to about 40 bits/sec at the seizure onset time of 126 hours 25 minutes and 28 seconds and the final postictal state where the L_{max} converges to its original mean value of about 30 bits/sec that it existed in preictally. In all these plots the time presented is relative to the beginning of corresponding recording.

We support our conjecture using more seizures from different animals at different times. First, Figures 6.3(a)-(b) is obtained from L_{max} profiles computed from Rat 12. A few channels had considerable amount of noise in Rat 12. Yet, we can see that the L_{max} profile clearly shows the transitions we discussed in the previous paragraph. Second, we look at

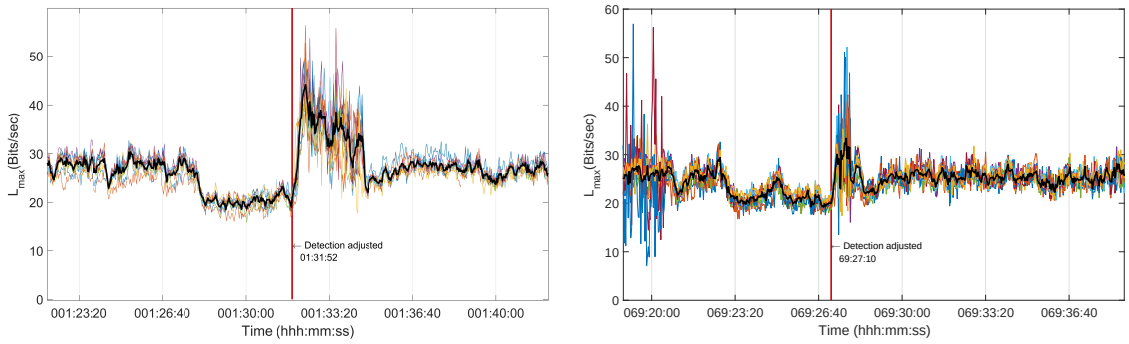

(a) (b)

Figure 6.4: Plots of Maximum Lyapunov Exponents computed using Kantz algorithm on all 10 channels of Rat 13. The thick black line is the mean of the L_{max} from all the channels at each time point. The L_{max} was computed using 10 seconds of data, sampled at 512 Hz, moving forward every 2 seconds in time. (a) Shows a seizure detection event at time 1 hours 31 minutes and 52 seconds from the beginning of recording; the seizure start time as seen from the EEG was 1 hours 31 minutes and 57 seconds. The red vertical line marks the beginning of the seizure. As can be seen the Lyapunov drops a little a few minutes before the seizure, then at the seizure, rises to a higher value than its mean before resetting to its interictal value after the seizure is complete. (b) Shows the same temporal profile for a separate recording file approximately 8 weeks later. Here the seizure detection algorithm shows the start time as 69 hours 27 minutes and 10 seconds compared to the start marked visually from EEG at 69 hours 27 minutes and 20 seconds.

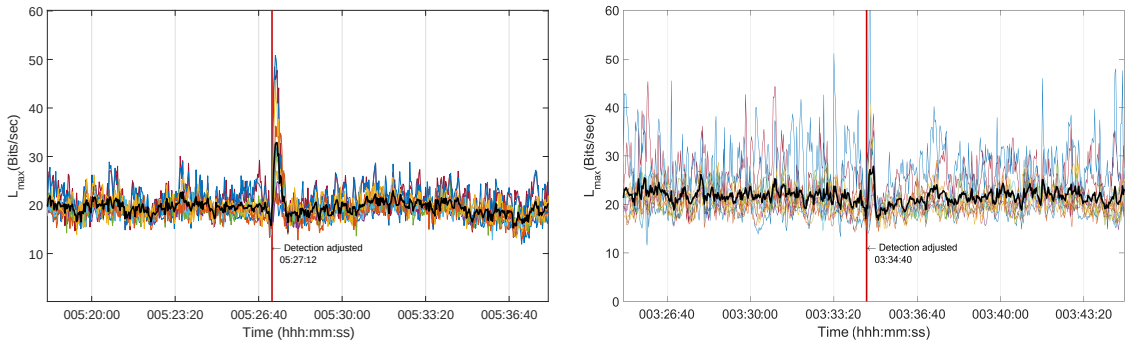

(a) (b)

Figure 6.5: Plots of Maximum Lyapunov Exponents computed using Kantz algorithm on all 10 channels of Rat 14. The thick black line is the mean of the L_{max} from all the channels at each time point. The L_{max} was computed using 10 seconds of data, sampled at 512 Hz, moving forward every 2 seconds in time. (a) Shows a seizure detection event at time 5 hours 27 minutes and 12 seconds from the beginning of recording; the seizure start time as seen from the EEG was 5 hours 27 minutes and 10 seconds. The red vertical line marks the beginning of the seizure. As can be seen the Lyapunov drops a little a few minutes before the seizure, then at the seizure, rises to a higher value than its mean before resetting to its interictal value after the seizure is complete. (b) Shows the same temporal profile for a separate recording file approximately 8 weeks later. Here the seizure detection algorithm shows the start time as 3 hours 34 minutes and 40 seconds compared to the start marked visually from EEG at 3 hours 34 minutes and 37 seconds.

two more seizures from Rat 13 in Figure 6.4(a)-(b). Both plots show very distinct L_{max} profiles as the EEG transitions from interictal to preictal to ictal and finally to postictal. In Figure 6.4(b) the beginning of the plot shows the L_{max} profiles from some of the channels to have higher variance. This is because the animal was being stimulated during that time, and stimulation artifacts do cause the L_{max} profiles of channels to show inconclusive results. However, ignoring the L_{max} from the stimulated channels will show us the characteristic L_{max} profile from a seizure as we will show soon. Finally, we observe the L_{max} profile computed from data collected on Rat 14. Rat 14 showed considerable degradation of EEG data quality after the first few months. Figure 6.5(a) shows data from the first week, while Figure 6.5(b) shows the same profile 9 weeks later. There was overall more noise in all the channels but a few suffered worse. Yet, the seizure profile is still quite distinguishable from the interictal data.

At this point it must be noted that although a similar profile in L_{max} can be seen

for all seizures, their lengths and amplitude changes are not the same. We now turn our attention to the case when data is obfuscated with stimulation artifacts/noise. We have shown how data from Rat 12 and Rat 14 contain noise yet the L_{max} seizure profile is clearly distinguishable through Figure 6.3(a)-(b) and Figure 6.5(b) respectively. In Figure 6.6 we can see how the seizure profile is still clearly distinguishable even in the presence of stimulation artifacts. This is data from Rat 14 whose channels already had a considerable amount of noise. A stimulation for 14 minutes was provided between electrodes LA-RA (refer to chapter 5 for location of electrodes and their abbreviated names) and a seizure occurred at time 14 hours, 42 minutes and 52 seconds from the start of the recording file. The transitions of the L_{max} profile can still be seen and the seizure detected through visual inspection.

The caveat to using the Kantz algorithm in such a setting is that it is computationally intensive. Thus, we implemented the tuned algorithm in a parallelizable fashion so as to allow for fast computations. Since, the Kantz algorithm tracks not one but a large number of trajectories (in the order of 100s) within a neighborhood, the information used is much greater than in either Wolf or Rosenstein algorithms. This is a double-edged sword since we would have to trade-off speed with accuracy. Our approach to circumvent this was to utilize the parallel-computing toolbox available in MATLAB and run these computations in parallel on 10 cores in a single hyper-threaded CPU. Each core computes L_{max} for 10 seconds of data on each rat EEG channel; this is the value for T shown in the algorithms in Chapter 3. This process takes about 0.1 seconds to complete when parallelized but about 3 seconds when run serially on an Intel Xeon Processor in offline mode. On humans, where the typical EEG has between 32 and 128 channels we can expect the process to take significantly longer. The process is repeated with new data every two seconds, i.e. every two seconds the past ten seconds of data is passed to the L_{max} algorithm to get a single value from each channel. Without the use of super-computing platforms offline data analysis would take days to weeks and online computations would be infeasible in the absence of accelerators

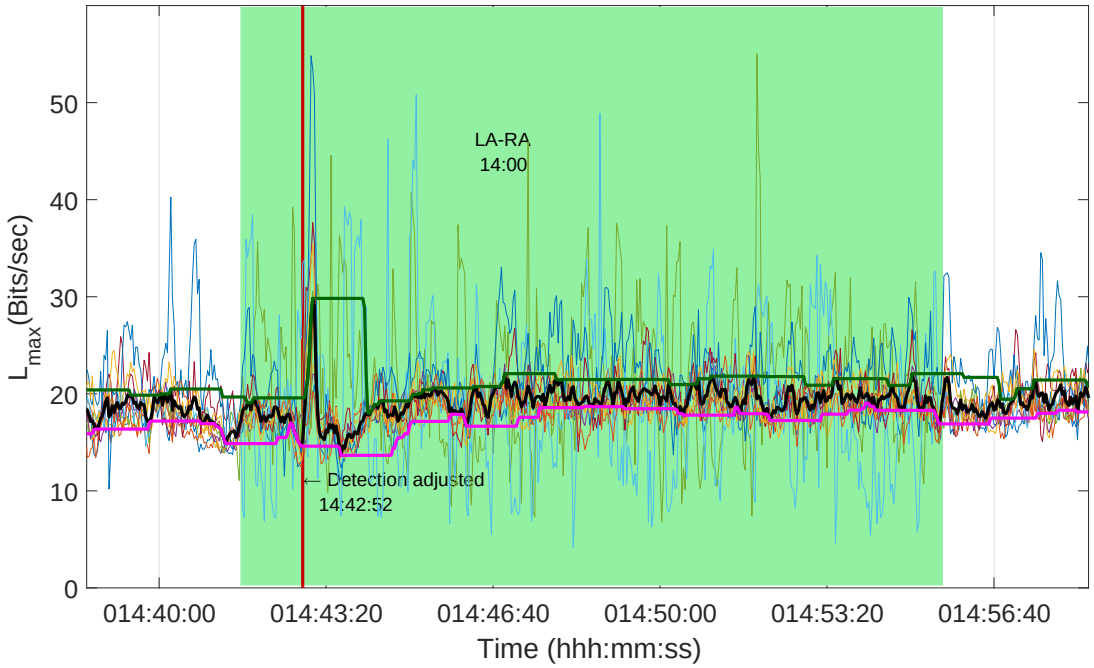

Figure 6.6: Plot of Maximum Lyapunov Exponents computed using Kantz algorithm on all 10 channels of Rat 14. The thick black line is the mean of the L_{max} from all the channels at each time point. The L_{max} was computed using 10 seconds of data, sampled at 512 Hz, moving forward every 2 seconds in time. In this figure we detail the automatic seizure detection algorithm. The seizure detection event as marked by the algorithm is at time 14 hours 42 minutes and 52 seconds from the beginning of recording; the seizure start time as seen from the EEG was 14 hours 42 minutes and 51 seconds. The red vertical line marks the beginning of the seizure using the automated detection algorithm. The thick green plot is the moving maximum of the black line (mean at every time point) and the thick magenta plot is the moving minimum. A detection event is marked when the moving maximum at an instance crosses a predetermined threshold higher than all the past 60 seconds of moving minimums.

such as GPUs and coprocessors.

The key difficulty in achieving these L_{max} profiles from the Kantz algorithm is the fine-tuning of the 12 parameters required as input arguments. Over 200,000 CPU hours were spent in the ASU supercomputing center and Gordon XSEDE resources in optimizing this program to the epilepsy problem With these tuned parameters, when the computed L_{max} profile is plotted over time, a distinct pattern emerges near the ictal periods, as we have already shown, but it is not seen at any other time. To a human operator, this profile stands out immediately with little training. Compared to learning to mark seizures from

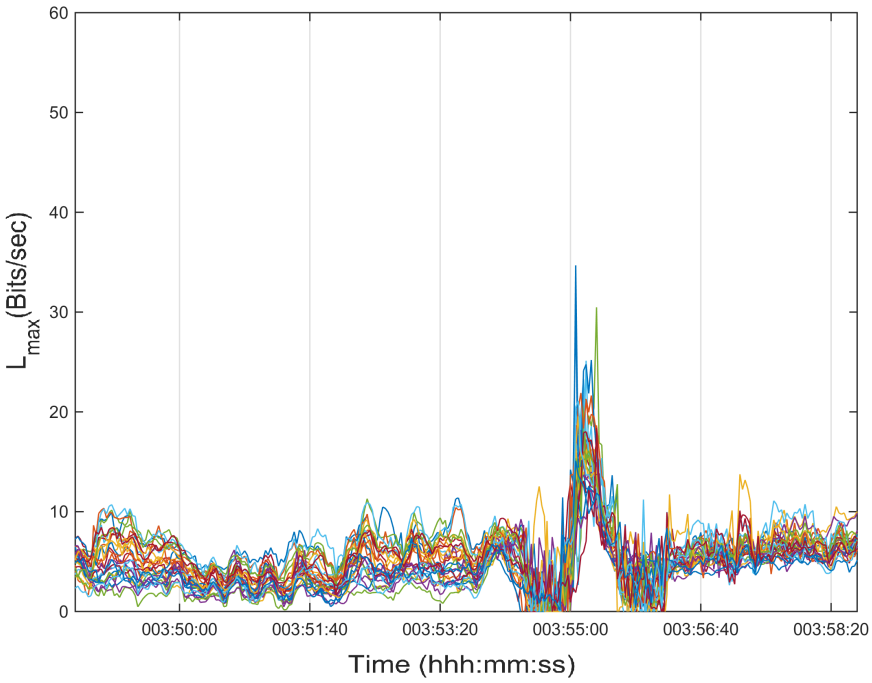

Figure 6.7: Plot of Maximum Lyapunov Exponents computed using Kantz algorithm on all 28 channels of de-identified human data. The EEG data was collected in differential mode. Seizure can be seen to start at about 3 hours 54 minutes from the beginning of recording.

EEGs this is over a factor of 10 increase in efficiency for rodent data. Preliminary tests on one set of human data has also shown promise. Figure 6.7 shows the same L_{max} profile against time plotted for human EEG. Here it can be clearly seen that the L_{max} profile goes through a characteristic drop in chaoticity at about time 3 hours and 54 minutes and then spikes at about 3 hours and 55 minutes and resets to normal around time 3 hours 55 minutes and 30 seconds. These transitions are quite similar to the rodent data presented previously and correlates to the hypothesis that the brain goes through chaos to order to more chaotic then resetting to chaotic state as a seizure evolves and completes. It is worth noting that, this set of analysis on human data was done using the same parameters for the Kantz algorithm that were used in rodent data. Although, these parameters have held true for all rodent data we have analyzed, the same claim cannot be made as yet for human data since only one seizure from a human was been analyzed so far.

6.2.1 *Automated Seizure Detection Algorithm*

Leading up to this point we have only provided a discussion of how the L_{max} profile evolves during a seizure. For now we are employing a simplistic thresholding algorithm to automate the L_{max} profile detection during a seizure. The methodology is explained with the help of Figure 6.6 where the thick line in **black** is the mean of the L_{max} values at every time point. This essentially tracks the center of the L_{max} of all channels; in cases where there are stimulations or we know that certain channels are bad (noisy) we exclude such channels from the mean computation. The thick **green** line tracks the maximum of the **black** line (mean), while the thick **magenta** line tracks its minimum. The detection algorithm essentially looks at the current value of the moving maximum of averages of L_{max} (**green** line) and compares it to the past 1 minute of the moving minimum of the average (**magenta** line). A detection is signaled whenever the difference between the moving maximum and the past 1 minute of minimums is greater than a threshold. Essentially this allows the current point in the average L_{max} plot (**black** line) to be marked when it moves from its lowest value at the start of the seizure to a high value once the seizure has progressed. This detection would in fact only show an alarm after the seizure has started; in order to see the start of the seizure a second algorithm adjusts for the time of detection by looking at the minimum value of the average L_{max} and plotting it in the output window using the red vertical line with the adjusted detection time adjacent to it as seen in all the plots. This does not perform as well if the data is extremely noisy; noise can be from air-waves or from various artifacts generated in the body, e.g. muscle, eye movement etc. and external inputs such as stimulation. A future goal to improvise the automated detection will be to investigate methods to accurately detect the L_{max} profile during a seizure using wavelet matching, neural networks etc.

Before concluding this section we present the Receiver Operating Characteristics (ROC) curve for our threshold based seizure detection algorithm in Figure 6.8(a) and the True Positive Rate (TPR) and False Positive Rate (FPR) against threshold in Figure 6.8(b).

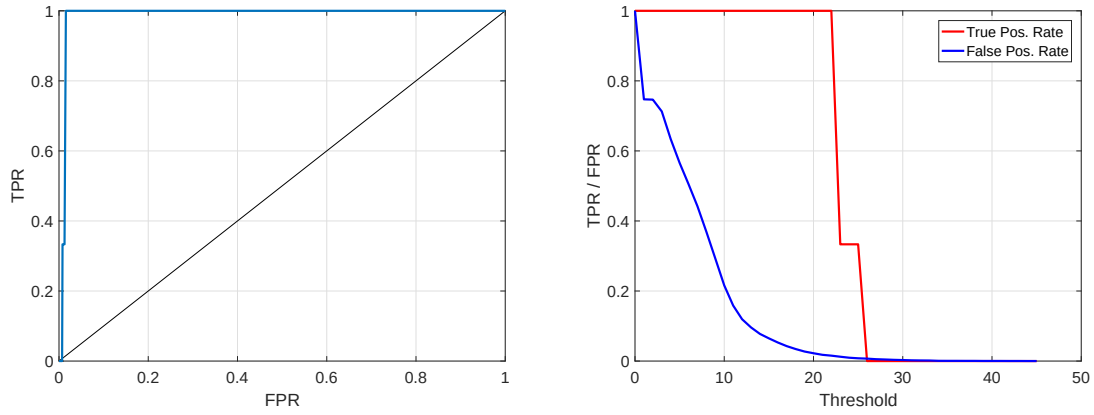

(a) (b)

Figure 6.8: Using Rat 13 week 1 data, which had 3 seizures, we determine the best threshold for the automated seizure detection scheme. (a) Shows the Receiver Operating Characteristics; with an area under the curve of 0.9882 we can say with certainty that the threshold based algorithm performs quite well. (b) Shows the True Positive Ration and False Positive Ration against detection threshold. The best value of threshold is 22 since it allows for TPR of 1 and FPR of 0.01545

TPR is the same as $Sensitivity$ and FPR is $1-Specificity$ (see Appendix B for definitions). This data is from Rat 13 Week 1; similar operations are performed on all rats to test out the best detection threshold. As can be seen the ROC curve has an area that is 0.9882 which is very close to 1 implying the feasibility of our classification technique based on thresholds. Additionally, looking at the TPR and FPR curves against threshold we can see that a value of $threshold = 22$ produces the highest $TPR = 1$ while simultaneously providing a low $FPR = 0.01545$.

6.3 Conclusions

In Chapter 3, we have shown a method of computing the maximum Lyapunov Exponent accurately. In this chapter we have presented a comparison of the Wolf and Rosenstein algorithm to our implementation of the tuned Kantz algorithm and shown that it provides a succinctly discernible temporal profile of L_{max} over time. We have produced many such L_{max} profiles and shown that it transitions through a drop to spike and then a resetting of its mean level during a seizure. Furthermore, after analyzing weeks of data over many

different rats we have seen that the modified Kantz algorithm is able to produce this profile consistently and prominently even in the presence of considerable noise. What is more important to acknowledge is that this method does not show such profiles when a seizure is not present; something that is not true for both Wolf and Rosenstein methods. The same is also true for healthy animals; plots from healthy are not shown since nothing is interesting enough to produce in this report.

The final objective of this work is to develop a highly reliable and fully automated computational algorithm that will enable real-time seizure detection. We hypothesize that such a tool will immediately benefit epileptologists and open up the possibility of wide acceptance by a number of commercially available implantable devices that attempt to treat epilepsy. Integrating this new technologoy to already existing portable neuro-modulators such as the Neurpace RNS system [31] and Cyberonics VNS system can strive to improve these automated stimulation devices by providing feedback on performance, i.e. how many seizures are occurring with the neuromodulator connected to the patient.

Currently the algorithm requires some human involvement. Complete automation will be achieved by testing out a number of shape detection algorithms through the use of neural networks and wavelet matching, not unlike the methods implemented in [101] albeit with better accuracy. The tuned Kantz algorithm uses almost 100's of times more information than any of the methods utilized in the past. While we have been able to program it efficiently, increase in the number of EEG channels to be analyzed will most certainly cause time constraints on computation. A possible hurdle to overcome in the future would be to implement it on parallelizable platforms such as GPUs while adhering to the real-time nature of the algorithm. If successfully implemented, such a product will become crucial in allowing medical practitioners to have a real-time seizure detection/warning system to help them better diagnose and treat patients with epilepsy.

Chapter 7

PREDICTION AND CONTROL OF SEIZURES

7.1 Introduction

AEDs are prone to creating systemic and central nervous system side effects and studies have shown that electrical stimulation as an alternative to seizure control may not have the same undesirable outcomes. On top of that, in comparison to surgery, with electrical stimulation, there is no need to resect the focus which is an irreversible process with side effects ranging from loss of memory to a number of possible permanent disruptions in brain function. Deep brain stimulation (DBS), principally of thalamic structures, has been reported to reduce seizure frequency in humans. Examples of DBS include 4-8 Hz electrical stimulation in the head of the caudate nucleus and 20-130 Hz centromedian nucleus (CM) stimulation. The stimulus delivery is either continuous (12-14hours/day), intermittent (10 min "on," 15-20 min "off" for 12-14 hours/day) or continuous periodic (20-30 minutes on, 3 or 4 times a day) [151, 162, 52, 73, 20].

The Vagus Nerve Stimulator (VNS) as an antiepileptic device was approved by the US Food and Drug Administration in 1997. This device stimulates the brain through the vagus nerve, at regular intervals, with predetermined intensity, frequency and pulse shapes. Although the reported side effects are minimal, only one-third of patients implanted with the VNS device experience a 50% reduction of seizure frequency, and fewer than 10% become seizure free [30]. Two further clinical trials of DBS for epilepsy management have also been conducted in the United States, one by Medtronic and the other by NeuroPace. Surgical implantation of stimulating electrodes into the thalamus and other deep brain structures is required for both. Like the VNS device, the Medtronic device is programmed to deliver intermittent stimulations independent of the presence or absence of seizure activity. The NeuroPace device attempts to detect seizures about their electrographic onset(see Appendix

B), and then try to abort them by delivering an electrical stimulation. Both devices have reported some success in reducing seizure frequency [73, 74, 107, 108].

While holding promise for a possible relief to epileptic patients, these devices could benefit from a quantum leap in conceptual and practical improvement whereby the stimulus is activated by certain preictal electrical activity in the brain, sufficiently early, to prevent the impending seizure from occurring. This would require the ability to detect predictive EEG changes of an impending seizure a long time (e.g. tens of minutes), before the seizure onset. Along these lines, a study reported that by stimulating after a seizure is predicted from EEG analysis, seizure frequency reduced markedly [130]. Such a technique would require considerable tuning, in order to improve performance, not only in the algorithm but in the shape of the stimulation signal as well [155]. Potential wireless implementations have shown that we could eliminate the hassle of having wires connected and hanging around the patient's body [163]. Although at this stage it is too early to claim whether the electrical stimulation approach will lead to a complete cure for epilepsy, or simply postpone seizures, the benefits to epileptic patients could be significant.

Based on work on seizure prediction it was shown that measures of spatial synchronization of dynamics, through the measurement of phase correlations, show that a preictal state can be characterized several minutes prior to seizure onset [118]. Dividing the EEG signal between six bands - delta (0.1–4 Hz), theta (4–8 Hz), alpha (8–12 Hz), beta (12–30 Hz), low-gamma (30–70 Hz), and high-gamma (70–180 Hz) and training a logistic regression classifier, [53] shows that seizures can be predicted in an animal model of epileptic dogs. On the other hand, using nonlinear dynamics as their primary focus, Iasemidis et al have shown the use of maximal Lyapunov exponent and its statistical distance metric (T-index) to provide decent prediction results [55, 63].

The contention to seizure prediction schemes come from studies which show that the solution to this problem is still at its infancy. As a few examples we cite [80], where the predictive power of the Lyapunov exponent is challenged; [66], where the variability of

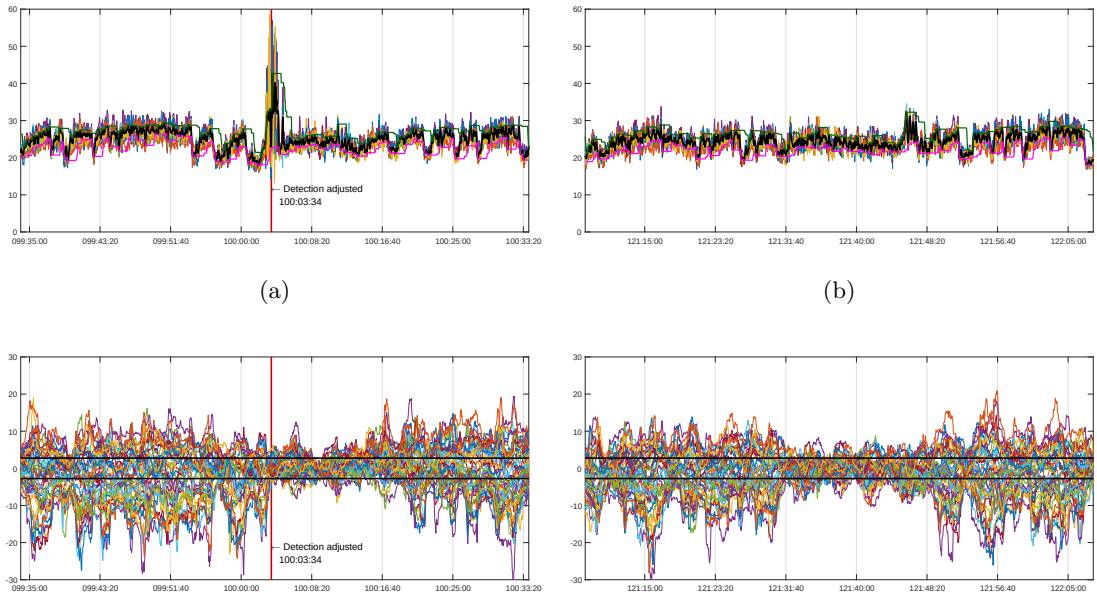

(a) (b)

(c) (d)

Figure 7.1: L_{max} and its paired T-index profiles computed on 1 hour of ictal and interictal data from Rat 13. L_{max} for ictal data and the corresponding T-index profile are shown in (a) and (c). Likewise, (b) and (d) show the same for interictal data. At first look not much can be said about the predictive power of the T-index.

sensitivity (65% - 100%) and specificity (65% - 80%) of prediction is quite poor and finally [98], which makes a concluding remark that while pre-seizure states have been shown to exist, no prospective prediction scheme with 100% senstivity and specificity respectively has been achieved. Our own investigation into using T-index computed on pairs of L_{max} profiles of channels show no discernible prediction measure. With the help of Figures 7.1(a),(c) and 7.1(b),(d) we provide evidence that little to no difference can be seen in the T-index profile during seizure and non seizure periods, thus T-index even on L_{max} computed from the optimized Kantz algorithm isn't quite effective at seizure prediction at first look; further analysis may contain the possibility of yielding better results. All these studies provide little solace to medical practitioners and epileptic patients.

Through our own studies, in particular the behavior of Lyapunov exponents of critical brain sites as shown in Chapter 6, we have shown that a good characterization of the transition to seizures and can be provided by the tuned Kantz algorithm and utilized in

the reliable issuance of warnings on impending seizures. As such, and in view of postulated models in [15], these interictal to preictal transitions can be interpreted as an increased seizure susceptibility state of the brain. This may not be entirely useful as a prediction measure, especially since in epileptic subjects such periods do arise frequently, compared to healthy subjects where they do not occur at all, but it creates the possibility of being used as an appropriate signal for feedback control and stimulation.

For the implemented closed-loop controller, the quantification of the controller's performance affects the control objective and the solvability of the control problem. A key issue in the control of the epileptic brain is that standard control objectives are not directly applicable. Desired trajectories are not known to enable the formulation of a tracking problem, either for aggregate outputs (measures of dynamics) like Lyapunov exponents, phase correlations etc. and more so for EEG states. The popular chaos control schemes for the stabilization of a periodic trajectory in [109, 116, 16] are inappropriate. To circumvent this problem, Tsakalis et al have shown through the use of chaotic oscillator models that seizures can be controlled by the application of an external feedback controller that compensates for the pathological tuning of the internal controller of the brain [147, 149]. While the results from such models produce a good hypothesis and validation from simulation, the problem with the methodology is its incorporation in the actual brain. Where does the control input go in the epileptic brain? In addition, we have seen through our work, that if the aggregate output (L_{max} profile) is what we are tracking, then the application of a stimulus that is larger than the EEG, will completely confound the EEG and tracking the output becomes near impossible during those times.

On top of answering the riddle to "when" the stimulation be applied, another potential difficulty comes from the question of "where" the stimulation should be provided. A partial direction towards the selection of an appropriate pair of electrodes for stimulation may be obtained by analyzing the EEG data for focus localization, using the GPDC method of [9], as refined by [154]. This method can provide an indication of the brain site that

is the most likely candidate for a focus, and hence a good first choice for stimulation. However, the drawback of this method is that the results are (so far) based on the analysis of averaged short-term data. Long term effects and possible plasticity have been observed in the work of [56], and therefore further analysis of the data is necessary to provide quantifiable relationships. Another direction that we have investigated during the course of this study is where stimulation of a particular site with a fixed amount of time will start to produce disentrainment as is validated by changes in the L_{max} profile. In the following sections we provide results from our GPDC implementation on preictal data, a creation of "control efficacy maps" through disentrainment with stimulation on specific pairs of sites and finally the results of control on seizure frequency and length.

7.2 Results of GPDC Algorithm on Localizing the Focus

As mentioned in the previous section, focus localization will have the benefit of allowing us to choose a location to apply the stimulus. Instead of taking all the interictal data as shown in [154], we utilize the preictal zone of seizures as identified by our tuned Kantz algorithm for computing L_{max}. The result of interest in this case is that during all preictal zones the same electrodes are active in almost the same manner in addition to the fact that looking at preictal data, we may gain better insight into the seizure activity than doing so at interictal periods. This result can be seen by observing Figures 7.2, 7.3, 7.4 and 7.5. These plots show results from GPDC applied to the four seizures which were recorded in the fifth week of experimentation where no stimulation was provided to Rat 13. For all figures, the first subplot is computed by measuring inflow in the GPDC epochs in the interictal period for each channel and then ranking them as a percentage of total inflow to all channels. The second subplot is the same but for outflow. The third subplot is the average of GPDC over all the epochs. Although GPDC is essentially a frequency dependent metric, which means that the plots should have looked like transfer functions, we took the total energy in each element of the GPDC matrix to represent it as a single number. Additionally, the bars marked in red are classified as outliers using Grubb's test with a confidence of $\alpha = 0.05$.

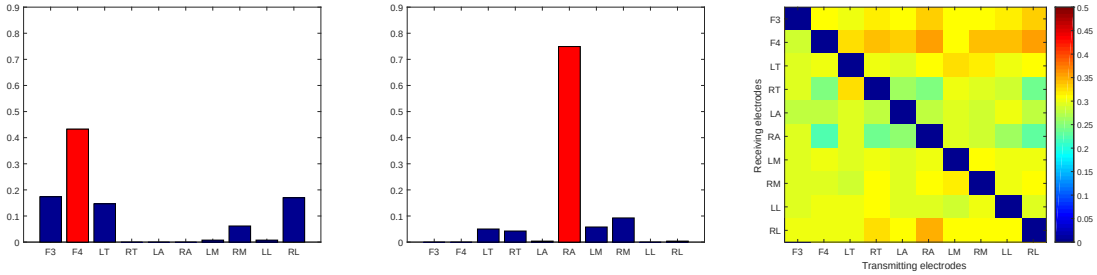

(a) (b) (c)

Figure 7.2: For the first seizure in "Week 5" of Rat 13 (a) shows the maximal inflow as computed from GPDC data. (b) Shows the maximal outflow and (c) the average GPDC for the entire preictal data set.

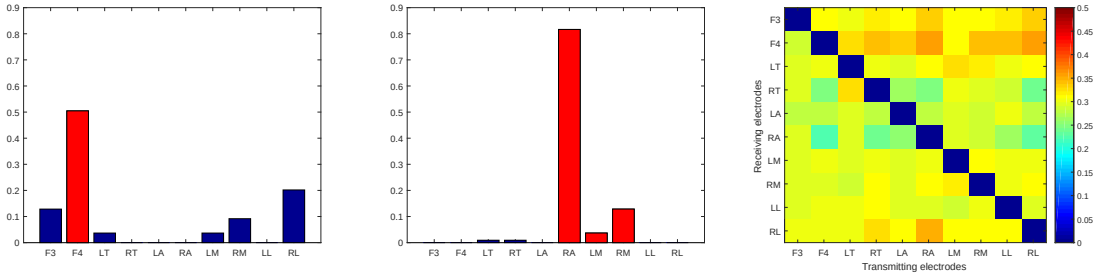

(a) (b) (c)

Figure 7.3: For the second seizure in "Week 5" of Rat 13 (a) shows the maximal inflow as computed from GPDC data. (b) Shows the maximal outflow and (c) the average GPDC for the entire preictal data set.

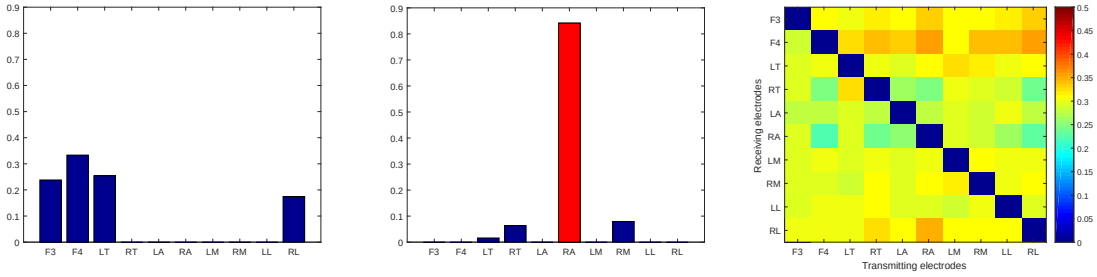

(a) (b) (c)

Figure 7.4: For the third seizure in "Week 5" of Rat 13 (a) shows the maximal inflow as computed from GPDC data. (b) Shows the maximal outflow and (c) the average GPDC for the entire preictal data set.

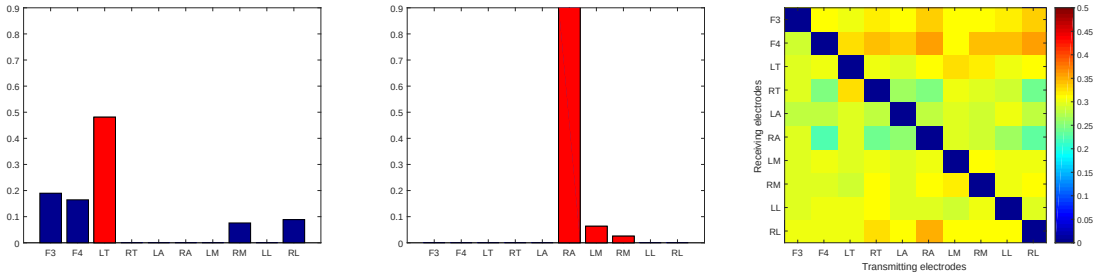

(a) (b) (c)

Figure 7.5: For the fourth seizure in "Week 5" of Rat 13 (a) shows the maximal inflow as computed from GPDC data. (b) Shows the maximal outflow and (c) the average GPDC for the entire preictal data set.

In computing the GPDC we employed the use of a small amount of white noise to provide an easy way of regularizing the MVAR parameters. The addition of noise (with variance $1e^{-5}$) to each channel creates a persistence of excitation condition, this essentially helps bias the parameters more towards the diagonal ones. Since for the purpose of localization, delayed self-inflow as measured by the parameters in the diagonal of the MVAR output are irrelevant, this "poor man's regularization" allows us to clean out effects of noise in the data that may falsely indicate stronger cross connectivity of information. Making the diagonal parameters larger in the MVAR solution helps alleviate such effects of noise whereby wrong inflow or outflow results could be potentially misleading. More elaborate methods of regularizing the parameters based on orthogonal projections could be used, however we forsook them and traded off sophistication for the benefit of speed. Observing the figures presented here together, it is quite clear that F4 and LT electrodes are the most active sinks for information inflow, while RA is the predominant source for information outflow. While [154] makes a claim about the channels involved in inflow being the focus, we intend to not focus on such results as these and try to generalize our findings in the following - if certain electrodes are more active than others at information inflow and outflow, we mark these locations as possibly interacting with the focus, wherever the focus may be. Where the focus really is, is difficult to tell for rat data; in contrast to human EEG, where the results of this method could be accurately verified through the eyes of a trained epileptologist. The

Table 7.1: Effect of stimulation on Lyapunov Profile for Rat12.

Pair	5m	10m	15m	20m	Sum
F3-F4	1	1	1	1	4
F3-LT	1	0	1	1	3
F3-RT	1	0	1	0	2
F3-LA	0	1	1	1	3
F3-RA	1	1	1	1	4
F3-LM	0	0	0	0	0
F3-RM	0	0	1	0	1
F3-LL	0	1	1	1	3
F3-RL	0	1	0	0	1
F4-LT	1	0	1	1	3
F4-RT	0	1	1	1	3
F4-LA	1	1	1	1	4
F4-RA	0	1	1	1	3
F4-LM	0	1	0	0	1
F4-RM	0	0	0	1	1
F4-LL	1	1	1	1	4
F4-RL	1	0	0	0	1
LT-RT	1	1	1	1	4
LT-LA	0	1	1	0	2
LT-RA	0	1	1	1	3
LT-LM	1	1	0	0	2
LT-RM	0	1	0	1	2
LT-LL	1	1	1	1	4

Pair	5m	10m	15m	20m	Sum
LT-RL	1	1	0	1	3
RT-LA	0	1	0	0	1
RT-RA	0	1	1	1	3
RT-LM	0	0	0	1	1
RT-RM	0	0	0	0	0
RT-LL	0	1	0	0	1
RT-RL	0	0	0	0	0
LA-RA	0	0	0	1	1
LA-LM	0	0	1	0	1
LA-RM	0	0	1	0	1
LA-LL	0	0	1	0	1
LA-RL	0	0	0	0	0
RA-LM	0	0	1	1	2
RA-RM	0	0	1	1	2
RA-LL	0	0	0	1	1
RA-RL	0	1	1	1	3
LM-RM	1	1	1	0	3
LM-LL	1	0	1	1	3
LM-RL	0	1	1	1	3
RM-LL	1	1	1	0	3
RM-RL	0	0	1	1	2
LL-RL	0	1	1	1	3

difficulty even for a trained EEG technician to pinpoint focus in a rat, from EEG data, lies partly due to the fact that the rat brain is so much smaller than that of a human, thus spatio-temporal differences in the EEG are difficult to discern.

Therfore, from these results we could ascertain that stimulating a combination of sites that involve these three (F4, LT, RA) would have the potential to abort a seizure. Further experimentation is required in order to substantiate these claims, however we do have promising preliminary data from such experiments that will be presented in Section 7.4.

Table 7.2: Aggregate effect of stimulation on Lyapunov Profile for Rat12.

	5m	10m	15m	20m
1	15	25	29	27
0	30	20	16	18

7.3 Control Efficacy Maps

A different way of answering the problem of "where" to stimulate could be through what we have come to call Control Efficacy Map (CEM). We arrived at this approach due to the difficulty in the design of a seizure control system that arises from the multivariable nature of the stimulation as well as its relation to the energy of the stimulus. From the figures of seizures in Chapter 6, we have already shown how during transitions to preictal periods, the L_{max} profile drops to below its mean value. Essentially, we use these transitions as precursors to seizures. These transitions also happen when not followed by a seizure, which makes prediction of seizures harder to track with great reliability. However, our hypothesis is that the epileptic brain is going through different transitions in its state all the time and not all such transitions end up in seizures. It was shown in [100], albeit with the use of L_{max} computed using Wolf's algorithm, that seizures have a way of resetting the brain dynamics and that the L_{max} profile ends up at a value equal to, higher or lower than its original mean after the seizure, depending on the age of animals. Notwithstanding the variability introduced by age of subjects, in our study, this concept has been generalized as we have seen from our own results that in the postictal state the L_{max} returns to its original level before it sunk to that of the preictal state. Following this, what could be argued is that if stimulation can act as an intermediary, i.e. pull the level of L_{max} up when it drops below the higher mean value, then a seizure may have been aborted; since the stimulation would have brought a change of state similar to postictal without the seizure ever occurring.

Table 7.1 shows a characterization of the stimulus efficacy (as a binary decision over a days-long set of experiments), when the stimulation is applied across a given electrode pair on Rat 12. Essentially, the methodology of the experiment is to apply stimulation on each

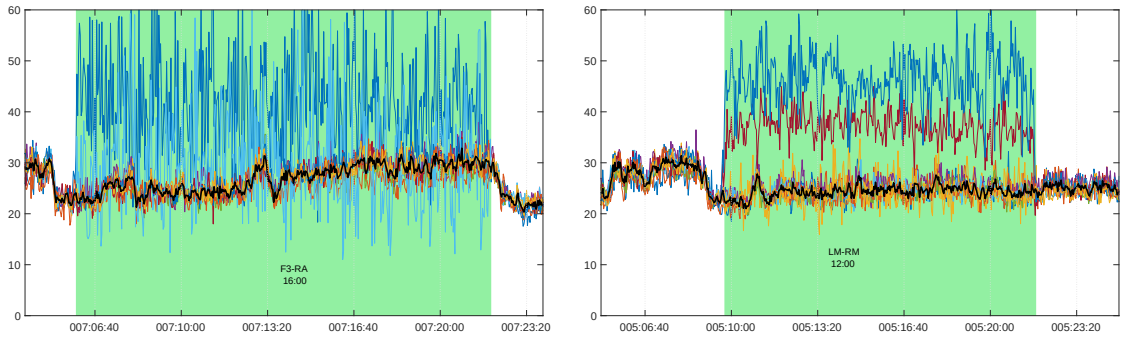

(a) (b)

Figure 7.6: (a) Shows the effect of stimulation electrodes F3-RA for 16 minutes. As can be seen, the stimulation was successful in bring the L_{max} up to the original level. The level dropped as soon as the stimulation ended indicating that more stimulation was necessary. (b) In this case a 12 minute stimulation on LM-RM was unsuccessful at affecting the L_{max} profile indicating either more stimulation energy was required or that stimulating this pair of sites would not have much effect.

of the 45 pairs of electrodes in increments of 5, 10, 15 and 20 minutes in a random order. An hour of wait time is provided between each stimulation so as to reduce any residual plasticity effects from the last one. Once all the combinations of stimulation ($45 \times 4 = 180$) are complete, we look at the the L_{max} trajectories and rank the effects of stimulation on them as a binary decision of 1 and 0. The value of 1 is assigned to cases where the L_{max} is at a lower value than its mean and the stimulation is able to pick it back up. This is illustrated with the help of Figure 7.6(a) where we can see that the L_{max} profile dropped from its mean level and as soon as stimulation started the profile was pulled back up. In this case however, as soon as stimulation was stopped the profile went back down, indicating that a longer stimulation may have been beneficial. Likewise a value of 0 is assigned to the case when the L_{max} drops but stimulation on a certain pair for a certain amount of time has no considerable effect on the L_{max} profile. To illustrate, we refer to Figure 7.6(b), where the stimulation had no effect but at all.

Once the table is filled, we look at the effects of stimulation. The column "Sum" in Table 7.1 is simply adding up the effects of stimulating a pair of electrodes. From this, we choose only those electrodes as maximally effective in disentraining the brain dynamics if

Table 7.3: Effect of stimulation on Lyapunov Profile for Rat13.

Pair	5m	10m	15m	20m	Sum	Pair	5m	10m	15m	20m	Sum
F3-F4	1	0	1	1	3	LT-RL	1	1	1	1	4
F3-LT	1	0	0	0	1	RT-LA	0	1	1	1	3
F3-RT	0	0	1	0	1	RT-RA	0	0	1	1	2
F3-LA	0	1	0	1	2	RT-LM	0	0	0	0	0
F3-RA	0	0	0	0	0	RT-RM	0	0	1	0	1
F3-LM	0	0	0	1	1	RT-LL	0	0	0	1	1
F3-RM	0	1	1	1	3	RT-RL	0	0	1	1	2
F3-LL	0	1	1	1	3	LA-RA	0	0	1	0	1
F3-RL	0	0	0	1	1	LA-LM	1	0	0	1	2
F4-LT	1	1	1	1	4	LA-RM	0	0	0	0	0
F4-RT	0	1	0	1	2	LA-LL	1	0	0	1	2
F4-LA	1	1	1	0	3	LA-RL	0	0	0	1	1
F4-RA	0	1	1	1	3	RA-LM	0	1	0	0	1
F4-LM	0	1	0	1	2	RA-RM	0	0	0	1	1
F4-RM	0	0	0	1	1	RA-LL	1	0	1	0	2
F4-LL	1	1	1	1	4	RA-RL	1	1	0	1	3
F4-RL	0	1	1	1	3	LM-RM	0	0	1	0	1
LT-RT	0	0	0	1	1	LM-LL	1	0	0	1	2
LT-LA	0	1	1	1	3	LM-RL	0	1	0	0	1
LT-RA	1	1	0	0	2	RM-LL	1	1	1	1	4
LT-LM	0	0	1	1	2	RM-RL	1	0	1	0	2
LT-RM	1	0	0	0	1	LL-RL	1	1	1	0	3
LT-LL	1	1	1	1	4						

Table 7.4: Aggregate effect of stimulation on Lyapunov Profile for Rat13.

	5m	10m	15m	20m
1	17	20	23	29
0	28	25	22	16

the sum is 4 or 3. Likewise Table 7.2 provides a summary of how the length of stimulation affects disentrainment irrespective of which channel is being stimulated. What is curious to find here is that as the length of stimulation is increased the number of pairs which get disentrained by stimulation increases (Row 1 in the table). Tables 7.3 and 7.4 show the results from the same experiments carried out on Rat 13. In the same manner as in Rat 12, with Rat 13, the increase in stimulation length causes more sites to disentrain.

From the creation of these control efficacy maps it is quite apparent that stimulation of arbitrary electrodes may not bring about the desired effect. The same is true if the duration (i.e., energy) of the stimulus is not high enough as given by the stimulation current, pulse width, frequency etc. So far in our study we have not investigated the effects of other parameters than the stimulation length. For these experiments the other parameters were chosen as specified in Section 5.3.2.1. Finally we are equipped with sufficient information of "where" and "when" to stimulate the epileptic brain. In the next section we provide results from our closed-loop experiments.

7.4 Results of Closed Loop Control Experiments

While seizures can be predicted with good sensitivity and specificity [57, 63, 85, 84], the question remains if we can intervene effectively to change the brain dynamics and prevent a seizure from occurring. We have already provided results from our work which shows that the applied electrical stimulation dynamically disentrains the brain sites. This constitutes evidence that electrical stimulation can actually change the spatio-temporal dynamics of the brain in the desired direction (Figure 7.6(a)), and hence has been used as actuation in a control scheme for epileptic seizure prevention in the work reported here. This work entails an expansion to our proof-of-concepts for the development of an efficacious controller for the epileptic brain using adaptive spatially distributed control. The developed controller (online) has been validated in vivo. Our main thrust includes multivariable stimulation with guidance from focus localization techniques and multivariable modeling that we have presented in the preceding sections in this chapter of the report, and the use of pulse-train-modulated signals for implementation of a realistic adaptive stimulation.

During the course of this study we have shown that impulsive electrical stimulation does desynchronize the rat's epileptic brain dynamics, provided that the stimulus duration and the electrode location is chosen wisely, i.e., based on a prior "control efficacy" experiment (Tables 7.1 and 7.3). So, our choice of electrical stimulation as a control input appears to be a viable candidate. For a realistic and feasible implementation of the desired effect, the input

to the system is chosen as a biphasic control signal with its pulse-width or pulse-number modulated to accomplish the desynchornization of the brain dynamics. Following the results shown in Tables 7.2, 7.4 we chose a minimum stimulation time of 5 minutes and a maximum of 20 minutes for the closed-loop control experiments. The length of stimulation starts off at 10 minutes when the experiment begins but adaptively increases in increments of 2 minutes if the number of seizure warnings keep increasing within a moving 2 hour window. This allows for more energy in stimulation to be delivered to the brain if the stimulation was not effective. Likewise, the stimulation length will be decreased by 2 minutes as well if in a moving 2 hour window the number of seizure precursor warnings decrease.

Although, data from Rat 12 was available to complete Table 7.1, the rat was euthanized due to head-cap breakage soon after and no closed-loop control experiment was performed on it. Figure 7.7 shows the efficacy of applying stimulation to Rat 13 over a 10 week period. The animal was allowed 4 weeks of rest after Status Epilepticus (SE) was induced so that the seizure frequency stabilized. Following this recuperation period the experiments started. The details of each experiment are provided in Table 7.5. Here the "Week" label does not always imply an actual week (typically +/- one day from a week) but a recording file which goes from the beginning to the end of the experiments. At first, 5 "weeks" of baseline recording was done and on the sixth week stimulation was applied to a set of electrodes, every time a "seizure warning" was generated by the computer system when it detected a drop of L_{max} beyond a threshold. The pairs of electrodes that were stimulated are F3-F4, F3-LT, F3-RA, F4-LT, F4-LA, F4-LL, LT-LL, LT-RL, RA-RL, LM-RM, LM-LL, LM-RL and RM-LL; these were selected based on the "control efficacy maps" we discussed earlier. Each time a seizure warning is generated the algorithm randomly picks one of these pairs and stimulates them. As we can see from the plot of seizure lengths and seizure frequency (seizures per 168 hours) in Figure 7.7(a) and Figure 7.7(b) respectively, the length of seizures decreased during the stimulation weeks. The 10th experiment ("week") was recorded after about a month of stimulation cessation and we can see that both seizure

Table 7.5: Beginning, end and length of experiments on Rat13. Information on whether closed-loop control was performed or not is provided in column 5.

File	Start Date	End Date	Duration	Stimulation
Week 1	25 Nov 2015	2 Dec 2015	175 hrs	No
Week 2	2 Dec 2015	10 Dec 2015	179 hrs	No
Week 3	21 Dec 2015	29 Dec 2015	187 hrs	No
Week 4	29 Dec 2015	7 Jan 2016	215 hrs	No
Week 5	7 Jan 2016	19 Jan 2016	287 hrs	No
Week 6	29 Jan 2016	6 Feb 2016	191 hrs	Yes
Week 7	6 Feb 2016	15 Feb 2016	238 hrs	Yes
Week 8	18 Feb 2016	25 Feb 2016	168 hrs	Yes
Week 9	26 Feb 2016	1 Mar 2016	91 hrs	Yes
Week 10	6 Apr 2016	12 Apr 2016	144 hrs	No

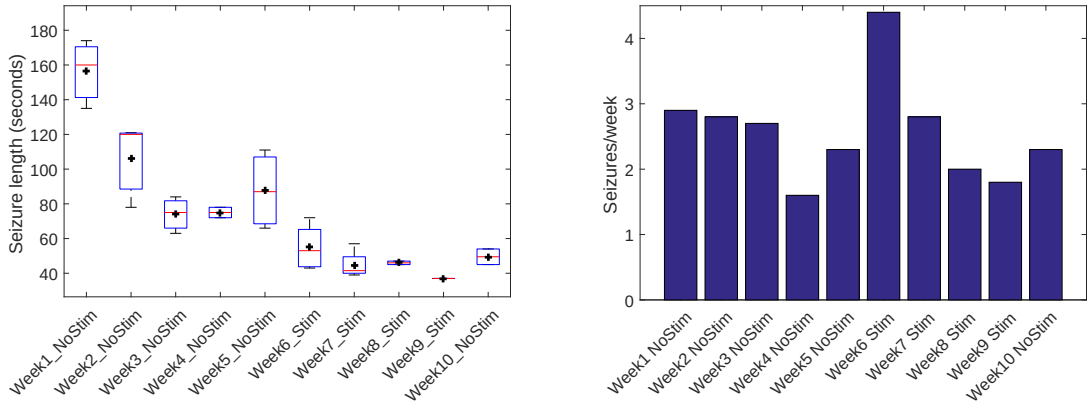

(a) (b)

Figure 7.7: (a) Shows the box and whisker plots of seizure lengths for Rat 13 over the course of 10 weeks preceded by 4 weeks of rest after status epilepticus induction. The black dots indicate the mean of each box. (b) Average number of seizures per day for the same rat over the same 10 week period of experimentation. Here week essentially imply a recording file which in general is never exactly 168 hrs. The first 5 weeks were baseline recording, thus no stimulation was provided. The files in which closed-loop control was provided shows shorter seizure lengths and lower seizure frequency as compared to those in the baseline period. Week 10 was another case of no stimulation but this was recorded 5 weeks after the end of the week 9 file. No stimulation was provided during those 5 weeks and it can be seen that the seizure lengths and the seizure rate per week both had started to increase gradually.

lengths and frequency had gone up; this is possibly due to any residual plasticity effects of the stimulation wearing out. On the other hand, through scrutiny it can be seen that during the first week of stimulation (week 5) both seizure length and frequency were higher than before they were stimulated. During this week the adaptive stimulation was not implemented. Every time a seizure warning was generated one of the pairs of sites mentioned earlier was stimulated with a fixed 5 minute duration. Based on this result we can say that small stimulations may in fact increase seizure susceptibility in epileptic rats. All other "weeks" of stimulation had the adaptive stimulation algorithm implemented.

One more finding in our study was that when the "Sum" for Rat 12 and Rat 13 had values of [4,4], [4,3] and [3,4] for an electrode pair, we assume that stimulation of those pairs are most likely to bring about disentrainment. This is justified since the same pairs seem to have similar disentrainment effect on both animals. While this result is not statistically accurate, it is a good starting point. Comparing Tables 7.1 and 7.3 such pairs are F3-F4, F4-LT, F4-LA, F4-LL, LT-LL, LT-RL, RA-RL and RM-LL. Inspecting the stimulation of these sites on Rat 13 we expect no seizure to follow. Looking at the results we see that a seizure occured in 2 minutes of when F4-LA was stimulated, this is probably because the stimulation did not start early enough. Another case was when F4-LA was stimulated only

Table 7.6: Details of number of times the best candidate electrode pairs were stimulated on Rat 13. The randomization algorithm missed stimulating RM-LL altogether due to an implementation error. Looking at the average performance each week we can see that stimulating these pairs reduced the number of warnings generated as time progressed with the exception of the second week, where an inverse response characteristic can be seen.

Electrodes	Week 6	Week 7	Week 8	Week 9	Total
F3-F4	22	24	13	6	65
F4-LT	22	23	10	4	59
F4-LA	28	34	11	6	79
F4-LL	26	25	13	3	67
LT-LL	21	44	13	9	87
LT-RL	23	22	15	9	69
RA-RL	19	22	12	5	58
Average	23	27.7	12.4	6	

for 5 minutes and a seizure occured about 20 mins following that; this can be justified by the fact that 5 minutes of stimulation was probably insufficient. A similar scenario was observed with F4-LL being stimulated for 5 minutes and a seizure occured 10 minutes after that; once again the stimulation had too low energy. The last case was when LT-LL was stimulated and a seizure occured within 2 minutes; once more stimulation was provided but not soon enough. Other than these cases there were no instances of a seizure following the stimulation of any of these pairs. A list of how many times each of these pairs were stimulated is provided in Table 7.6. It can be seen here, that as the weeks progressed, the number of seizure warnings started to decrease as well, indicating that these pairs were positively affecting brain dynamics to remain more in the chaotic (healthy) stages.

Overall, our results are encouraging since [131] had shown that seizures can be made shorter by stimulation at the detection of a seizure and [108] reported on how stimulation had brought about a mean reduction in seizure frequency of 75.6% over 36 month period in 4 patients. We now focus our attention to Rat 14 which was stimulated in sites F3-F4, F3-LT, F3-RA, F4-LT, F4-LA, F4-LL, LT-LL, LT-RL, RA-RL, LM-RM, LM-LL, LM-RL and RM-LL based on results from GPDC analysis. Table 7.7 provides the duration of experiments carried out on Rat 14 after the 4 weeks of recuperation time. It must be pointed out that Rat 14 had almost 30 times as many seizures as Rat 13. Figures 7.8(a) and 7.8(b) show the seizure lengths and average seizure frequency (per 168 hours) respectively. All stimulation experiments in this case had the adaptive implementation. While seizure frequency was seen to decrease, no conclusive statement about the length of seizures can be made. What can be commented on, is the fact that the length of seizures in Rat 14 was already less than half that of Rat 13 before stimulation. Since Rat 14 seizes so often its seizure lengths probably had to be shorter because the neurons need to re-energize before discharging and could not get sufficient time to do so. Thus reducing the length of the seizures did not seem feasible, however, the seizure frequency clearly reduced, albeit not to a great extent. A summary of the results from Rat 13 and 14 are provided in Table 7.8.

Table 7.7: Beginning, end and length of experiments on Rat14. Information on whether closed-loop control was performed or not is provided in column 5.

File	Start Date	End Date	Duration	Stimulation
Week 1	10 Mar 2016	18 Mar 2016	189 hrs	No
Week 2	18 Mar 2016	24 Mar 2016	139 hrs	No
Week 3	12 Apr 2016	14 Apr 2016	34 hrs	No
Week 4	14 Apr 2016	20 Apr 2016	138 hrs	No
Week 5	22 Apr 2016	28 Apr 2016	152 hrs	Yes
Week 6	28 Apr 2016	5 May 2016	147 hrs	Yes
Week 7	5 May 2016	12 May 2016	147 hrs	Yes
Week 8	17 May 2016	25 May 2016	191 hrs	Yes
Week 9	25 May 2016	5 Jun 2016	263 hrs	Yes
Week 10	7 Jun 2016	17 Jun 2016	241 hrs	Yes
Week 11	23 Jun 2016	27 Jun 2016	93 hrs	Yes
Week 12	27 Jun 2016	5 Jul 2016	188 hrs	Yes

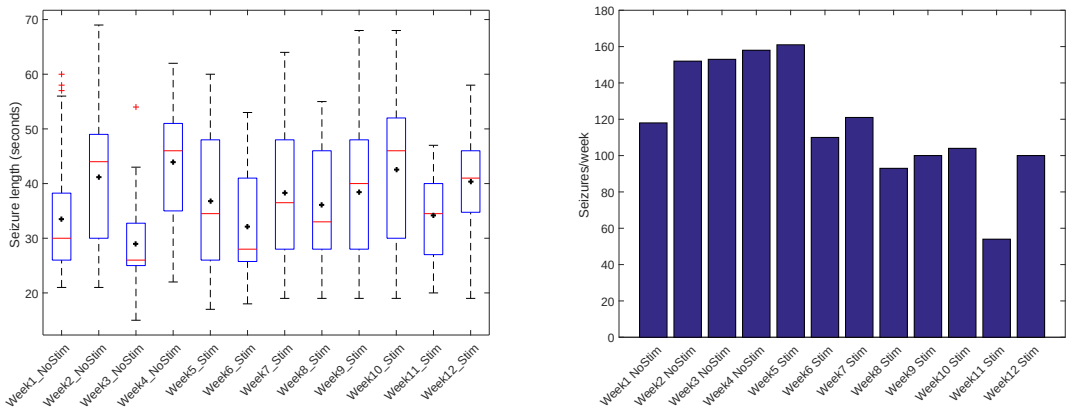

(a) (b)

Figure 7.8: (a) Shows the box and whisker plots of seizure lengths for Rat 14 over the course of 15 weeks preceded by 4 weeks of rest after status epilepticus induction. The black dots indicate the mean of each box. (b) Average number of seizures per day for the same rat over the same 15 week period of experimentation. Here week essentially imply a recording file which in general is never exactly 168 hrs. The first 4 weeks were baseline recording, thus no stimulation was provided. A clear difference in seizure frequency can be observed when comparing non-stimulation files to the ones where closed-loop control was provided. The same cannot be said about seizure lengths for this rat.

Table 7.8: Summary of average seizure length ("seconds") and average seizure frequency ("seizures/hour") along with the percentage changes for both Rat 13 and Rat 14. The comparisons in the "Before" and "After" columns imply the results before closed-loop control experiments were performed and the ones after.

	Rat 13			Rat 14		
	Before	After	% Change	Before	After	% Change
Avg. length	100.73	48.58	51.77	38.69	37.99	1.81
Avg. freguency	0.0144	0.014	2.78	0.8404	0.6365	24.26

7.5 Conclusions

In this chapter we finally presented results from closed-loop control experiments. While the problem is not anywhere near being solved, our results indicate certain advantages are to be gained from multivariable spatial inputs of stimulation. A key ingredient that could be incorporated into our L_{max} computation profile is along the lines of what was reported in [19], where preictal states were classified using support vector machines but then arbitrary tranistions in the output profile was smoothed out using a Kalman filter. Such an implementation could possibly reduce the number of false warnings that our seizure prediction algorithms generate. This would benefit the closed-loop strategy by being more power efficient and not stimulating the brain when not needed. Additionally, the Control Efficacy Maps presented here are essentially tables of binary decisions. A more elegant approach would be to create a dynamical system from the control input(stimulation) to the output(L_{max}) after which PID controllers could be designed using methods described in [129]. While we do recognize that results from only two animals is not statistically relevant, it does shine light on our conjecture that controlling seizures will require proper tuning of stimulation length, location and possibly more parameters in the stimulation signal; essentially an expansion to our Control Efficacy Maps.

Chapter 8

CONCLUSIONS AND FUTURE DIRECTIONS

As the ability to better detect and predict leads to the possibility of control, research in control of seizures is expected to flourish in the near future, much to the benefit of patients with intractable epilepsy. Investigations in stimulation and control of the brain have attracted the attention of the academic community at an explosive rate. Likewise, medical device companies have spun off into designing and implementing intervention devices for epilepsy, with clinical trials underway to test potential prediction and intervention methodology and devices for FDA approval.

Electromagnetic stimulation and/or administration of anti-epileptic drugs at the beginning of the preictal period, to disrupt the observed entrainment of the brain with the epileptogenic focus, may result in a significant reduction of the number and severity of epileptic seizures. Our underlying hypothesis is that an epileptic seizure will be prevented if an external intervention successfully resets the brain prior to the seizure's occurrence. Results from our experiments produced in this document have shown that both the length of seizures and the rate can be lowered by such means. However, it is very important to investigate the parameters that lead to maximum efficacy and minimum side effects of such an intervention. Experimental results provided so far proves that this is not an intractable problem any longer.

We have shown that a successful and robust controller should be correcting the pathological part of the system, that is where the coupling between brain sites increases excessively; a situation the existing internal feedback in the brain cannot compensate for. To this end, we have shown how L_{max} computed using the tuned Kantz algorithm can be treated as a synchronization measure (output) of interest. The method exploited in our work involving the reliable computation of Lyapunov exponents can be utilized

in generating a highly accurate automated seizure detection system as well. A reliable seizure detection mechanism will aid medical practitioners by reducing time to diagnose and therefore strategize a better treatment plan for patients in epilepsy.

Based on results provided in the preceding chapters, we expect that the envisioned active real-time seizure detection and feedback control techniques will mature into a technology for intervention and control of the transition of the brain towards epileptic seizures and would result in a novel and effective treatment of epilepsy. The "heavy machinery" of computing Lyapunov exponents is a significant overhead to be paid, as compared to existing linear measures, in order to improve the reliability of seizure detection and prevention algorithms. Computational power is definitely of great concern, especially if the technology is to be applied in a portable fashion so that patients can go on with their day-to-day lives without interference. Considerations must be taken into account of how the devices can perform big data operations while at the same time being small enough to be portable. The ultimate goal is to provide a seizure-free epileptic brain capable of functioning "normally", with minimum time-wise and power-wise intervention and side effects with the help of these advancements. We envision that this technology will eventually enable a long anticipated new mode of treatment for other brain dynamical disorders too, with neuromodulation, anti-epileptic drugs and electromagnetic stimuli as its actuators.

In this dissertation we were only able to produce closed-loop control experiment results from two animals. The reason being these experiments are long, in the order of weeks, thus analysis of results and producing meaningful interpretations take quite a while. Added to the difficulty is when an animal will cease due to health issues. In such cases the experiments have to be restarted with a new animal. Mortality rates for animals are typically between 40% - 60% after Status Epilepticus is induced. Another miscreant to the mortality rate is headcap breakage, whereby during a seizure a rat would violently hit the cage walls and the recording headcap will break off; in such cases euathanizing the animal is the only remaining option. Additionally as in the case of Rat 14, we have seen significant degradation of signal

quality after a few months of electrode implantation. The theory is that the accumulation of glial cells around the electrodes change their impedance and therefore SNR output. A future study is being planned where better electrodes will be utilized to get clean signals for longer experiments. With this, we conclude this dissertation by listing the topics covered in preceding chapters followed by a discussion of possible future directions that can further the results we have obtained so far.

A brief review of the history of epilepsy and the research done in the field is presented in Chapter 1. Chapter 2 discussed the theory of nonlinear dynamics, chaotic systems and its relevance to the epilepsy problem. The maximum Lyapunov exponent, a measure of chaoticity of a dynamical system, was introduced in Chapter 3 and the most robust method of computing it was presented. In Chapter 4, the algorithm to compute the generalized partial directed coherence was presented along with justification for the choice of GPDC computation parameters. Chapter 5 went into the details of the experimental setup, starting from how the animals are made epileptic to the construction of the multivariable control input system and all the relevant hardware and software utilized in the study. Chapters 6 and 7 provides results in seizure detection, focus localization, control efficacy maps and closed-loop control that we obtained during the course of this work. We showed how, although many researchers are looking into an accurate prediction scheme, it may be noteworthy that given a good control action, 100% accurate prediction may not be necessary. Any warning for seizure may be utilized to desyncrhonize the epileptic dynamics in the brain and abort an impending seizure.

8.1 Future Work

To wrap up, we present in the following, a list of prospective future work that may further the advancement of research in this topic of interest -

- The GPDC algorithm suffers largely from the MVAR modeling process. MVAR modeling by nature generates systems that are high pass; this is not very reliable. One future work would be to incorporate some frequency weighting in the MVAR

process so as to get models that are low pass and contain only frequencies of interest.

- GPDC is essentially a normalized inverse transfer function of a sampled data system. After such a light has been shed on the matter, it becomes possible to think of other such measures to try and achieve GPDC-like interaction measures. To that end, future work could involve applying well known system identification techniques as is abundant in the control systems literature. One such method is treating each channel as an input and determining the transfer function that has the rest of the channels as an output.

- Improvement of seizure detection algorithm will entail tuning for both rat and human data. Additionally some form of artificial neural networks may be employed over the simplistic threshold based algorithm being used currently. Thus, feature detection algorithms based either in wavelet matching methods or neural networks such as support vector machines (SVM) or deep-learning algorithms could make the automation of seizure detection more robust to artifacts in the data.

- Another potential addition to the seizure detection algorithm would be to accurately mark the electrographic onset (see Appendix B) of a seizure based on L_{max} profiles. If successful this could lend a hand to doctors in marking the exact time that a seizure is starting and not just an approximate time of when the seizure is detected.

- Porting the L_{max} code to a GPU or other accelerator device would improve speed of analysis by orders of magnitude. Efficient GPU code development will involve data pipelining, increased parallelism and efficient memory usage. The application benefit of such a scheme may allow real-time detection for human EEG that involves high volumes of data to be analyzed.

- A possible future direction in this work will entitle generating dynamical system models from the applied stimulus (input) to the Lyapunov exponents (outputs) as an improvement to the "Control Efficacy Maps". The inputs, as always, will be

time modulated with a biphasic impulse train since this is the type of signal that gave us better decoupling results so far. It is worth mentioning that the measure of synchronization can include, but not be limited to, Lyapunov exponents computed from EEG and other biomarkers such as heart rate, pulse oxygen levels, body temperature, etc. A parameterization of these signals in terms of their duration, frequency, and location should also be considered in order to eventually develop a comprehensive input-output model from the average stimulus power to the output of interest.

- A great challenge at this moment is that whenever stimulation is applied the EEG signal is corrupted, thus computing L_{max} accurately becomes difficult. A future improvement could involve stimulating with currents in the range of or lower than EEG signals. Additionally the stimulation could be EEG like in shape and form instead of being biphasic.

REFERENCES

[1] A-M Systems, "Digital stimulus isolator model 2300", URL http://www.a-msystems.com/s-140-digital-stimulus-isolator-model-2300.aspx (2013).

[2] Aarabi, A., R. Fazel-Rezai and Y. Aghakhani, "Eeg seizure prediction: Measures and challenges", in "2009 Annual International Conference of the IEEE Engineering in Medicine and Biology Society", pp. 1864–1867 (2009).

[3] Abarbanel, H. D. and J. P. Gollub, "Analysis of observed chaotic data", Physics Today **49**, 86 (1996).

[4] Albo, Z., G. V. D. Prisco, Y. Chen, G. Rangarajan, W. Truccolo, J. Feng, R. P. Vertes and M. Ding, "Is partial coherence a viable technique for identifying generators of neural oscillations?", Biol. Cybern. **90**, 5, URL http://dx.doi.org/10.1007/s00422-004-0475-5 (2004).

[5] Annegers, J. F., W. A. Rocca and W. A. Hauser, "Causes of epilepsy: contributions of the rochester epidemiology project", in "Mayo Clinic Proceedings", vol. 71, pp. 570–575 (Elsevier, 1996).

[6] Aram, P., R. Postoyan and M. Cook, "Patient-specific neural mass modeling-stochastic and deterministic methods", Recent Advances in Predicting and Preventing Epileptic Seizures p.63 (2013).

[7] Astolfi, L., F. Cincotti, D. Mattia, M. Marciani, L. Baccalá, F. Fallani, S. Salinari, M. Ursino, M. Zavaglia and F. Babiloni, "Assessing cortical functional connectivity by partial directed coherence: simulations and application to real data", IEEE Transactions on Biomedical Engineering **53**, 9, 1802–1812, URL http://dx.doi.org/10.1109/TBME.2006.873692 (2006).

[8] Baccalá, L., K. Sameshima, G. Ballester, A. Do Valle and C. Timo-Iaria, "Studying the interaction between brain structures via directed coherence and granger causality", Applied Signal Processing **5**, 1, 40 (1998).

[9] Baccalá, L. A. and K. Sameshima, "Partial directed coherence: a new concept in neural structure determination", Biological Cybernetics **84**, 6, 463–474, URL http://dx.doi.org/10.1007/PL00007990 (2001).

[10] Baccalá, L. A., K. Sameshima and D. Y. Takahashi, "Generalized partial directed coherence", in "2007 15th International Conference on Digital Signal Processing", pp. 163–166 (2007).

[11] Beverlin, B. and T. I. Netoff, "Dynamic control of modeled tonic-clonic seizure states with closed-loop stimulation", Frontiers in Neural Circuits **6**, URL http://dx.doi.org/10.3389/fncir.2012.00126 (2013).

[12] Boroojerdi, B., A. Prager, W. Muellbacher and L. G. Cohen, "Reduction of human visual cortex excitability using 1-hz transcranial magnetic stimulation", Neurology **54**, 7, 1529–1531 (2000).

[13] Center for Disease Control and Prevention, "Epilepsy fast facts", URL http://www.cdc.gov/epilepsy/basics/fast-facts.htm (2016).

[14] Chakravarthy, N., *A feedback systems perspective for modeling and controlling epileptic seizures*, Ph.D. thesis, Arizona State University, URL http://login.ezproxy1.lib.asu.edu/login?url=http://search.proquest.com/docview/304895784?accountid=4485, copyright - Copyright UMI - Dissertations Publishing 2007; Last updated - 2015-08-23; First page - n/a (2007).

[15] Chakravarthy, N., S. Sabesan, K. Tsakalis and L. Iasemidis, "Controlling epileptic seizures in a neural mass model", J Comb Optim **17**, 1, 98–116, URL http://dx.doi.org/10.1007/s10878-008-9182-9 (2008).

[16] Chakravarthy, N., K. Tsakalis, L. D. Iasemidis and A. Spanias, "A multi-dimensional scheme for controlling unstable periodic orbits in chaotic systems", Physics Letters A **349**, 1-4, 116-127, URL http://www.sciencedirect.com/science/article/pii/S0375960105013642 (2006).

[17] Cheung, B. L. P., R. Nowak, H. C. Lee, W. Drongelen and B. D. Veen, "Cross validation for selection of cortical interaction models from scalp eeg or meg", IEEE Transactions on Biomedical Engineering **59**, 2, 504–514 (2012).

[18] Cheung, B. L. P., B. A. Riedner, G. Tononi and B. V. Veen, "Estimation of cortical connectivity from EEG using state-space models", IEEE Transactions on Biomedical Engineering **57**, 9, 2122–2134, URL http://dx.doi.org/10.1109/TBME.2010.2050319 (2010).

[19] Chisci, L., A. Mavino, G. Perferi, M. Sciandrone, C. Anile, G. Colicchio and F. Fuggetta, "Real-time epileptic seizure prediction using AR models and support vector machines", IEEE Transactions on Biomedical Engineering **57**, 5, 1124–1132, URL http://dx.doi.org/10.1109/TBME.2009.2038990 (2010).

[20] Chkhenkeli, S. A., M. Šramka, G. S. Lortkipanidze, T. N. Rakviashvili, E. S. Bregvadze, G. E. Magalashvili, T. S. Gagoshidze and I. S. Chkhenkeli, "Electrophysiological effects and clinical results of direct brain stimulation for intractable epilepsy", Clinical neurology and neurosurgery **106**, 4, 318–329 (2004).

[21] Cignetti, F., L. M. Decker and N. Stergiou, "Sensitivity of the wolf's and rosenstein's algorithms to evaluate local dynamic stability from small gait data sets", Annals of Biomedical Engineering **40**, 5, 1122–1130, URL http://dx.doi.org/10.1007/s10439-011-0474-3 (2011).

[22] Citizens for Research in Epilepsy., "Epilepsy facts", http://www.cureepilepsy.org/aboutepilepsy/facts.asp, URL http://www.cureepilepsy.org/aboutepilepsy/facts.asp (2016).

[23] Claassen, J., S. A. Mayer, R. G. Kowalski, R. G. Emerson and L. J. Hirsch, "Detection of electrographic seizures with continuous eeg monitoring in critically ill patients", Neurology **62**, 10, 1743–1748, URL http://www.neurology.org/content/62/10/1743.abstract (2004).

[24] Curia, G., D. Longo, G. Biagini, R. S. Jones and M. Avoli, "The pilocarpine model of temporal lobe epilepsy", Journal of Neuroscience Methods **172**, 2, 143–157, URL http://dx.doi.org/10.1016/j.jneumeth.2008.04.019 (2008).

[25] Da Silva, F. L., W. Blanes, S. N. Kalitzin, J. Parra, P. Suffczynski and D. N. Velis, "Epilepsies as dynamical diseases of brain systems: basic models of the transition between normal and epileptic activity", Epilepsia **44**, s12, 72–83 (2003).

[26] Dodson, W. E. and M. J. Brodie, "Efficacy of antiepileptic drugs", Epilepsy: A comprehensive textbook **2**, 1185–1192 (2008).

[27] Edward, L., "Predictability: Does the flap of a butterfly's wings in brazil set off a tornado in texas?", American Association for the Advancement of Science, Washington, DC (1972).

[28] Engel, J., *Seizures and epilepsy*, vol. 83 (Oxford University Press, 2013).

[29] Faes, L., S. Erla and G. Nollo, "Measuring connectivity in linear multivariate processes: Definitions, interpretation, and practical analysis", Computational and Mathematical Methods in Medicine **2012**, 1–18, URL http://dx.doi.org/10.1155/2012/140513 (2012).

[30] Fisher, R. S., G. L. Krauss, E. Ramsay, K. Laxer and J. Gates, "Assessment of vagus nerve stimulation for epilepsy: report of the therapeutics and technology assessment subcommittee of the american academy of neurology", Neurology **49**, 1, 293–297 (1997).

[31] Food and Drug Administration., "RNS System", URL http://www.fda.gov/MedicalDevices/ProductsandMedicalProcedures/DeviceApprovalsandClearances/Recently-ApprovedDevices/ucm376685.htm (2015).

[32] Forsgren, L., "Prospective incidence study and clinical characterization of seizures in newly referred adults", Epilepsia **31**, 3, 292–301 (1990).

[33] Gabor, A., R. Leach and F. Dowla, "Automated seizure detection using a self-organizing neural network", Electroencephalography and clinical Neurophysiology **99**, 3, 257–266 (1996).

[34] Gardner, A. B., A. M. Krieger, G. Vachtsevanos and B. Litt, "One-class novelty detection for seizure analysis from intracranial eeg", J. Mach. Learn. Res. **7**, 1025–1044, URL http://dl.acm.org/citation.cfm?id=1248547.1248584 (2006).

[35] Georgis, G., G. Menoutis, D. Reisis, K. Tsakalis and A. B. Shafique, "Towards real-time neuronal connectivity assessment: A scalable pipelined parallel generalized partial directed coherence engine", in "2015 IEEE International Conference on Electronics, Circuits, and Systems (ICECS)", pp. 13–16 (2015).

[36] Georgis, G., D. Reisis, P. Skordilakis, K. Tsakalis, A. B. Shafique, G. Chatzikonstantis and G. Lentaris, "Neuronal connectivity assessment for epileptic seizure prevention: Parallelizing the generalized partial directed coherence on many-core platforms", in "Embedded Computer Systems: Architectures, Modeling, and Simulation (SAMOS XIV), 2014 International Conference on", pp. 359–366 (IEEE, 2014).

[37] Gómez-Herrero, G., M. Atienza, K. Egiazarian and J. L. Cantero, "Measuring directional coupling between EEG sources", NeuroImage **43**, 3, 497–508, URL http://dx.doi.org/10.1016/j.neuroimage.2008.07.032 (2008).

[38] Good, L. B., S. Sabesan, S. T. Marsh, K. Tsakalis, D. Treiman and L. Iasemidis, "Control of synchronization of brain dynamics leads to control of epileptic seizures in rodents", International Journal of Neural Systems **19**, 03, 173–196, URL http://www.worldscientific.com/doi/abs/10.1142/S0129065709001951 (2009).

[39] Gotman, J. and V. Levtova, "Amygdala-hippocampus relationships in temporal lobe seizures: a phase-coherence study", Epilepsy research **25**, 1, 51–57 (1996).

[40] Granger, C. W., "Investigating causal relations by econometric models and cross-spectral methods", Econometrica: Journal of the Econometric Society pp. 424–438 (1969).

[41] Grassberger, P. and I. Procaccia, "Characterization of strange attractors", Physical review letters **50**, 5, 346–349 (1983).

[42] Grassberger, P. and I. Procaccia, "Measuring the strangeness of strange attractors", Physica D: Nonlinear Phenomena **9**, 1, 189–208 (1983).

[43] Grassberger, P., T. Schreiber and C. Schaffrath, "Nonlinear time sequence analysis", International Journal of Bifurcation and Chaos **01**, 03, 521–547, URL http://www.worldscientific.com/doi/abs/10.1142/S0218127491000403 (1991).

[44] Guo, X., M. Dave and S. Mohamed, "HPCmatlab: A framework for fast prototyping of parallel applications in matlab", Procedia Computer Science **80**, 1461–1472 (2016).

[45] Harlan Laboratories Inc., "Sprague dawley outbred rat", URL http://www.harlan.com/products_and_services/research_models_and_services/research_models/sprague_dawley_outbred_rat/hsdsprague-dawley-sd/us.hl (2013).

[46] Hasselblatt, B. and A. Katok, *A first course in dynamics: with a panorama of recent developments* (Cambridge University Press, 2003).

[47] He, F., S. A. Billings, H.-L. Wei and P. G. Sarrigiannis, "A nonlinear causality measure in the frequency domain: Nonlinear partial directed coherence with applications to EEG", Journal of Neuroscience Methods **225**, 71–80, URL http://dx.doi.org/10.1016/j.jneumeth.2014.01.013 (2014).

[48] He, F., H.-L. Wei, S. A. Billings and P. G. Sarrigiannis, "A nonlinear generalization of spectral granger causality", IEEE Transactions on Biomedical Engineering **61**, 6, 1693–1701, URL http://dx.doi.org/10.1109/TBME.2014.2300636 (2014).

[49] Heck, C. N., D. King-Stephens, A. D. Massey, D. R. Nair, B. C. Jobst, G. L. Barkley, V. Salanova, A. J. Cole, M. C. Smith, R. P. Gwinn *et al.*, "Two-year seizure reduction in adults with medically intractable partial onset epilepsy treated with responsive neurostimulation: Final results of the rns system pivotal trial", Epilepsia **55**, 3, 432–441 (2014).

[50] Hegger, R., H. Kantz and T. Schreiber, "Practical implementation of nonlinear time series methods: The tisean package", Chaos **9**, 2, 413–435, URL http://scitation.aip.org/content/aip/journal/chaos/9/2/10.1063/1.166424 (1999).

[51] Hirtz, D., D. J. Thurman, K. Gwinn-Hardy, M. Mohamed, A. R. Chaudhuri and R. Zalutsky, "How common are the "common" neurologic disorders?", Neurology **68**, 5, 326–337, URL http://www.neurology.org/content/68/5/326.abstract (2007).

[52] Hodaie, M., R. A. Wennberg, J. O. Dostrovsky and A. M. Lozano, "Chronic anterior thalamus stimulation for intractable epilepsy", Epilepsia **43**, 6, 603–608 (2002).

[53] Howbert, J. J., E. E. Patterson, S. M. Stead, B. Brinkmann, V. Vasoli, D. Crepeau, C. H. Vite, B. Sturges, V. Ruedebusch, J. Mavoori, K. Leyde, W. D. Sheffield, B. Litt and G. A. Worrell, "Forecasting seizures in dogs with naturally occurring epilepsy", PLoS ONE **9**, 1, e81920, URL http://dx.doi.org/10.1371/journal.pone.0081920 (2014).

[54] Iasemidis, L., P. Pardalos, J. Sackellares and D.-S. Shiau, "Quadratic binary programming and dynamical system approach to determine the predictability of epileptic seizures", Journal of Combinatorial Optimization **5**, 1, 9–26, URL http://dx.doi.org/10.1023/A:1009877331765 (2001).

[55] Iasemidis, L., A. Prasad, J. Sackellares, P. Pardalos and D. Shiau, "On the prediction of seizures, hysteresis and resetting of the epileptic brain: insights from models of coupled chaotic oscillators", Order and chaos **8**, 283–305 (2003).

[56] Iasemidis, L., S. Sabesan, L. Good, K. Tsakalis and D. Treiman, "Closed-loop control of epileptic seizures via deep brain stimulation in a rodent model of chronic epilepsy", in "World Congress on Medical Physics and Biomedical Engineering, September 7-12, 2009, Munich, Germany", pp. 592–595 (Springer, 2009).

[57] Iasemidis, L., D.-S. Shiau, J. Sackellares, P. Pardalos and A. Prasad, "Dynamical resetting of the human brain at epileptic seizures: Application of nonlinear dynamics and global optimization techniques", IEEE Transactions on Biomedical Engineering **51**, 3, 493–506, URL http://dx.doi.org/10.1109/TBME.2003.821013 (2004).

[58] Iasemidis, L., H. Zaveri, J. Sackellares, W. Williams and T. Hood, "Nonlinear dynamics of electrocorticographic data", J. Clin. Neurophysiol **5**, 339 (1988).

[59] Iasemidis, L. D., "Epileptic seizure prediction and control", IEEE Transactions on Biomedical Engineering **50**, 5, 549–558 (2003).

[60] Iasemidis, L. D., J. Chris Sackellares, H. P. Zaveri and W. J. Williams, "Phase space topography and the Lyapunov exponent of electrocorticograms in partial seizures", Brain Topography **2**, 3, 187–201, URL http://dx.doi.org/10.1007/BF01140588 (1990).

[61] Iasemidis, L. D., J. C. Principe and J. C. Sackellares, "Measurement and quantification of spatiotemporal dynamics of human epileptic seizures", Nonlinear Biomedical Signal Processing: Dynamic Analysis and Modeling, Volume 2 pp. 294–318, URL http://dx.doi.org/10.1109/9780470545379.ch12 (2000).

[62] Iasemidis, L. D. and J. C. Sackellares, "The evolution with time of the spatial distribution of the largest Lyapunov exponent on the human epileptic cortex", Measuring chaos in the human brain pp. 49–82 (1991).

[63] Iasemidis, L. D., D.-S. Shiau, W. Chaovalitwongse, J. C. Sackellares, P. M. Pardalos, J. C. Principe, P. R. Carney, A. Prasad, B. Veeramani and K. Tsakalis, "Adaptive epileptic seizure prediction system", Biomedical Engineering, IEEE Transactions on **50**, 5, 616–627 (2003).

[64] Iasemidis, L. D., H. P. Zaveri, J. C. Sackellares and W. J. Williams, "Phase space analysis of eeg in temporal lobe epilepsy", in "Engineering in Medicine and Biology Society, 1988. Proceedings of the Annual International Conference of the IEEE", pp. 1201–1203 vol.3 (1988).

[65] Intan Technologies LLC., "RHD2000 evaluation system", URL http://intantech.com/RHD2000_evaluation_system.html (2015).

[66] James, C. J. and D. Gupta, "Seizure prediction for epilepsy using a multi-stage phase synchrony based system", in "2009 Annual International Conference of the IEEE Engineering in Medicine and Biology Society", pp. 25–28 (2009).

[67] Jansen, B. H. and V. Rit, "Electroencephalogram and visual evoked potential generation in a mathematical model of coupled cortical columns", Biological Cybernetics **73**, 4, 357–366 (1995).

[68] Johnson, M. D., H. H. Lim, T. I. Netoff, A. T. Connolly, N. Johnson, A. Roy, A. Holt, K. O. Lim, J. R. Carey, J. L. Vitek and B. He, "Neuromodulation for brain disorders: Challenges and opportunities", IEEE Transactions on Biomedical Engineering **60**, 3, 610–624, URL http://dx.doi.org/10.1109/TBME.2013.2244890 (2013).

[69] Kalitzin, S. N., D. N. Velis and F. H. L. da Silva, "Stimulation-based anticipation and control of state transitions in the epileptic brain", Epilepsy & Behavior **17**, 3, 310–323, URL http://dx.doi.org/10.1016/j.yebeh.2009.12.023 (2010).

[70] Kaminski, M. J. and K. J. Blinowska, "A new method of the description of the information flow in the brain structures", Biological Cybernetics **65**, 3, 203–210, URL http://dx.doi.org/10.1007/BF00198091 (1991).

[71] Kantz, H., "A robust method to estimate the maximal Lyapunov exponent of a time series", Physics letters A **185**, 1, 77–87 (1994).

[72] Katherine Miller, "Seizures, in theory: Computational neuroscience and epilepsy", URL http://biomedicalcomputationreview.org/content/seizures-theory-computational-neuroscience-and-epilepsy (2014).

[73] Kerrigan, J. F., B. Litt, R. S. Fisher, S. Cranstoun, J. A. French, D. E. Blum, M. Dichter, A. Shetter, G. Baltuch, J. Jaggi *et al.*, "Electrical stimulation of the anterior nucleus of the thalamus for the treatment of intractable epilepsy", Epilepsia **45**, 4, 346–354 (2004).

[74] Kossoff, E. H., E. K. Ritzl, J. M. Politsky, A. M. Murro, J. R. Smith, R. B. Duckrow, D. D. Spencer and G. K. Bergey, "Effect of an external responsive neurostimulator on seizures and electrographic discharges during subdural electrode monitoring", Epilepsia **45**, 12, 1560–1567 (2004).

[75] Kramer, U., S. Kipervasser, A. Shlitner and R. Kuzniecky, "A novel portable seizure detection alarm system: preliminary results", Journal of Clinical Neurophysiology **28**, 1, 36–38 (2011).

[76] Krishnan, B., I. Vlachos, Z. Wang, J. Mosher, I. Najm, R. Burgess, L. Iasemidis and A. Alexopoulos, "Epileptic focus localization based on resting state interictal {MEG} recordings is feasible irrespective of the presence or absence of spikes", Clinical Neurophysiology **126**, 4, 667 – 674, URL http://www.sciencedirect.com/science/article/pii/S1388245714004052 (2015).

[77] Kuncel, A. M. and W. M. Grill, "Selection of stimulus parameters for deep brain stimulation", Clinical Neurophysiology **115**, 11, 2431–2441, URL http://dx.doi.org/10.1016/j.clinph.2004.05.031 (2004).

[78] Kuroda, Y., "Neurocritical care update", Journal of Intensive Care **4**, 1, 1–10, URL http://dx.doi.org/10.1186/s40560-016-0141-8 (2016).

[79] Lado, F. A., L. Velíšek and S. L. Moshé, "The effect of electrical stimulation of the subthalamic nucleus on seizures is frequency dependent.", Epilepsia (Series 4) **44**, 2, 157 – 164, URL http://search.ebscohost.com.ezproxy1.lib.asu.edu/login.aspx?direct=true&db=aph&AN=9019667&site=ehost-live (2003).

[80] Lai, Y.-C., M. A. F. Harrison, M. G. Frei and I. Osorio, "Inability of Lyapunov exponents to predict epileptic seizures", Phys. Rev. Lett. **91**, 6, URL http://dx.doi.org/10.1103/PhysRevLett.91.068102 (2003).

[81] Le Van Quyen, M., J. Martinerie, V. Navarro, M. Baulac and F. J. Varela, "Characterizing neurodynamic changes before seizures", Journal of Clinical Neurophysiology **18**, 3, 191–208 (2001).

[82] Lehnertz, K., "Epilepsy and nonlinear dynamics", J Biol Phys **34**, 3-4, 253–266, URL http://dx.doi.org/10.1007/s10867-008-9090-3 (2008).

[83] Lehnertz, K., R. G. Andrzejak, J. Arnhold, T. Kreuz, F. Mormann, C. Rieke, G. Widman and C. E. Elger, "Its possible use for interictal focus localization, seizure anticipation, and prevention: Nonlinear eeg analysis in epilepsy", Journal of Clinical Neurophysiology **18**, 3, 209–222 (2001).

[84] Lehnertz, K., S. Bialonski, M.-T. Horstmann, D. Krug, A. Rothkegel, M. Staniek and T. Wagner, "Synchronization phenomena in human epileptic brain networks", Journal of Neuroscience Methods **183**, 1, 42–48, URL http://dx.doi.org/10.1016/j.jneumeth.2009.05.015 (2009).

[85] Lehnertz, K., F. Mormann, H. Osterhage, A. Müller, J. Prusseit, A. Chernihovskyi, M. Staniek, D. Krug, S. Bialonski and C. E. Elger, "State-of-the-art of seizure prediction", Journal of Clinical Neurophysiology **24**, 2, 147–153 (2007).

[86] Lehnertz, K., G. Widman and C. Elger, "Predicting seizures of mesial temporal and neocortical origin", Epilepsia **39**, suppl 6, 205 (1998).

[87] Lennox, W. G., *Science and seizures: new light on epilepsy and migraine* (Harper & Brothers, 1946).

[88] Li, Y., H.-L. Wei, S. A. Billings and X.-F. Liao, "Time-varying linear and nonlinear parametric model for granger causality analysis", Physical Review E **85**, 4, URL http://dx.doi.org/10.1103/PhysRevE.85.041906 (2012).

[89] Liang, S.-F., Y.-C. Liao, F.-Z. Shaw, D.-W. Chang, C.-P. Young and H. Chiueh, "Closed-loop seizure control on epileptic rat models", Journal of Neural Engineering **8**, 4, 045001, URL http://stacks.iop.org/1741-2552/8/i=4/a=045001 (2011).

[90] Lorenz, E. N., "Deterministic nonperiodic flow", Journal of the Atmospheric Sciences **20**, 2, 130–141, URL http://dx.doi.org/10.1175/1520-0469(1963)020⟨0130:DNF⟩2.0.CO;2 (1963).

[91] Lothman, E. W., E. H. Bertram, J. W. Bekenstein and J. B. Perlin, "Self-sustaining limbic status epilepticus induced by "continuous" hippocampal stimulation: electrographic and behavioral characteristics", Epilepsy research **3**, 2, 107–119 (1989).

[92] Lowenstein, D. H., "Epilepsy after head injury: An overview", Epilepsia **50**, 4–9, URL http://dx.doi.org/10.1111/j.1528-1167.2008.02004.x (2009).

[93] Lulic, D., A. Ahmadian, A. A. Baaj, S. R. Benbadis and F. L. Vale, "Vagus nerve stimulation", Neurosurgical focus **27**, 3, E5, URL http://dx.doi.org/10.3171/2009.6.FOCUS09126 (2009).

[94] Milton, J. G., J. Gotman, G. M. Remillard and F. Andermann, "Timing of seizure recurrence in adult epileptic patients: a statistical analysis", Epilepsia **28**, 5, 471–478 (1987).

[95] Mina, F., P. Benquet, A. Pasnicu, A. Biraben and F. Wendling, "Modulation of epileptic activity by deep brain stimulation: a model-based study of frequency-dependent effects", Front. Comput. Neurosci. **7**, URL http://dx.doi.org/10.3389/fncom.2013.00094 (2013).

[96] Montgomery, D. C., *Design and analysis of experiments*, vol. 7 (Wiley New York, 1984).

[97] Mormann, F., T. Kreuz, R. G. Andrzejak, P. David, K. Lehnertz and C. E. Elger, "Epileptic seizures are preceded by a decrease in synchronization", Epilepsy Research **53**, 3, 173–185, URL http://dx.doi.org/10.1016/S0920-1211(03)00002-0 (2003).

[98] Mormann, F., T. Kreuz, C. Rieke, R. G. Andrzejak, A. Kraskov, P. David, C. E. Elger and K. Lehnertz, "On the predictability of epileptic seizures", Clinical Neurophysiology **116**, 3, 569–587, URL http://dx.doi.org/10.1016/j.clinph.2004.08.025 (2005).

[99] Mountcastle, V. B., "The columnar organization of the neocortex.", Brain **120**, 4, 701–722, URL http://brain.oxfordjournals.org/content/120/4/701 (1997).

[100] Nair, S. P., P. I. Jukkola, M. Quigley, A. Wilberger, D. S. Shiau, J. C. Sackellares, P. M. Pardalos and K. M. Kelly, "Absence seizures as resetting mechanisms of brain dynamics", Cybernetics and Systems Analysis **44**, 5, 664–672, URL http://dx.doi.org/10.1007/s10559-008-9051-7 (2008).

[101] Nandan, M., S. S. Talathi, S. Myers, W. L. Ditto, P. P. Khargonekar and P. R. Carney, "Support vector machines for seizure detection in an animal model of chronic epilepsy", Journal of Neural Engineering **7**, 3, 036001, URL http://stacks.iop.org/1741-2552/7/i=3/a=036001 (2010).

[102] Natus Medical Inc., "Natus Neurolink IP128", URL http://www.natus.com/index.cfm?page=products_1&crid=223 (2016).

[103] Niedermeyer, E. and F. H. L. da Silva, *Electroencephalography: basic principles, clinical applications, and related fields* (Wolters Kluwer Health, 2005).

[104] Nissinen, J., T. Halonen, E. Koivisto and A. Pitkänen, "A new model of chronic temporal lobe epilepsy induced by electrical stimulation of the amygdala in rat", Epilepsy research **38**, 2, 177–205 (2000).

[105] Oestreicher, C., "A history of chaos theory", Dialogues in clinical neuroscience **9**, 3, 279–89 (2007).

[106] Omidvarnia, A. H., M. Mesbah, M. S. Khlif, J. M. O'Toole, P. B. Colditz and B. Boashash, "Kalman filter-based time-varying cortical connectivity analysis of newborn eeg", in "2011 Annual International Conference of the IEEE Engineering in Medicine and Biology Society", pp. 1423–1426 (2011).

[107] Osorio, I., M. G. Frei, S. Sunderam, J. Giftakis, N. C. Bhavaraju, S. F. Schaffner and S. B. Wilkinson, "Automated seizure abatement in humans using electrical stimulation", Annals of neurology **57**, 2, 258–268 (2005).

[108] Osorio, I., J. Overman, J. Giftakis and S. B. Wilkinson, "High frequency thalamic stimulation for inoperable mesial temporal epilepsy", Epilepsia **48**, 8, 1561–1571 (2007).

[109] Ott, E., C. Grebogi and J. A. Yorke, "Controlling chaos", Physical review letters **64**, 11, 1196 (1990).

[110] Packard, N. H., J. P. Crutchfield, J. D. Farmer and R. S. Shaw, "Geometry from a time series", Physical Review Letters **45**, 712–716, URL http://link.aps.org/doi/10.1103/PhysRevLett.45.712 (1980).

[111] Pardalos, P. M., W. Chaovalitwongse, L. D. Iasemidis, J. C. Sackellares, D.-S. Shiau, P. R. Carney, O. A. Prokopyev and V. A. Yatsenko, "Seizure warning algorithm based on optimization and nonlinear dynamics", Mathematical Programming **101**, 2, URL http://dx.doi.org/10.1007/s10107-004-0529-4 (2004).

[112] Parker, T. S. and L. O. Chua, "Chaos: A tutorial for engineers", Proceedings of the IEEE **75**, 8, 982–1008 (1987).

[113] Paz, J. T. and J. R. Huguenard, "Microcircuits and their interactions in epilepsy: is the focus out of focus?", Nature neuroscience **18**, 3, 351–359 (2015).

[114] Penfield, W., "The evidence for a cerebral vascular mechanism in epilepsy", Annals of Internal Medicine **7**, 3, 303–310 (1933).

[115] Poincaré, H., *New methods of celestial mechanics*, vol. 13 (Springer Science & Business Media, 1992).

[116] Pyragas, K., "Control of chaos via an unstable delayed feedback controller", Physical Review Letters **86**, 11, 2265 (2001).

[117] Qu, H. and J. Gotman, "A patient-specific algorithm for the detection of seizure onset in long-term eeg monitoring: possible use as a warning device", IEEE Transactions on Biomedical Engineering **44**, 2, 115–122 (1997).

[118] Quyen, M. L. V., "Anticipating epileptic seizures: from mathematics to clinical applications", Comptes Rendus Biologies **328**, 2, 187–198, URL http://dx.doi.org/10.1016/j.crvi.2004.10.014 (2005).

[119] Racine, R. J., "Modification of seizure activity by electrical stimulation: Ii. motor seizure", Electroencephalography and clinical neurophysiology **32**, 3, 281–294 (1972).

[120] Rosenstein, M. T., J. J. Collins and C. J. De Luca, "A practical method for calculating largest Lyapunov exponents from small data sets", Physica D: Nonlinear Phenomena **65**, 1, 117–134 (1993).

[121] Ruelle, D. and F. Takens, "On the nature of turbulence", Communications in Mathematical Physics **20**, 3, 167–192, URL http://dx.doi.org/10.1007/BF01646553 (1971).

[122] Ruffini, G., F. Wendling, I. Merlet, B. Molaee-Ardekani, A. Mekonnen, R. Salvador, A. Soria-Frisch, C. Grau, S. Dunne and P. C. Miranda, "Transcranial current brain stimulation (tCS): Models and technologies", IEEE Trans. Neural Syst. Rehabil. Eng. **21**, 3, 333–345, URL http://dx.doi.org/10.1109/TNSRE.2012.2200046 (2013).

[123] Sabesan, S., *Spatiotemporal brain dynamics in epilepsy: Application to seizure prediction and focus localization*, Ph.D. thesis, Arizona State University (2008).

[124] Sabesan, S., L. B. Good, K. S. Tsakalis, A. Spanias, D. M. Treiman and L. D. Iasemidis, "Information flow and application to epileptogenic focus localization from intracranial eeg", Neural Systems and Rehabilitation Engineering, IEEE Transactions on **17**, 3, 244–253 (2009).

[125] Sackellares, J. C., L. D. Iasemidis, D.-S. Shiau, R. L. Gilmore and S. N. Roper, "Epilepsy - when chaos fails", Chaos in the Brain pp. 112–133 (2000).

[126] Saito, Y. and H. Harashima, "Tracking of information within multichannel {EEG} record causal analysis in {EEG}", Yamaguchi N, Fujisawa K (eds) Recent advances in {EEG} and {EMG} data processing. Elsevier pp. 133–146 (1981).

[127] Sazonov, A. V., C. K. Ho, J. W. M. Bergmans, J. B. A. M. Arends, P. A. M. Griep, E. A. Verbitskiy, P. J. M. Cluitmans and P. A. J. M. Boon, "An investigation of the phase locking index for measuring of interdependency of cortical source signals recorded in the EEG", Biological Cybernetics **100**, 2, 129–146, URL http://dx.doi.org/10.1007/s00422-008-0283-4 (2009).

[128] Schelter, B., J. Timmer and M. Eichler, "Assessing the strength of directed influences among neural signals using renormalized partial directed coherence", Journal of Neuroscience Methods **179**, 1, 121–130, URL http://dx.doi.org/10.1016/j.jneumeth.2009.01.006 (2009).

[129] Shafique, A. B. and K. Tsakalis, "Discrete-time pid controller tuning using frequency loop-shaping", in "Advances in PID Control", vol. 2, pp. 613–618 (2012).

[130] Shiau, D., S. Nair, L. Iasemidis, P. Carney, W. Norman, J. Principe, P. Pardalos, W. Suharitdamrong, J. Cho and J. Sackellares, "Seizure warning system and dynamic response to electrical stimulation in a rodent model of chronic limbic epilepsy", in "3rd European Medical and Biological Engineering Conference (EMBEC). Prague", vol. 11 (2005).

[131] Shoeb, A., T. Pang, J. Guttag and S. Schachter, "Non-invasive computerized system for automatically initiating vagus nerve stimulation following patient-specific detection of seizures or epileptiform discharges", International Journal of Neural Systems **19**, 03, 157–172, URL http://www.worldscientific.com/doi/abs/10.1142/S0129065709001938, pMID: 19575506 (2009).

[132] Simon, P., M. de Laplace, F. W. Truscott and F. L. Emory, *A philosophical essay on probabilities*, vol. 166 (Dover Publications, 1951).

[133] Slooter, A., E. Vriens, F. Leijten, J. Spijkstra, A. Girbes, A. van Huffelen and C. Stam, "Seizure detection in adult icu patients based on changes in eeg synchronization likelihood", Neurocritical care **5**, 3, 186–192, URL http://dx.doi.org/10.1385/NCC:5:3:186 (2006).

[134] Socolar, J. E. S., *Nonlinear Dynamical Systems*, pp. 115–140 (Springer US, Boston, MA, 2006), URL http://dx.doi.org/10.1007/978-0-387-33532-2_3.

[135] Srinivasan, R., D. M. Tucker and M. Murias, "Estimating the spatial nyquist of the human eeg", Behavior Research Methods, Instruments, & Computers **30**, 1, 8–19, URL http://dx.doi.org/10.3758/BF03209412 (1998).

[136] Stoegbauer, H., L. Yang, P. Grassberger, R. Andrzejak, T. Kreuz, A. Kraskov, C. Elger and K. Lehnertz, "Lateralization of the focal hemisphere in mesial temporal lobe epilepsy using independent component analysis", Epilepsia **43**, 7, 51 (2002).

[137] Tafreshi, A. K., A. M. Nasrabadi and A. H. Omidvarnia, "Epileptic seizure detection using empirical mode decomposition", in "2008 IEEE International Symposium on Signal Processing and Information Technology", pp. 238–242 (2008).

[138] Takahashi, D. Y., L. A. Baccalá and K. Sameshima, "Connectivity inference between neural structures via partial directed coherence", Journal of Applied Statistics **34**, 10, 1259–1273, URL http://dx.doi.org/10.1080/02664760701593065 (2007).

[139] Takens, F., "Dynamical systems and turbulence (detecting strange attractors in fluid turbulence)", Lecture Notes In Mathematics (1981).

[140] Tassinari, C. A., M. Cincotta, G. Zaccara and R. Michelucci, "Transcranial magnetic stimulation and epilepsy", Clinical neurophysiology **114**, 5, 777–798 (2003).

[141] Taxidis, J., B. Coomber, R. Mason and M. Owen, "Assessing cortico-hippocampal functional connectivity under anesthesia and kainic acid using generalized partial directed coherence", Biological Cybernetics **102**, 4, 327–340, URL http://dx.doi.org/10.1007/s00422-010-0370-1 (2010).

[142] Temkin, O., *The falling sickness: a history of epilepsy from the Greeks to the beginnings of modern neurology* (Johns Hopkins University Press Baltimore, 1994).

[143] Tergau, F., U. Naumann, W. Paulus and B. J. Steinhoff, "Low-frequency repetitive transcranial magnetic stimulation improves intractable epilepsy", The Lancet **353**, 9171, 2209 (1999).

[144] Thiel, M., B. Schelter, M. Mader and W. Mader, "Signal processing of the eeg: Approaches tailored to epilepsy", in "Recent Advances in Preventing and Predicting Epileptic Seizures", edited by R. Tetzlaff, C. E. Elgar and K. Lehnertz, pp. 119–131 (World Scientific, 2013).

[145] Traub, R. D. and A. Bibbig, "A model of high-frequency ripples in the hippocampus based on synaptic coupling plus axon–axon gap junctions between pyramidal neurons", The Journal of Neuroscience **20**, 6, 2086–2093 (2000).

[146] Tsakalis, K., N. Chakravarthy and L. Iasemidis, "Control of epileptic seizures: Models of chaotic oscillator networks", in "Proceedings of the 44th IEEE Conference on Decision and Control", pp. 2975–2981 (2005).

[147] Tsakalis, K., N. Chakravarthy, S. Sabesan, L. Iasemidis and P. Pardalos, "A feedback control systems view of epileptic seizures", Cybernetics and Systems Analysis **42**, 4, 483–495 (2006).

[148] Tsakalis, K. and L. Iasemidis, "Prediction and control of epileptic seizures", in "International Conference and Summer School Complexity in Science and Society European Advanced Studies Conference V, Patras and Ancient Olympia, Greece", pp. 14–26 (2004).

[149] Tsakalis, K. and L. Iasemidis, "Control aspects of a theoretical model for epileptic seizures", International Journal of Bifurcation and Chaos **16**, 07, 2013–2027, URL http://www.worldscientific.com/doi/abs/10.1142/S0218127406015866 (2006).

[150] Tzallas, A., M. Tsipouras and D. Fotiadis, "Epileptic seizure detection in eegs using time–frequency analysis", IEEE Transactions on Information Technology in Biomedicine **13**, 5, 703–710, URL http://dx.doi.org/10.1109/TITB.2009.2017939 (2009).

[151] Velasco, A. L., M. Velasco, F. Velasco, D. Menes, F. Gordon, L. Rocha, M. Briones and I. Márquez, "Subacute and chronic electrical stimulation of the hippocampus on intractable temporal lobe seizures: preliminary report", Archives of Medical Research **31**, 3, 316–328 (2000).

[152] Venkataraman, V., I. Vlachos, A. Faith, B. Krishnan, K. Tsakalis, D. Treiman and L. Iasemidis, "Brain dynamics based automated epileptic seizure detection", in "2014 36th Annual International Conference of the IEEE Engineering in Medicine and Biology Society", pp. 946–949 (2014).

[153] Vercueil, L., A. Benazzouz, C. Deransart, K. Bressand, C. Marescaux, A. Depaulis and A. Benabid, "High-frequency stimulation of the sub-thalamic nucleus suppresses absence seizures in the rat: comparison with neurotoxic lesions", Epilepsy research **31**, 1, 39–46 (1998).

[154] Vlachos, I., B. Krishnan, J. Sirven, K. Noe, J. Drazkowski and L. Iasemidis, "Frequency-based connectivity analysis of interictal iEEG to localize the epileptogenic focus", in "2013 29th Southern Biomedical Engineering Conference", (Institute of Electrical & Electronics Engineers (IEEE), 2013), URL http://dx.doi.org/10.1109/SBEC.2013.90.

[155] Volkmann, J., J. Herzog, F. Kopper and G. Deuschl, "Introduction to the programming of deep brain stimulators", Movement Disorders **17**, S3, S181–S187, URL http://dx.doi.org/10.1002/mds.10162 (2002).

[156] Walton, N. Y. and D. M. Treiman, "Response of status epilepticus induced by lithium and pilocarpine to treatment with diazepam", Experimental neurology **101**, 2, 267–275 (1988).

[157] Wendling, F., F. Bartolomei, F. Mina, C. Huneau and P. Benquet, "Interictal spikes, fast ripples and seizures in partial epilepsies - combining multi-level computational models with experimental data", European Journal of Neuroscience **36**, 2, 2164–2177, URL http://dx.doi.org/10.1111/j.1460-9568.2012.08039.x (2012).

[158] World Health Organizations, "Epilepsy fact sheet no. 999", URL http://www.who.int/mediacentre/factsheets/fs999/en/ (2016).

[159] Williamson, J. R., D. W. Bliss and D. W. Browne, "Epileptic seizure prediction using the spatiotemporal correlation structure of intracranial eeg", in "2011 IEEE International Conference on Acoustics, Speech and Signal Processing (ICASSP)", pp. 665–668 (2011).

[160] Williamson, J. R., D. W. Bliss, D. W. Browne and J. T. Narayanan, "Seizure prediction using eeg spatiotemporal correlation structure", Epilepsy & Behavior **25**, 2, 230–238 (2012).

[161] Wolf, A., J. B. Swift, H. L. Swinney and J. A. Vastano, "Determining Lyapunov exponents from a time series", Physica D: Nonlinear Phenomena **16**, 3, 285–317 (1985).

[162] Yamamoto, J., A. Ikeda, T. Satow, K. Takeshita, M. Takayama, M. Matsuhashi, R. Matsumoto, S. Ohara, N. Mikuni, J. Takahashi *et al.*, "Low-frequency electric cortical stimulation has an inhibitory effect on epileptic focus in mesial temporal lobe epilepsy", Epilepsia **43**, 5, 491–495 (2002).

[163] Young, C.-P., S.-F. Liang, D.-W. Chang, Y.-C. Liao, F.-Z. Shaw and C.-H. Hsieh, "A portable wireless online closed-loop seizure controller in freely moving rats", IEEE Trans. Instrum. Meas. **60**, 2, 513–521, URL http://dx.doi.org/10.1109/TIM.2010.2050358 (2011).

[164] Zhao, Y., S. A. Billings, H. Wei and P. G. Sarrigiannis, "Tracking time-varying causality and directionality of information flow using an error reduction ratio test with applications to electroencephalography data", Physical Review E **86**, 5, URL http://dx.doi.org/10.1103/PhysRevE.86.051919 (2012).

[165] Zhong, X.-L., J.-T. Yu, Q. Zhang, N.-D. Wang and L. Tan, "Deep brain stimulation for epilepsy in clinical practice and in animal models", Brain Research Bulletin **85**, 3-4, 81–88, URL http://dx.doi.org/10.1016/j.brainresbull.2011.03.020 (2011).

[166] Zhou, K. and J. C. Doyle, *Essentials of robust control*, vol. 104 (Prentice hall Upper Saddle River, NJ, 1998).

APPENDIX A

DETAILS OF THE SWITCHING CIRCUIT

Figure A.1 shows how the complete switching circuit works in conjunction with the Intan board, the Arduino Mega and the stimulator from A-M Systems. To recap, the 10 electrodes we use are F3, F4, LT, RT, LA, RA, LM, RM, LL, RL which are correspondingly connected from the Intan board to the animal's head-cap using the switches EEG 1 through EEG 10 as shown in the Figure. As an example, if at a certain point in time, it is intended to stimulate the F3-F4 electrode pair, the computer sends out this command to the Arduino. The Arduino carries out the instruction by holding voltages on its digital pins accordingly to switch off the EEG 1 and EEG 2 switches and switch on the StimR1 and StimB2 switches. This will allow stimulation current to flow between the chosen pair of electrodes while simultaneously disconnecting the first two Intan ADCs. This ensures that the ADCs are protected from the stronger stimulating current. When the time to end stimulation comes about, the computer program will send a stop command to the Arduino Mega. Then the Arduino will respond by switching off the StimR1 and StimB2 switches and switching back on the EEG 1 and EEG 2 switches. Thus, re-establishing recording capability in those two channels.

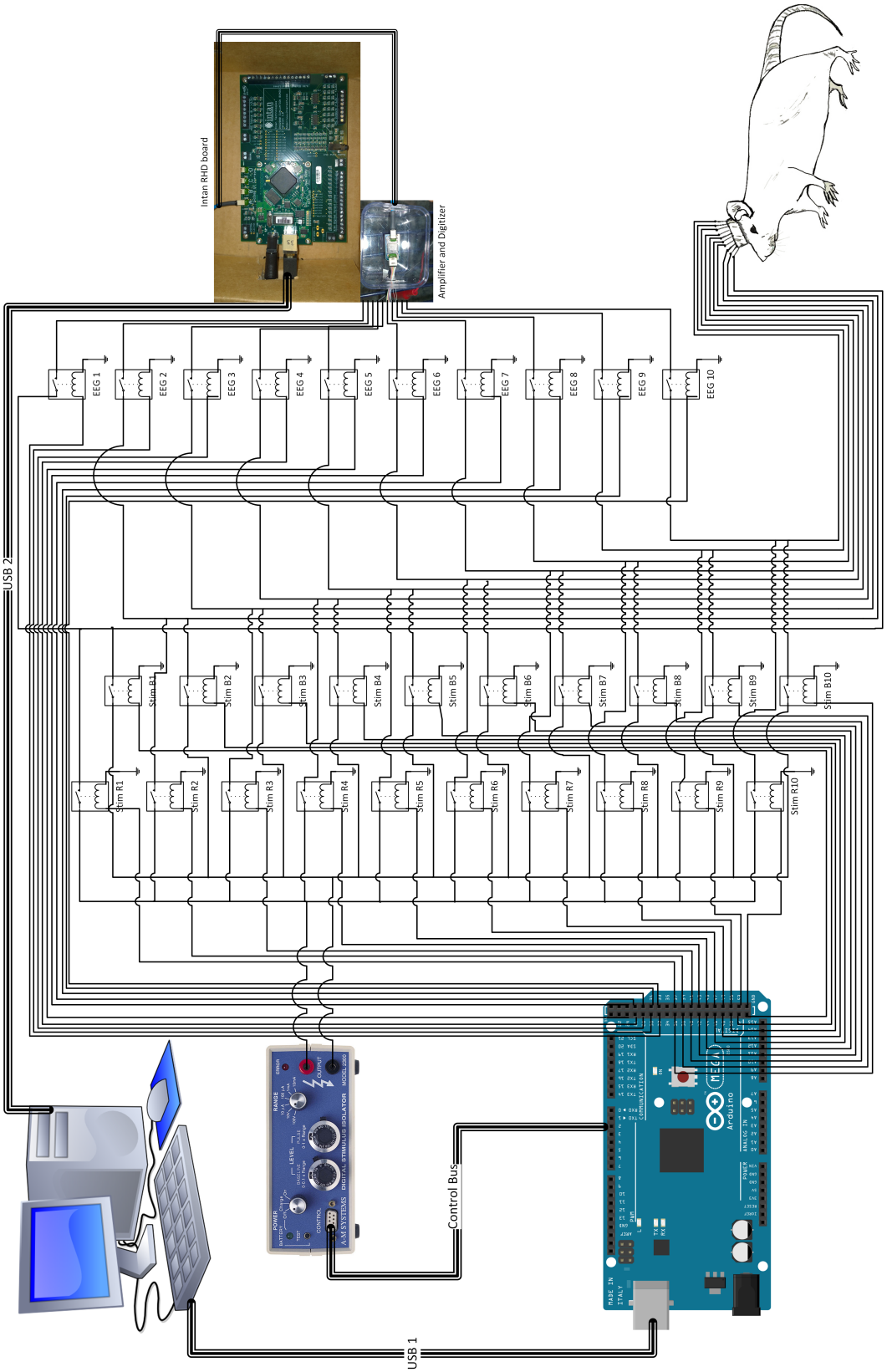

Figure A.1: Schematic of the switching circuit.

APPENDIX B

TERMS AND ACRONYMS

Some of the terms and Acronyms used in this report are explained here.

- Ictal - During seizure.
- Interictal - Between seizures.
- Preictal - Tens of seconds before seizure.
- Postictal - Tens of seconds after seizure.
- Electrographic Onset (EO) – The time at which the seizure is marked to have begun through expert visual analysis of the EEG/ECoG.
- Electrographic End (EE) – The time at which the seizure is marked to have ended through expert visual analysis of the EEG/ECoG.
- Clinical Onset (CO) – The time at which an expert observer, or an observer familiar with the patient's seizures first identifies a behavioral manifestation of a seizure.
- False Positive (FP) – The occurrence of a seizure detection at a time when no seizure is occurring.
- False Negative (FN) – The failure to detect a seizure that has occurred.
- True Positive (TP) – The detection of a seizure that has occurred.
- True Negative (TN) – Correctly being in the state of non-detection during a time when a seizure is not occurring.
- Sensitivity – A measure of how likely an epoch during a seizure is to be detected. The classical definition, for a binary classifier, is given by

$$Sensitivity = \frac{\#TruePositives}{\#TruePositives + \#FalseNegatives}$$

- Specificity - A measure of how likely an epoch during a non-seizure epoch is to be detected. The classical definition, for a binary classifier, is given by

$$Specificity = \frac{\#TrueNegatives}{\#TrueNegatives + \#FalsePositives}$$

APPENDIX C

EEG DATA SAMPLES

Here, we present two samples of EEG data collected from Rat 13. Both data were sampled at 512 Hz. First, in Figure C.1 we show 1 minute and 40 seconds of interictal data that starts at 125 hours 13 minutes and 48 seconds from the beginning of the record. Next, in Figure C.2 we show ictal data from a seizure that occurs roughly an hour after the interactal data. The data starts at 125 hours 25 minutes and 17 seconds from the beginning of the EEG file. Visual comparison shows a clear distinction of the seizure during the ictal period as compared to the interictal one. The seizure start is marked at 126 hours 25 minutes and 39 seconds from the beginning of the record file.

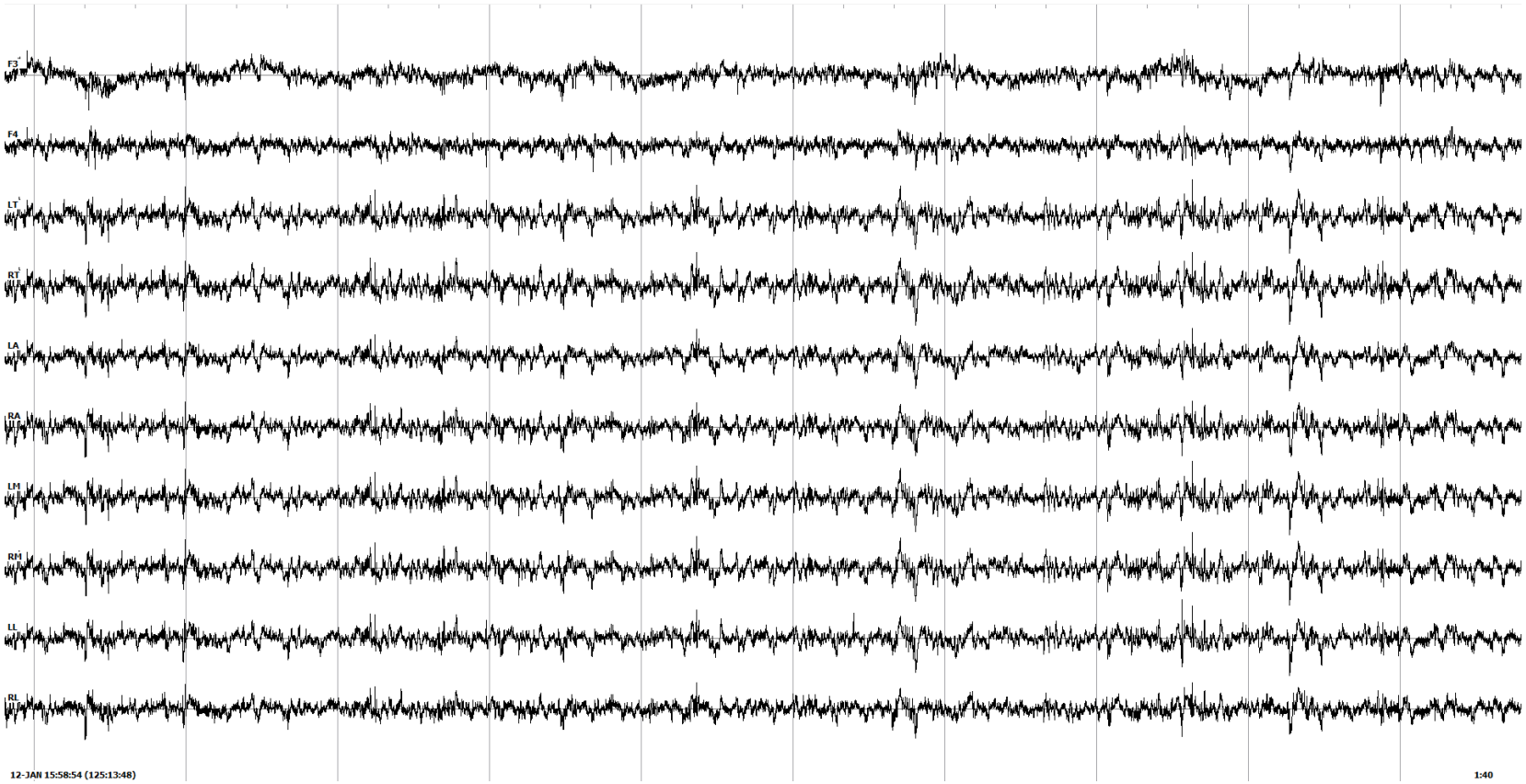

Figure C.1: Interictal EEG data from Rat 13.

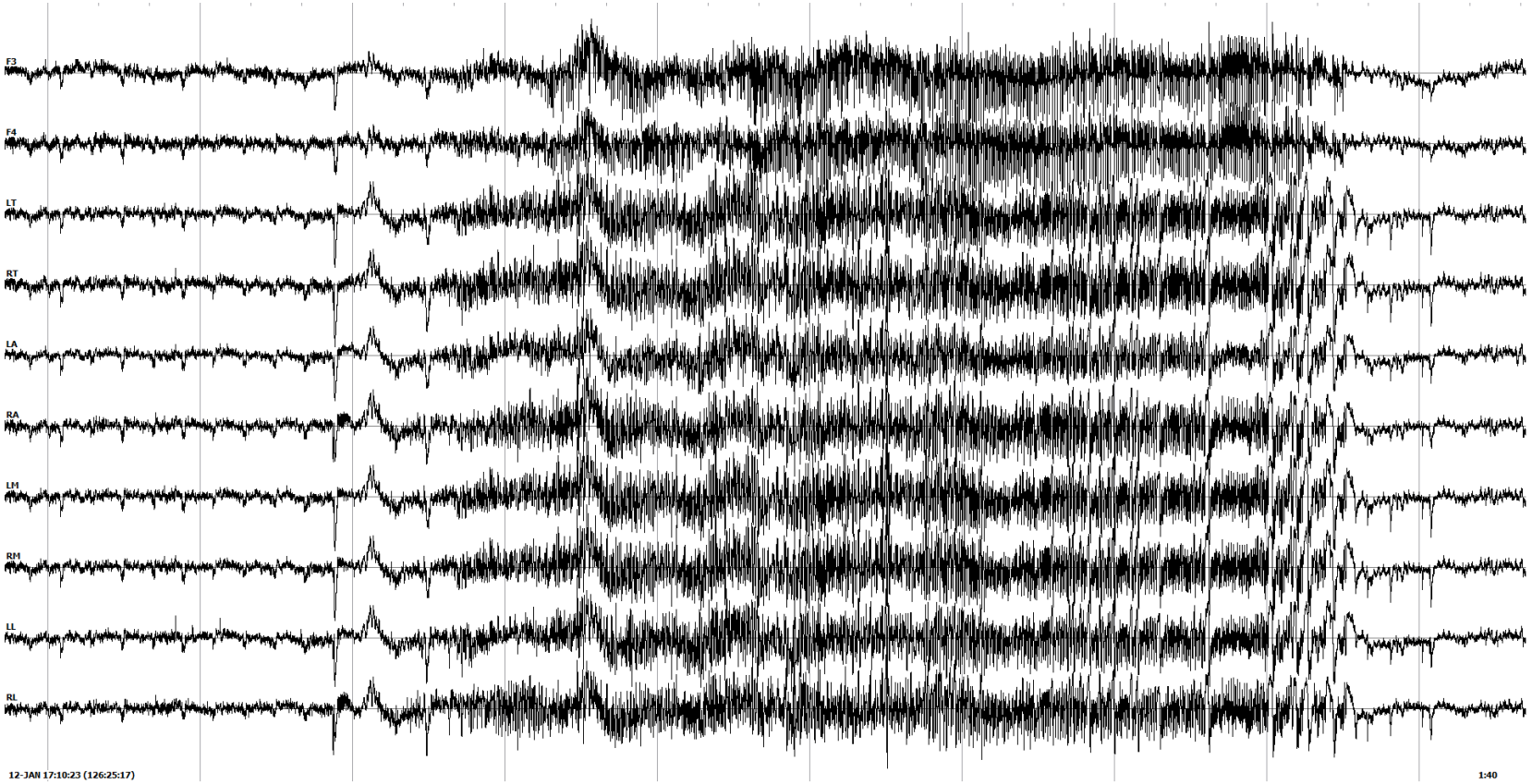

Figure C.2: Ictal EEG data from Rat 13.